Organo-chalcogen Supramolecular Building Blocks

SYNTHETIC, STRUCTURAL AND COMPUTATIONAL STUDIES OF ORGANO-CHALCOGEN SUPRAMOLECULAR BUILDING BLOCKS

BY

LUCIA MYONGWON LEE, B.SC.

A THESIS
SUBMITTED TO THE SCHOOL OF GRADUATE STUDIES
IN PARTIAL FULFILLMENT OF THE REQUIREMENTS
FOR THE DEGREE
DOCTORATE OF PHILOSOPHY

MCMASTER UNIVERSITY

© COPYRIGHT BY LUCIA MYONGWON LEE, AUGUST 2017

Ph.D (2017) McMaster University
(Chemistry) Hamilton, ON

TITLE: Synthetic, Structural and Computational Studies of Organo-chalcogen Supramolecular Building Blocks

AUTHOR: Lucia Myongwon Lee

SUPERVISOR: Associate Professor Ignacio Vargas-Baca

NUMBER OF PAGES: pages i-xxxi, pages 158.

LAY ABSTRACT

Supramolecular chemistry is a prominent area of research that pursues the construction of large structures by the spontaneous assembly and organization of molecular building blocks. Its fundamental premise is that the judicious use of intermolecular forces allows the design of a structure and control of its properties. Most of the work in supramolecular chemistry has relied on hydrogen atoms bridging molecules and the bonding of metal ions to atoms rich in electrons. This thesis pursued the use of a different type of intermolecular force, termed "secondary bonding", which is characteristic of the heaviest elements at the right of the periodic table (the "main-group" of elements).

Previous work at McMaster demonstrated that cyclic molecules containing carbon, nitrogen and tellurium were particularly efficient as supramolecular building blocks. However, they are easily degraded by atmospheric water, this fact severely limits practical applications of these compounds.

In this thesis, the tellurium atoms are replaced by selenium, a lighter element in the same family. The resulting molecules are more tolerant of atmospheric conditions but form weaker intermolecular links. Through a combination of quantum mechanical, synthetic, spectroscopic and structural studies, it is shown that certain modifications to the molecular structure increase the affinity of the selenium atoms for electrons. In this way, it is possible to strengthen the intermolecular interactions and promote the spontaneous assembly of supramolecular structures.

These investigations eminently fall in the category of fundamental research but have broad-reaching implications for practical applications in optical and electronic technologies.

ABSTRACT

Previous studies of supramolecular association through chalcogen-centred secondary bonding interactions (SBIs) demonstrated the versatility of 1,2,5-telluradiazoles and their annulated congeners, the benzo-2,1,3-telluradiazoles, as supramolecular building blocks. Key to the properties of those compounds is their propensity to undergo auto-association through the $[Te\text{-}N]_2$ supramolecular synthon leading to dimers or supramolecular ribbon polymers. Moderate steric repulsion induces structural distortions of $[Te\text{-}N]_2$ without dissociation and, in doing so, enables properties of practical interest such as chromotropism and second-order non-linear optical responses. However, moisture sensitivity discourages wide-spread application of these compounds. While being more tolerant of the atmosphere, the analogous selenadiazoles form weaker intermolecular interactions. Using a combined experimental and computational approach, this thesis investigates methods by which the selenium-centred supramolecular interactions can be enhanced and applied in the construction of supramolecular architectures.

The quantum mechanical description of the SBIs formed by 1,2,5-chalcogenadiazoles was updated with the application of modern dispersion corrections to relativistic density functional theory calculations (PBE-D3, ZORA). While in all cases the dispersion effect on optimized SBI distances is small (< 0.03 Å), the dispersion corrections to the calculated interaction energy range from 6 to 10 kJ mol^{-1} and increase with the weight of the chalcogen. The total interaction energy increases faster, however, therefore the relative weight of dispersion for the telluradiazole (10%) is significantly less than for the sulfur analogue (40%).

The same dispersion-corrected functional was applied to the identification of the secondary ions observed in the Laser Desorption Ionization mass spectrum of benzotelluradiazoles. The most stable structure of the $[2M+H]^+$ ion was shown to feature the $[Te\text{-}N]_2$ supramolecular synthon and would be preferred over alternatives held by hydrogen bonding alone, one Te···N SBI, a combination of the two or π-stacking. The $[2M]^+$ would also feature the $[Te\text{-}N]_2$ supramolecular synthon. Shortening of the Te···N distances in these ions implies that electron withdrawing groups strengthen the SBIs.

The updated computational method was also applied to characterize the bonding in the adducts of a N-heterocyclic carbene with benzo-2,1,3-telluradiazole and 3,4-dicyano-2,1,5-telluradiazole recently prepared by the Zibarev group. The long Te···C distances (2.53 and 2.34 Å) correspond to fractional bond orders (<0.6) but display a significant covalent character. Attachment of the carbene nearly erases the remaining σ-hole on tellurium, raises the LUMO energy and consequently prevents the dimerization of these adducts, in contrast to what has been observed with the pyridine and DMSO adducts of other telluradiazoles.

Benzo-2,1,3-selenenadiazole reacted with boranes (BR_3, R = Ph, F, Cl, Br) yielding 1:1 (R = Ph, F, Cl, Br) and 1:2 (R = Cl) adducts. The crystal structure the BPh_3 adduct features molecules organized in pairs connected by long Se···Cπ SBIs but no Se···N SBIs. The BF_3 and BCl_3 1:1 adducts dimerize forming the $[Se\text{-}N]_2$ supramolecular synthon. In contrast, the BBr_3 adduct does not dimerize although Se···Br, Br···Br SBIs are formed through the lattice. The 1:2 adduct displays Se···Cl SBIs accompanied by distortion of the N-B-Cl bond angle due to the enhanced electrophilicity of the chalcogen. DFT calculations were performed to evaluate the energies of dimerization of the 1:1 adducts, the calculated SBI energies are greater than those for the dimer of the parent heterocycle (benzo-2,1,3-selenadiazole, **3b**).

The products of the combination of benzo-2,1,3-selenenadiazole with chloride salts of divalent Mn, Fe, Co, Ni, and Cd crystallized from DMSO in two distinct structural types. While the smaller ions (Fe^{II}, Co^{II} and Ni^{II}) form infinite chains of metal atoms N,N'-bridged by the heterocycle´ the larger ions (Mn^{II} and Cd^{II}) stabilize infinite chains of metal atoms bridged by μ^2 halide ions. In the latter case, two heterocycle molecules cap each metal ion and are able to establish a link to the next chain in the lattice through the $[Se\text{-}N]_2$ supramolecular synthon. Despite the large (>9.2 Å) distance between $[M(\mu\text{-}Cl)_2]_\infty$ chains, the manganese derivative is only paramagnetic, not ferromagnetic. Symmetry-broken DFT calculations for small models were unable to quantitatively reproduce the measured couplings (J) but do indicate that the heterocycle acquires significant spin density in the Mn^{II} compound enabling paramagnetic coupling through the $[Se\text{-}N]_2$ supramolecular synthon.

General methods for the synthesis of N-alkylated selenadiazolium cations were investigated. Methyl, *iso*-propyl and *tert*-butyl benzo-2,1,3-selenadiazolium cations were prepared by direct alkylation or cyclo-condensation of the alkyl-phenylenediamine with selenous acid. While the former reaction only proceeds with the primary and tertiary alkyl iodides, the latter is very efficient. Difficulties reported in earlier literature are attributable to the formation of adducts of benzoselenadiazole with its alkylated cations and side reactions initiated by aerobic oxidation of iodide. However, the cations themselves are

resilient to oxidation and stable in acidic to neutral aqueous media. X-ray crystallography was used in the identification and characterization of the following compounds: $[C_6H_4N_2(R)Se]^+X^-$, ($R = CH(CH_3)_2$, $C(CH_3)_3$; $X = I^-$, I_3^-), $[C_6H_4N_2(CH_3)Se]^+I^-$, and $[C_6H_4N_2Se][C_6H_4N_2(CH_3)Se]_2I_2$. Formation of Se···N SBIs was only observed in the last structure because anion binding to selenium is stronger. The relative strengths of those forces and the structural preferences they enforce were assessed with DFT-D3 calculations supplemented by AIM analyses of the electron density.

The methods developed for the preparation of N-alkyl benzoselenadiazolium cations were extended to the syntheses of dications intended for use as building blocks of supramolecular polymers. The structure of several salts was established by single-crystal X-ray diffraction. $[H_4C_6NSeN\text{-}CH_2\text{-}CH_2\text{-}NSeNC_6H_4]Cl_2$ crystallized forming a macrocyclic structure in which two dications are bridged by Se···Cl SBIs; a third halide anion sits at the centre of the macrocycle. $[1,2\text{-}(H_4C_6NSeN)_2\text{-}C_6H_{10}]Cl_2$ features two selenadiazolium cations bridged by a 1-(R),2-(R)-substituted cyclohexane and short Se···Cl SBIs. $[1,4\text{-}(H_4C_6NSeN\text{-}CH_2)_2\text{-}C_6H_4](BF_4)_2$, featuring a *p*-xylene bridge, crystallizes in two pseudopolymorphs; with dications in anti or syn conformations making Se···F contacts. $[H_4C_6NSeN\text{-}CH_2\text{-}CH_2\text{-}NSeNC_6H_4](CF_3SO_3)_2$ does dimerize though the $[Se\text{-}N]_2$ supramolecular synthon, although Se···O interactions with the anions cap the second selenium atom. In contrast, $[H_4C_6NSeN\text{-}CH_2\text{-}CH_2\text{-}CH_2\text{-}NSeNC_6H_4](CF_3SO_3)_2$ only displays Se···O contacts.

An oligonucleotide analogue containing N-substituted selenadiazolium cations was designed to create foldamers with structures controlled by main-group secondary bonding. The target structures take advantage of the methods developed in this thesis for the functionalization of selenadiazoles and is meant to be compatible with automated methods for oligonucleotide synthesis. The proposed synthesis begins with the preparation of 1-(α,β)-O-methyl-2-deoxy-D-ribose, which was chlorinated and treated with phenylenediamine. High-resolution mass spectrometry confirmed the attachment of the diamine to the ribose, however, the yield was too low to continue this synthetic project.

A ground-breaking development in the application of secondary bonding in supramolecular chemistry is the discovery of the reversible auto-association of *iso*-tellurazole *N*-oxides through Te···O SBIs into annular structures. These rings are persistent in solution and behave as actual macrocycles able to complex transition metal ions, form adducts with fullerenes, and host small molecules. Single-crystal X-ray diffraction was critical to the characterization of these structures and required careful disorder modelling for tetrahydrofuran molecules included in a macrocyclic hexamer and the occupational disorder of CH_2Cl_2 and BF_4^- anions due to metal depletion in the crystal of a Pd^{II} complex.

ACKNOWLEDGEMENTS

I thank my supervisor, Dr. Ignacio Vargas-Baca, whom I think, is the greatest graduate supervisor a graduate student can ask for. I very much admire his passion for chemistry, patient guidance and encouragement he has provided during my time at McMaster University. He is such an inspiration.

I express my gratitude towards my supervisory committee members, Dr. G. J Schrobilgen and Dr. W. J. Leigh for their helpful suggestions.

I thank the NMR spectroscopy facility (Drs. Hilary Jenkins, Bob Berno), mass spectrometry facility, and the X-ray diffraction facility (Drs. Hilary Jenkins, and Jim Britten).

I thank my funding sources: McMaster University, the Department of Chemistry & Chemical Biology, the Natural Science Engineering Research Council of Canada (NSERC), and the Ontario Graduate Scholarship (OGS).

I acknowledge the staff and facilities of the Shared Hierarchical Academic Research Computing Network (SHARCNET:www.sharcnet.ca).

I thank both past & present lab members and summer/undergraduate thesis students (Victoria Corless, Dora Hsieh, Faisal Adam-Pani, Michael Tran, Andy Tran, Helen Luu, Sophia Jeon, and Jiwon Lee)

I also thank wonderful friends I have made during my time at McMaster University: Meera Mehta, Jeff Price, María Gonzalez, Patricia Edem, Brad Cowie, Lisa Walter, Vinodh Rajendra, Salma Al-Karmi, Chris Gendy, Alex Hudson, Faraz, Blossom Yan, Peter Ho, Sam Ros, Derek Morim, Kathryn Benincasa, Fariha Mahmood, Natalie D'Silva, Jamie

Goettel, Fan Fei, Gil the stuffed sheep, and Frens (Alison Stewart, Jennifer Wild, Christal Zhou, and Sheilan Sinjari).

I also thank my family members (my parents and my brother Jiwon Lee) for their constant love and encouragement.

TABLE OF CONTENTS

LIST OF FIGURES

LIST OF SCHEMES

LIST OF TABLES

LIST OF ABBREVIATIONS AND SYMBOLS

δ	chemical shift, ppm (parts per million)
λ	wavelength
μ	linear absorption coefficient (in crystallography)
ρ	density of a material (in crystallography)
Å	Angstrom (1Å = 10^{-10} m.
a, b, c, α, β, γ	unit cell parameters (in crystallography)
ACN	acetonitrile
ADF	Amsterdam Density Functional software
ALDA	Adiabatic Local Density Approximation
a.u.	atomic units
B97	GGA exchange correlation functional, Becke exchange and correlation
BP86	GGA exchange correlation functional, Becke exchange and Perdew correlation
CI	chemical ionization (in mass spectrometry)
cm^{-1}	inverse centimetres (wavenumbers)
COSY	Correlation Spectroscopy
CSD	Cambridge Structural Database
D	donor atom within an SBI
DCE	1,2-dichloroethane
DCM	dichloromethane
DFT	density functional theory
DMF	dimethyl formamide
DMSO	dimethyl sulfoxide
DMT	Dimethoxytrityl
DZ	double-ζ (basis set)
DZP	double-ζ with one-polarization function (basis set)
E	energy
e	electrons (in crystallography)
EA	elemental analysis
EI	electron ionization (in mass spectrometry)
ESI	electrospray ionization
ETS-NOCV	extended-transition-state method from the natural orbitals for chemical valence
esu	electrostatic units
FT	Fourier transform
GGA	generalized gradient approximation

GUI	graphical user interface
HF	Hartree-Fock
HOMO	highest occupied molecular orbital
HR	high resolution
HMBC	heteronuclear multiple-bond coherence (pulse sequence)
iPr	*iso*-propyl
IR	infrared
IUPAC	International Union of Pure and Applied Chemistry
K	Kelvin
KS	Kohn-Sham
LUMO	lowest unoccupied molecular orbital
MALDI	matrix-assisted laser desorption/ionization
Me	methyl
MO	molecular orbital
MS	mass spectrometry
nm	nanometer
NMR	nuclear magnetic resonance (spectroscopy)
PAC	phenoxyacetyl
PBE	GGA DFT exchange and correlation functional by Perdew, Burke, and Ernzerhoff
pm	picometer
ppm	parts per million
PW91	GGA exchange exchange and correlation functional by Perdew and Wang
Pyr	pyridine
R_1	unweighted residual factor (in crystallography)
r_{vdW}	van der Waals radii
SBI	secondary bonding interaction
T	temperature
TBDMS	*tert*-butyldimethylsilyl
TEA	triethylamine
^{t}Bu	*tert*-butyl
TD-DFT	time-dependant density functional theory
THF	tetrahydrofuran
TMS	tetramethylsilane
TOF	time-of-flight (in mass spectrometry)
TZ2P	triple-ζ with two-polarization functions (basis set)
TZP	triple-ζ with one polarization function (basis set)
UV-Vis	ultraviolet-visible (spectroscopy)

V	unit cell volume (in crystallography)
VT	variable temperature (in NMR)
wR_2	weighted residual factor (in crystallography)
Z	molecules per unit cell (in crystallography)
ZORA	zeroth-order regular relativistic approximation

LIST OF COMPOUNDS

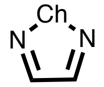

1

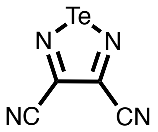

2

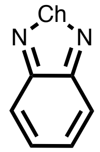

3
a= S
b= Se
c= Te

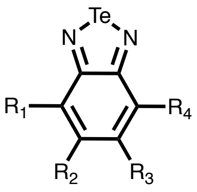

4 $R_{1,4}$ = Br; $R_{2,3}$ = H
5 $R_{1,2,34}$= F
6 $R_{1,4}$=Cl; $R_{2,3}$= H
7 $R_{1,3}$=^{t}Bu; $R_{2,4}$= H

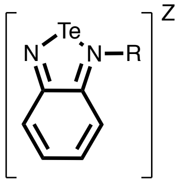

8
a R= BPh_3; Z= 0
b R= CH_3; Z= +1

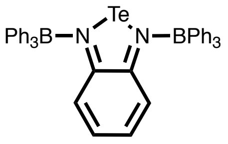

9

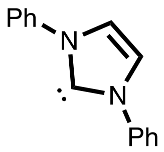

10

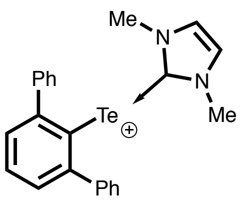

11

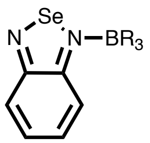

12
a R= Ph
b R= F
c R= Cl
d R= Br
e R= I

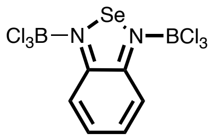

13

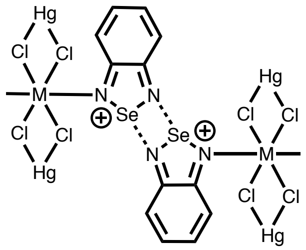

14 M= Mn

15 M= Cd

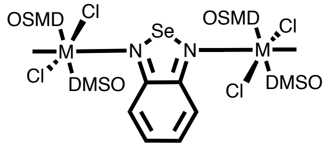

16 M= Fe

17 M= Co

18 M= Ni

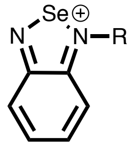

19
a R= CH_3
b R = iPr
c R= ^{t}bu

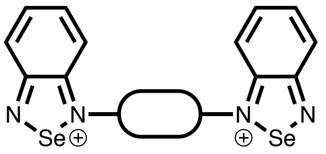

20

a N-$(CH_2)_2$-N
b N-$(CH_2)_3$-N

c

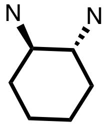

d

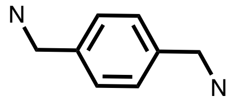

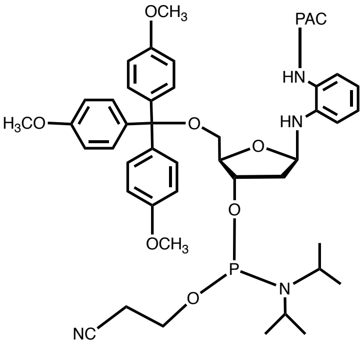

21

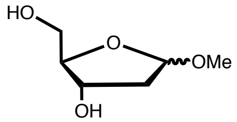

22

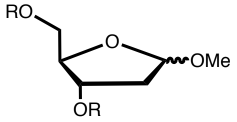

23
a R= Ac
b R= pTolC(O)

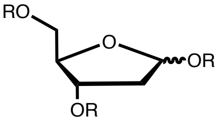

24
a R= Ac
b R= pTolC(O)

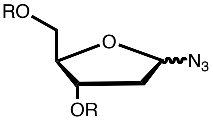

25
a R= Ac
b R= pTolC(O)

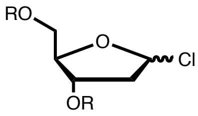

26
a R= Ac
b R= pTolC(O)

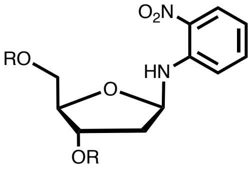

27
a R= Ac
b R= pTolC(O)

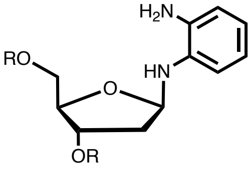

28
a R= Ac
b R= pTolC(O)

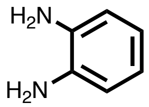

29

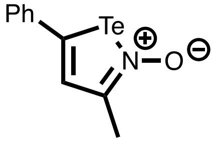

30

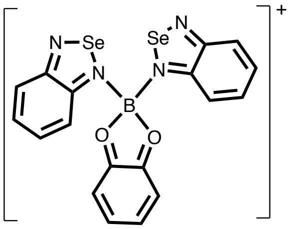

31

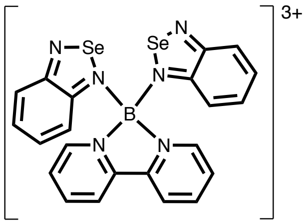

32

Chapter 1. Introduction

1.1 Supramolecular Chemistry

This interdisciplinary area of research uses weak intermolecular forces to precisely control the organization of organic and inorganic molecules in large structures. The rapid progress in supramolecular chemistry began in late 1960s and became much more prominent after the 1987 Nobel Prize for Chemistry was awarded to Lehn, Cram and Pedersen for contributions that greatly expanded the field. Continuous interest in supramolecular chemistry has resulted in a wide variety of supramolecular structures; some of them possess magnetic, photoactive, redox and other remarkable and useful properties, including the "molecular machines" that earned Stoddart, Sauvage and Feringa the 2016 Nobel Prize.

There are several supramolecular interactions that can be used in the assembly of large *supramolecules*: ion-ion interactions, ion-dipole interactions, dipole-dipole interactions, cation-π interactions, π-π stacking, van der Waals forces, hydrogen bonding, the coordination of the metal ions, and the hydrophobic effect. Yet, most of all that progress has been achieved using just the last two types of supramolecular interactions in the list.

1.2 Hydrogen Bonding

Formally defined by the International Union for Pure and Applied Chemistry (IUPAC), a hydrogen bond is "an attractive interaction between a hydrogen atom from a molecule or a molecular fragment X-H in which X is more electronegative than H, and an atom or a group of atoms in the same or a different molecule, in which there is evidence of bond formation".[1] The attractive interaction between the hydrogen atom of X-H molecular fragments and electron-rich atoms can be fairly strong (4 to 120 kJ mol^{-1}) and is dependent on the environment. Its high directionality and applications have been extensively recognized by a wealth of theoretical and experimental work.

One of the most remarkable examples of its natural application is the self-assembling double helix of DNA (Figure 1.1)[2], which is present in every living cell as the basis of genetic inheritance and storage of information required for the functions of the entire organism. In reality, the double helical structure of DNA results not just from the precise pairings of nucleobases through H-bonding, but also the additional contributions of π-stacking, electrostatic interactions and the hydrophobic effect. Inspired by the cooperative interplay of these interactions, DNA is being considered as an attractive tool in the field of structural nanotechnology.[3,4] Novel supramolecular architectures have been developed by incorporating polymers and transition metals which take advantage of the self-assembly of DNA oligonucleotides.[5-7]

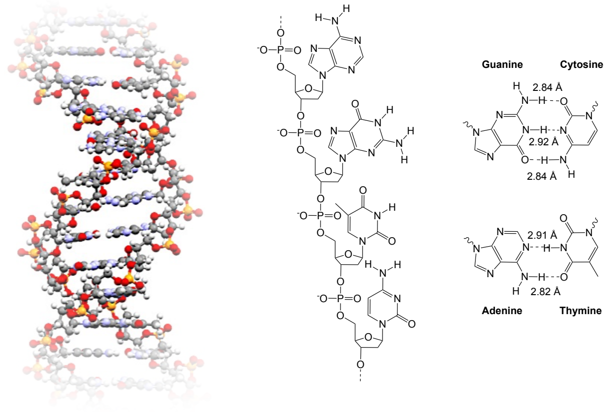

Figure 1.1 Structure of the DNA double helix, example of a nucleotide chain and nucleobase pairing.

1.3 Coordination of Metal Ions

The affinity of metal ions for atoms with lone pairs of electrons has been used to manipulate molecular structure and properties for more than a century. *Ligand design*, the purposeful synthesis of organic compounds exclusively intended to bind metal ions remains a central part of inorganic chemistry. In most instances the metal is bound to a previously built ligand, but there are also cases in which the organic molecule is built around a metal ion which acts as a template. The synthesis of Schiff-base macrocycles is a prominent example of this type of chemistry. Here, the size of the macrocycle is dependent on the size of the metal ions; smaller cations result in small macrocycles whereas the use of larger cations results in bigger structures.[8,9] Transition metal coordination centres are commonly used to control and hold the shape of large structures. Extensive research has gone into construction of complex two- and three-dimensional self-assembled structures at molecular (rings and cages)[10-17] and crystalline –macroscopic– scale.[18-20] (Figure 1.2)

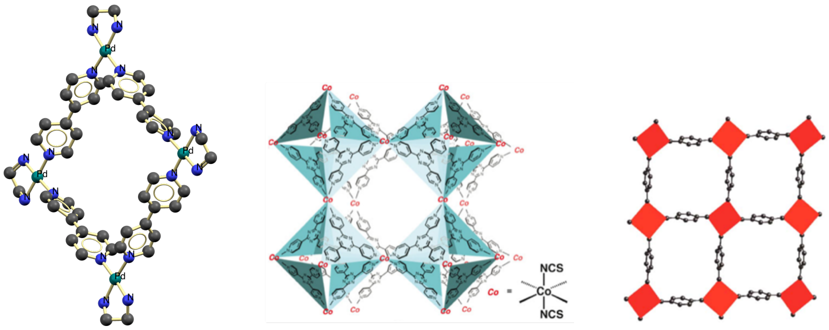

(a) (b) (c)

Figure 1.2 Examples of metal organic (a) ring (b) cage and (c) framework (built from Zn^{II} and terephthalate). a) is drawn from original data in reference 21; b) and c) are reproduced with permission from references 17 and 20 respectively.

1.4 Secondary Bonding and σ-hole Interactions

Other supramolecular interactions such as, ion-dipole, dipole-dipole, cation-π, and π-π stacking are as well capable of stabilizing supramolecular structures but, in comparison to hydrogen bonding and the coordination of transition metal ions, have received much less attention. Even less investigated have been the supramolecular interactions that are characteristic of the heavy p-block elements.

Once X-ray diffraction developed into a routine technique for the characterization of inorganic compounds, it became apparent that compounds that contain heavy p-block elements pack in structures that place the heavy atom in close proximity to electron rich centres (lone pairs, π-electron clouds) at distances shorter that the corresponding sum of van der Waals radii but significantly longer than typical single bonds. This was observed even when the element in question was already in a molecule compliant with the Lewis octet rule or could be described by a hypervalent model. Moreover, such contacts appeared to defy the expected repulsion between lone-pairs of electrons. Initially dismissed as mere packing accidents or simple "van der Waals contacts", these interatomic contacts were poorly understood for a long time, as illustrated by the diversity of labels given to describe this phenomenon: soft-soft interactions, closed-shell interactions, nonbonding interactions, semibonding interactions, weakly-bonding interactions, and charge-transfer interactions, to list just the most frequent occurrences in literature.

Analysis of these interactions with modern computational methods has identified three main stabilizing contributions:

i) Electrostatic. As the heavy p-block elements are often bonded to more electronegative atoms, they acquire positive charges and become attracted to electron rich centres. Politzer has shown that the effect is more pronounced in the region of space opposite to a bond and is easily visualized by plotting the electrostatic potential over an *iso*-density surface of the molecule. The region of positive potential is termed a "σ hole"[22] as it is the result of localization of electron density in the inter-nuclear region by formation of a bonding molecular orbital. The effect is thus not exclusive of polar bonds, even homodiatomic molecules such as I_2 feature prominent sigma holes (Figure 1.3).

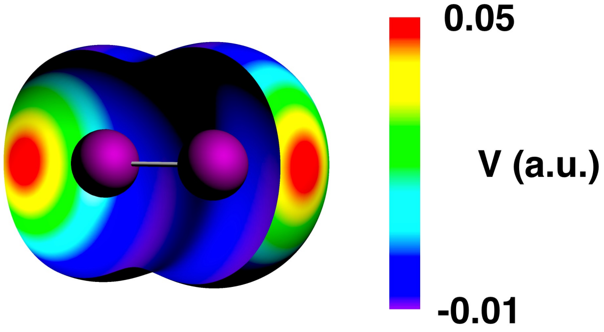

Figure 1.3 DFT (PBE, ZORA, TZ2P) Electrostatic potential of I_2 mapped on the molecular surface defined by the 10^{-3} a.u. contour of the electron density. A section of the surface is hidden for clarity and the sigma-holes are shown in red.

ii) Covalent. The sigma hole exerts a polarizing effect on a neighbouring electron-rich centre, which can be strong enough to cause orbital mixing and sharing of electron density. The heavy element is a particular type of Lewis acid that accepts electrons into the antibonding orbital that arises from the same bond that generates the sigma hole in the first place (Figure 1.4).

Figure 1.4 Pictorial representation of the molecular orbital mixing involved in the interaction of I_2 with a Lewis base.

iii) Dispersion. As the heavy p-block elements are very polarizable, electron correlation manifested in the London dispersion force is a non-negligible contribution to the stabilization of these supramolecular interactions.

Opposing those effects is the Pauli or "steric" repulsion that results from the interaction of electrons in occupied orbitals. Parsed by Energy Decomposition Analysis (EDA), the relative weights of these contributions vary widely from one system to another. Due to the computational expense, Density Functional Theory (DFT) is preferred for computational modelling of molecules with heavy p-block atoms. Although dispersion corrections are now available for selected functionals, accurate evaluation of electron correlation requires methods such as Symmetry-Adapted Perturbation Theory which are only practical for small molecules. Even so, such calculations have identified systems in which dispersion is the dominant contribution.[23]

While there are instances in which calculations have shown the dominant role of the donation of electrons into σ* orbitals, the model that emphasizes the electrostatic contributions has gained high visibility and the term "σ-hole interaction" is frequently used in current literature. However, that denomination and the others above listed highlight the bonding model rather than the physical observation.

This phenomenon appears in the structures of compounds of elements that span most of the p-block, from group 14 to group 18. As the cases of group 17 have received most attention in recent years, the term "halogen bonding" was proposed by analogy to hydrogen bonding interactions as was recently sanctioned by the IUPAC, which formally defined it as a "*net attractive interaction between an electrophilic region associated with a halogen atom in a molecular entity and a nucleophilic region in another, or the same, molecular entity*".[24] By extension, terms such as "tetrel bonding" (group 14),[25,26] "pnictogen bonding" (group 15), "chalcogen bonding" (group 16), "aerogen bonding" (group 18),[27] are frequently used in current literature. However, such proliferation of names can be misleading because all those are just particular cases of a general phenomenon that is observable with elements across the p-block. As early as 1970, N. Alcock proposed the term "secondary bonding"[28] to denote the structures in which heavy main-group atoms appear to engage in attractive interactions beyond their primary (Lewis or hypervalent) valencies. This thesis will use throughout *secondary bonding interaction* (SBI) to refer to such supramolecular interactions centred on heavy p-block elements. The next sections review prominent cases of secondary bonding involving group 14, 15, 16 and 18 elements from recent literature. group 17 is omitted in view of the many reviews recently published.[22,29-32]

1.4.1 Group 14 – Carbon, Silicon, Germanium, Tin, and Lead

In early investigations, the *p* character of the participating orbitals was thought to be critical for strength, consequently secondary interactions centred on group 14 elements (the *tetrels,* Tr) were mostly overlooked because the relevant frontier orbitals feature extensive contribution (hybridization) from the valence *s* orbital. However, Politzer et al.

noted that there is considerable experimental evidence and computational data that show atoms of the group 14 elements acting as Lewis acid centres towards bases. In fact, the initial addition step in the classical SN_2 nucleophilic substitution mechanism would be an example, albeit not a stable one. Similar to halogen bonding, the strength of such interaction increases with the atomic number of the element in the order C < Si < Ge < Pb.[33,34]

A number of studies of group-14 SBIs have focused on theoretical studies of binary complexes with electron-rich groups, applying the σ-hole model. Bauzá and Frontera conducted an extensive survey of crystal structures in the Cambridge Structural Database (CSD) that contain short contacts between anions and group-14 atoms,[25,26,35] this section highlights their most recent findings.

The Pb(II) complexes of N’-(phenyl(pyridin-2-yl)methylene-isonicotinohydrazine show that the Pb···N secondary bond is important in stabilizing the overall architecture.[36] (Figure 1.5) Supplementary topological analysis of the electron density confirmed the existence of a σ-hole at the Pb centre.[36,37] The stability of the Pb-centred bis-pyridyl hydrazone complex[38] arises from the cooperativity of tetrel SBIs and covalent bonding. Computational and experimental evidence of the influence of the carbon-centred SBIs on NMR parameters in the solid state has been reported.[39]

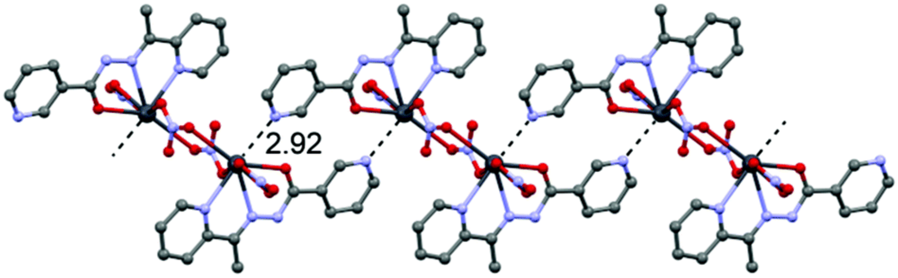

Figure 1.5 Packing in the crystal of the Pb(II) complex of 2-acetyl-pyridyl-nicotinoylhydrazone. Intermolecular Pb···N SBI are highlighted with dashed lines and the distance is shown in Å. Reproduced with permission from reference 36.

Among the group-14 atoms, carbon is the least studied element due to its small size and lowest polarizability within the family. However, the crystal structure of 1,2,3,3,-tetracyanocyclopropane revealed that multiple C···N bonding interactions are present and their distances range from 3.02 to 3.17 Å[35] (Cf. Σr_{vdW} = 3.25 Å).

1.4.2 Group 15 – Phosphorus, Arsenic, Antimony, and Bismuth

Similar to other σ-hole interactions, interactions centred on group-15 elements (the pnictogens, Pn) have been reported in the literature for several decades, but are receiving more attention. Monomeric units in the dianionic complexes are linked to neighbouring molecules through Pn···S SBIs (Pn = Sb, Bi)[40] (Figure 1.6).

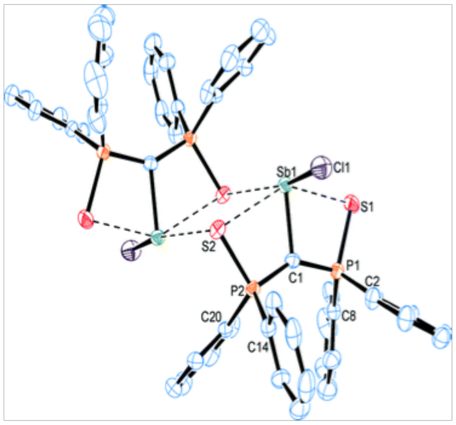

Figure 1.6 30% Displacement ellipsoid ORTEP plot for $\{SbCl[C(Ph_2PS)_2]\}_2{\cdot}C_4H_8O$. Hydrogen atoms of phenyl groups have been omitted for clarity. The lattice THF molecule is not shown. Reproduced with permission from reference 40.

A recent computational study showed that the intramolecular P···N interactions in 8-phosphinonapthalen-1-amine derivatives can be strengthened upon substitution of H atoms by electron withdrawing groups on phosphorus.[41] In the case of isocyano derivatives, analysis of the Electron Localization Function (ELF) highlighted the attraction of the nitrogen lone pair towards the P-CN σ-hole. The use of organic thiol-based ligands with As, Sb, Pb to explore the pnictogen-centred SBIs with halogens, chalcogen ethers and aryl-π electrons has been documented over the two last decades.[42-45] One notable example is an antimony centred supramolecular structure stabilized by Sb···Cl, Sb···Br and Sb···Cπ SBIs.[46]

1.4.3 Group 16 – Oxygen, Sulfur, Selenium, and Tellurium

As in the pnictogens case, supramolecular interactions centred on group-16 elements (G16, the chalcogens, Ch) are subject of increasing interest in current literature. This section reviews the most significant recent developments in chalcogen-centred SBIs. Only the interactions with interatomic distances that clearly are shorter than sum of van der Waals radii are included in this section. Special attention is given to the two families of compounds that best illustrate the abilities of G16 SBIs to control supramolecular structure and properties: the dichalcogenaalkynes and 1,2,5-chalcogenadiazoles.

Several theoretical studies have been concerned with bimolecular complexes held by group 16 SBIs. The analyses have included EDA and AIM methods for combinations that include:

- $D(H)S\cdots F\text{-}CH_3$ (D= H, F, Cl, OH, OCH_3, NH_2, $NHCH_3$, NO_2, CN)[47] in which the $S\cdots F$ binding energy strongly depends on D and the electrostatic and exchange energy are dominant components to these interactions.
- $(CH_3)_2Ch1\cdots Ch2(Z)CH_3$ (Ch1= O, S, Se, Te; Ch2= O, Se, Te; Z= CH_3, $C\equiv CH$, CN).[23,48] In this case, SBI strength increases with the polarizability of the chalcogen centre and the electron withdrawing ability of Z. With the addition of the electron withdrawing groups to O, the electrostatic interaction becomes more attractive whereas the polarization and dispersion components remain unchanged. For the heavier chalcogens, the electrostatic component becomes more repulsive as the polarization and dispersion effects become stronger.

- Y_2Ch1=Ch2 and Ch2=Ch1Y_2 (Y= H, F, CH_3; Ch1= O, S, Se; Ch2= O, S) for which Atoms in Molecules (AIM) analysis showed that the Ch1···Ch2 interaction actually is a highly polarized σ-bond.[49]
- F_2CSe and a wide range of bases (N_2, NCH, NH_3, $NHCH_2$, NCLi, $N(CH_3)_3$ (Scheme 1.1). Here the SBI is strongest for sp^2 hybridized $NHCH_2$ and weakest for *sp* hybridized NCH. The dispersion contribution is dominant in the N_2 complex.[50]
- Ch=C=S or Y_2C=S (Y = F, Cl) with singlet H_2C: which only display a weak S···C SBI mainly stabilized by electrostatic contributions.[51]
- Complexes of ChO_3 (Ch= S, Se) with electron-donating chalcogen bases ChHD (D=H, Cl, Br, CCH, NC, OH, OCH_3) in which the SBI energies range from -4.4 to -12.1 kcal mol^{-1} and their stability is governed by electrostatic effects. Modelling of the ternary HCN···ChO_3···ChHX complexes revealed competition between the Ch···N and the Ch···Ch SBIs.[52]

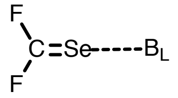

B_L = N_2, NCH, NH_3, $NHCH_2$, NCLi, $N(CH_3)_3$

Scheme 1.1 Binary complexes of CF_2Se with a variety of electron donor molecules.

The solution NMR studies of organo-ditellurides, R-Te-Te-R (R= 4-$CH_3C_6H_4$, 2—$(CH_3)_2NCH_2C_6H_4$, $C(Si(CH_3)_2C_6H_5)_3$) show that the ^{125}Te chemical shift is very sensitive to environmental conditions. Once solvent effects and diamagnetic susceptibility are accounted for, a small but measurable dependence on concentration for the non-hindered molecules can be attributed to intermolecular association through SBIs.[53]

The SBIs in $[(ChPR_2)_2N][(TePR'_2)_2N]$ (Ch=S, Se, Te; R= ^{t}Bu, R'=^{i}Pr) were structurally and computationally examined. The observed trend is that as the Te-Te bond length in the cation decreases, the strength of the Ch···Te secondary bond increases. The stability of the interaction was attributed to electron donation from the anion into the σ*(Te-Te) of the cation.[54]

The reaction of isocyanide-palladium(II) complex with 1,3-thiazole- and 1,3,4-thiadiazole-2 amine derivatives afforded a mixture of two regioisomeric binuclear diaminocarbene Pd(II) complexes.[55] In the case of 1,3-thiazole-2-amines, the thermodynamically controlled isomer features S···N SBIs and S···Cl for the kinetically controlled isomer (Figure 1.7).[55] In the zinc(II) complex of 1,3-diaminopropane, $[Zn(Dap)(NCS)_2][Zn(Dap)\ (NCS)_2]_3$ the trivalent sulfur centre is stabilized by hydrogen bonds and S···N SBIs.[56]

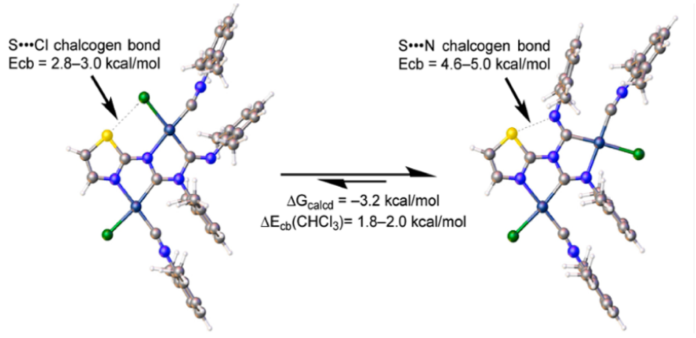

Figure 1.7 Two distinct types of G16 SBIs observed in the regioisomerization of a binuclear diaminocarbene Pd(II) complex. Reproduced with permission from reference 55.

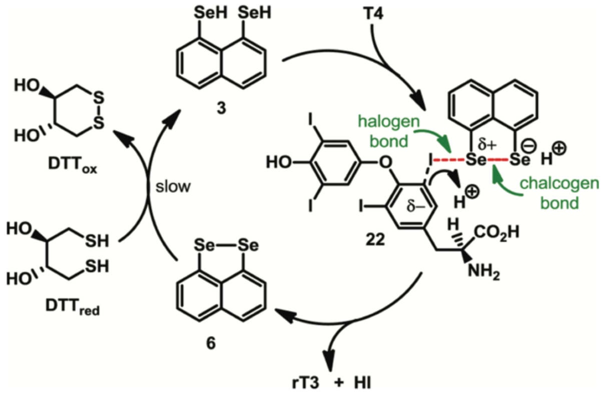

Figure 1.8 SBIs postulated in the mechanism of regioselective deiodination of thyroxine. Reproduced with permission from reference 57.

A naphthylene diselenol was shown to mimic the deiodination function of thyroxine more efficiently than the analogous dithiols or a thiol-selenol pair. Mechanistic studies suggest that formation of I···Se and Se···Se SBIs is critical to the enhanced activity of the molecule (Figure 1.8)[57]

Anion binding of dithieno[3,2-b;2’3’-d]thiophenes (DTTs) derivatives was experimentally and theoretically explored. With various substituent groups on the sulfur heterocycle, the transport activities were monitored in large unilamellar vesicles. The cyano derivative features the deepest σ-hole, and showed the most efficient anion binding in solution and anion transport across lipid bilayers.[58] Interactions of electron deficient perfluorinated 2,5-diaryl tellurophene derivatives with anions such as bromide, nitrate, benzoate and toluenesulfonate were probed by UV-vis spectroscopy. Bis(perfluoroaryl) tellurophene solely participates in an anion-arene interaction whereas the ethylene bridged derivative displays Te···Cl SBIs.[59]

1.4.3.1 Dichalcogenaalkynes

Four different tubular structures containing chalcogen centres have been synthesized and characterized by X-ray crystallography (Figure 1.9). The sulfur containing 25-membered ring is arranged in a helical pattern with a short S···S SBI (3.52 Å) and its cavity is large enough to include hexanes.[60] Other tubular structures containing S and Se cyclohexaynes led to even larger cavities that are also stabilized by Ch···Ch SBIs.[61] Recrystallization of these compounds in toluene and hexanes yields similar structures with different intertubular Ch···Ch distances. The 2,7-ditelluraocta-3,5-diyne molecules is heavily dominated by zigzag Te···Te SBIs, which forms a rectangular cavity that is large enough for potential host-guest chemistry.[60] Rigid tetrachalcogenadiyne structures consist of sulfur and selenium centres stabilized by short Ch···Ch (Ch= S, Se) SBIs and other minor directional forces such as π-π stacking and C-H···donor interactions.[60,62] A variety of macrocycles based on 1,4-dichalcogeno-1,3-butadiynes linked by n-alkane chains have been structurally characterized. Due to the rigid 1,3-butadiyne rods, structures are flexible enough to host polar and nonpolar solvent molecules.

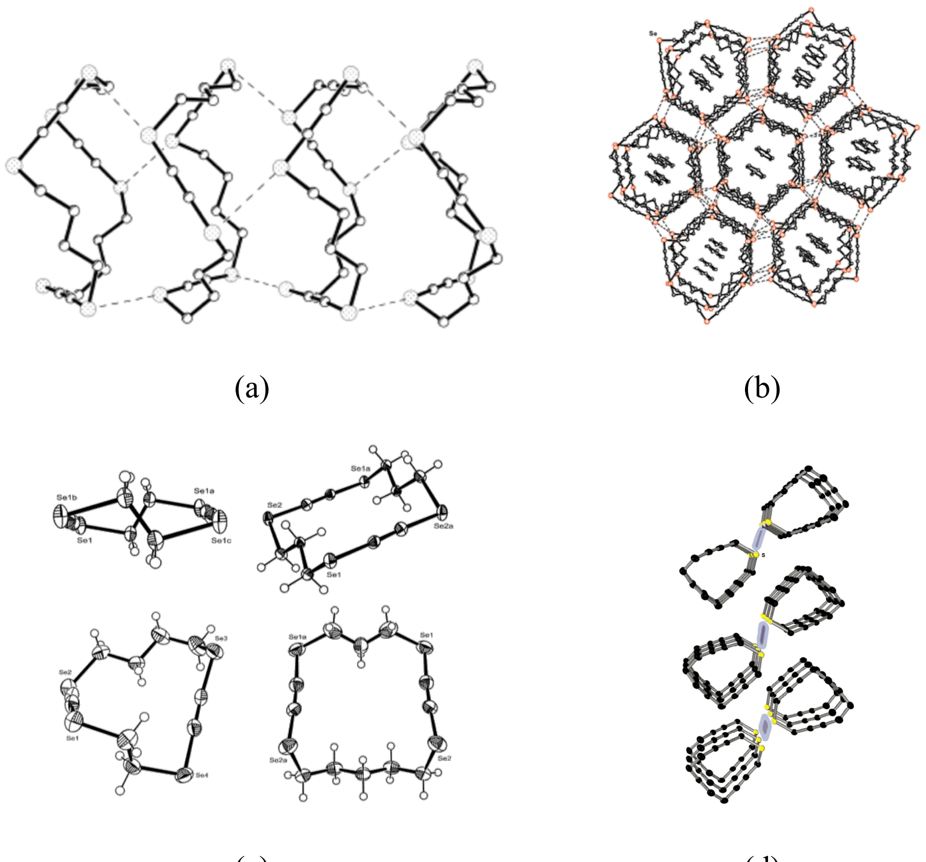

(a) (b)

(c) (d)

Figure 1.9 a) Side view of a 24-membered ring composed of 3 S-C≡C-S units featuring S···S SBIs; b) Top view of 1,6,11,16,21,26-Hexaselenacyclotriaconta-2,4,-12,14,22,24-hexayne highlighting Se···Se distances and included toluene; c) Tetraselenacycloalkadiynes d) columnar structure of 1-thiacyclododeca-3,10-diyne featuring S···S SBIs. Figures reproduced with permission from references 60, 61,63, and 62 .

1.4.3.2 1,2,5-Chalcogenadiazoles

The crystal structures of molecules that contain the 1,2,5-chalcogenadiazole ring (**1-3**) are of special interest because they frequently display a *supramolecular synthon* made by two molecules associated through two antiparallel Ch···N SBIs defining a virtual four-membered ring. This structural motif will be denoted from this point on as [Ch-N]$_2$. Repetition of the [Ch-N]$_2$ synthons leads to supramolecular ribbon-polymers in the solid state (Scheme 1.2).[64] A survey of the crystal structures of tellurium compounds that display intermolecular interactions classified the most recurrent supramolecular synthons and, using the Te···N SBI distance as a gauge, established that the [Te-N]$_2$ supramolecular synthon is especially strong.[65]

1a Ch = S
1b Ch = Se
1c Ch = Te

1a$_2$ Ch = S
1b$_2$ Ch = Se
1c$_2$ Ch = Te

1a$_\infty$ Ch = S
1b$_\infty$ Ch = Se
1c$_\infty$ Ch = Te

Scheme 1.2 1,2,5-Chalcogenadiazoles, and their aggregates (dimers and ribbon polymers). The [Ch-N]$_2$ supramolecular synthon is the four-membered ring in the dimers.

The telluradiazoles usually display the shortest intermolecular Ch···N distances (2.77 Å Cf. Σr_{vdw}= 3.61 Å) in the solid state. A potential energy surface for the dimer of 1,2,5-telluradiazole (**1c$_2$**) (Figure 1.10) was modeled using Density Functional Theory to examine the bonding contributions and evaluate the strength of the [Ch-N]$_2$ supramolecular synthon. A well-defined minimum in the surface indicates the formation of a stable dimer with a stabilizing energy of 50 kJ mol^{-1} in the tellurium case. Along the d$_2$ axis two large potential barriers prevent the lateral displacement of the rings.[66] No such potential barrier was observed along the d$_1$ axis, which would be consistent with the possibility of error selfcorrection. These observations highlighted the potential of telluradiazoles as promising supramolecular building blocks due to the formation of strong and directional supramolecular synthons. The calculated interaction energies for the selenadiazole (**1b$_2$**) and thiadiazole (**1a$_2$**) heterocycles are smaller and the corresponding SBI distances are larger. In apparent agreement, the derivatives of these heterocycles are less frequently found to associate in their crystal structures.

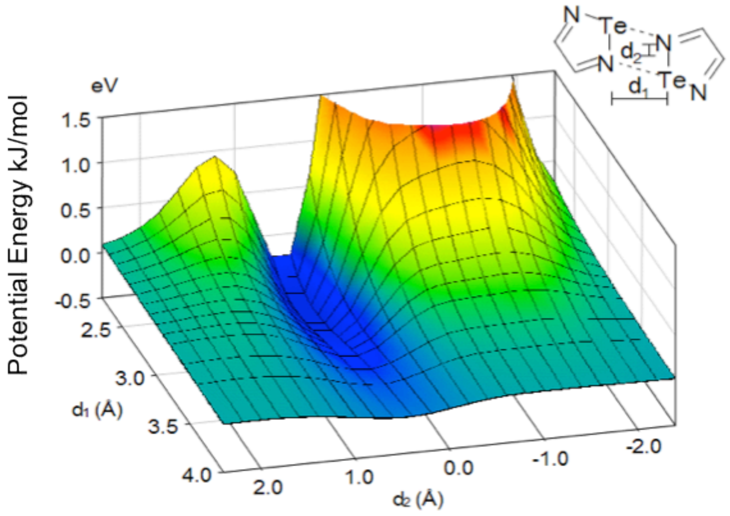

Figure 1.10 Potential energy surface for the in-plane distortion of the [Te-N]$_2$ supramolecular synthon. Reproduced with permission from reference 66.

The study showed that the Ch···N SBIs that link the chalcogenadiazoles result from a balance of electrostatic attraction of opposite partial charges, repulsive interactions between electrons in occupied orbitals, the donation of the nitrogen lone pairs into chalcogen-nitrogen σ* orbitals. However, the contribution of dispersion could not be evaluated at the time of that study. Overall, these molecules are double Lewis acid-base pairs; DFT studies of their acidity and basicity is discussed in Chapter 3.

The effect of steric repulsion on the stability of the Te···N SBIs was subject of a computational and experimental study. DFT analysis predicted that the Te···N secondary bonds in two derivatives of 1,2,5-telluradiazoles: benzo-2,1,3-telluradiazole (**3c**) and 3,6-dibromobenzo-2,1,3-telluradiazole (**4**) are strong enough to overcome the aromatic hydrogen and bromine repulsions. Crystal structures were consistent with the predictions in that the **3c** forms infinite ribbons chains in the solid state while the dibromo-substituted derivative was isolated as discrete dimers.[67] The first benzotelluradiazole isolated, **7**, is also dimeric.[68] The dibromo derivative and its DMSO adduct feature other SBIs between the tellurium atom and oxygen of the DMSO and a bromine atom of a neighbouring molecule.[69]

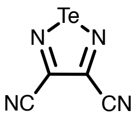

2

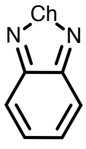

3a = S
3b = Se
3c = Te

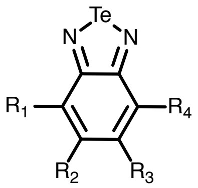

4 $R_{1,4}$= Br; $R_{2,3}$= H
5 $R_{1,2,3,4}$= F
6 $R_{1,4}$= Cl; $R_{2,3}$= H
7 $R_{1,3}$= ^{t}Bu; $R_{2,4}$= H

In pursuit of controlling the association by capping the nitrogen atoms with a Lewis acid, both 2:1 (**9**) and 1:1 triphenylborane (**8a**) adducts were synthesized and structurally characterized.[70] The disubstituted adduct consists (**9**) of one molecule of benzo-telluradiazole with BPh_3 attached to each nitrogen atom. No Te···N SBIs are formed as the phenyl rings hinder access to the chalcogen. However, the chalcogen is in close proximity to the centroids of the phenyl rings (3.1188(2) and 3.1311(2) Å, indicating that the electrophilicity of the chalcogen increases upon binding of the borane to nitrogen.

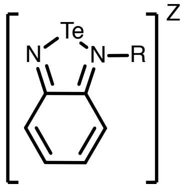

8

a R= BPh_3; Z= 0
b R= CH_3; Z= +1

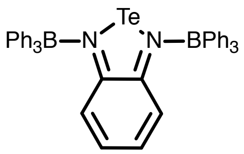

9

The effect of steric hindrance on the formation of SBIs was further studied by two polymorphs of 4,5,6,7-tetrafluorobenzo-2,1,3-telluradiazole (**5**) resulted from two types of distortions of the $[Te\text{-}N]_2$ SBI due to the steric interaction between neighbouring fluorine atoms.[71] The yellow β polymorph consists of molecules arranged in ribbon chains with centrosymmetric Te···N SBIs in which Te···N distances are 2.75(1) and 2.884(6) A. The β phase is metastable, and it switches to the thermodynamically preferred structure upon heating. In the red α structure, all the Te···N secondary bonds are distorted and have equal distances (Figure 1.11). This distortion arises from in-plane motion and the rotation of the rings with respect to each other and each of these on its own leads to removal of the inversion centre of the $[Te\text{-}N]_2$ SBIs. Such system is a remarkable example to illustrate the substantial effect that SBIs have on the macroscopic properties of a material.

Inspired by the α phase of **5**, Cozzolino et al. sought a system with distorted Te···N SBIs that are propagated through the lattice to create a noncentrosymmetric crystal with second-order nonlinear optical properties.[72] For this, the steric repulsion between molecules would have to be enough to induce the non-centrosymmetric distortion but not so large as to prevent association. This concept was demonstrated with 3,4-dicyano-1,2,5-telluradiazole (**2**) and 5,6-dichlorobenzo-2,1,3-telluradiazole (**6**). Their second harmonic generation efficiency confirmed the presence of a second-order NLO response that arise from their noncentrosymmetric crystal lattice.

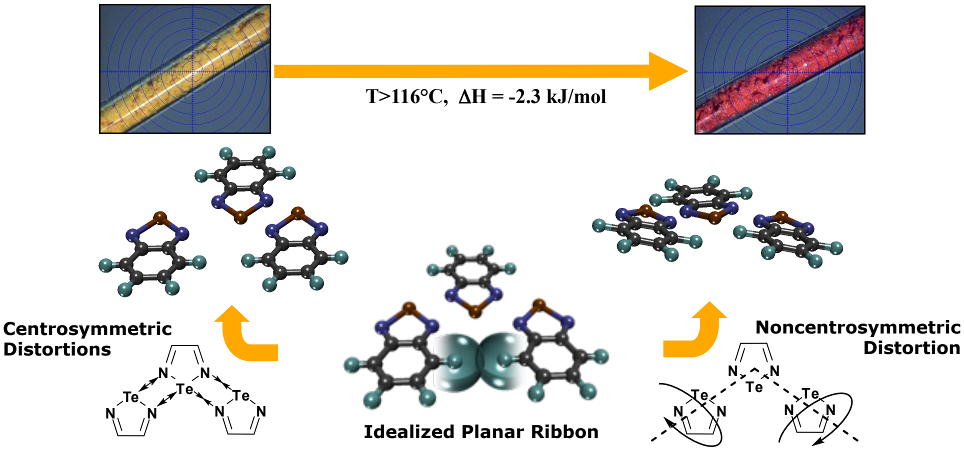

Figure 1.11 Two chromotropic crystalline phases (α red, β yellow) of 4,5,6,7-tetrafluorobenzo-2,1,3-telluradiazole (**5**). Reproduced with permission from reference 71.

Cozzolino et al. also used telluradiazoles to search for evidence of Te···N SBIs in the gas phase. UV photoelectron spectroscopy was unable to detect aggregation, only individual molecules were observed. However, the electrospray mass spectrum acquired from benzo-2,1,3-chalcogenadiazoles (**3**) under UV-LDI conditions featured aggregates of singly protonated ion of the parent heterocycles. Details of the DFT-D studies used to identify the most stable structures of such aggregates are discussed in Chapter 3.[73]

In later studies, Zibarev prepared coordination complexes of **2** with F^-, I^-, PhS^-. Both experimental and computational studies show that the E-X bonds are donor-acceptor interactions with distances much shorter than the sum of van der Waals radii.[74]

Investigation of the redox properties of the N-methyl- benzo-2,1,3-telluradiazolium (**8b**) cation showed an unusual behavior which was attributed to the association of the molecules in solution.[75] Recently, Taylor et al. used UV-vis absorption and ^1H NMR spectroscopies to probe the solution-phase thermodynamics of bonding interactions between **3c** and Lewis bases (Cl^-, Br^-, I^-, NO_3^- and quinuclidine). The strength of SBIs was dependent on the functional groups on the aromatic ring as well as the solvent. Binding constants determined in THF were in agreement with calculated values (B97-D3).[76] A unique trimer featuring the $[S\text{-}N]_3$ supramolecular synthon has been observed in the co-crystal of triptycenetris(thiadiazole) and C_{60}.[77]

1.4.4 Group 18

$Xe\cdots F$ SBIs were identified in the salt of $[XeOXeOXe][\mu\text{-}F(ReO_2F_3)_2]_2$[78] (Figure 1.12). X-ray crystallographic data revealed contacts longer than the sum of van der Waals radii and the supplementary computational results showed that the F atoms donate electron density to a σ-hole on the Xe atoms. Other structures such as $(OsO_3F_2)_2{\cdot}2(XeOF_4)$[79], $[H_5F_4][SbF_6].2[XeF_3{\cdot}HF][Sb_2F_{11}]$[80], $[XeF_3{\cdot}HF][Sb_2F_{11}]$[80], $[XeF_3][SbF_6]$[80], $[XeF][Bi_2F_{11}]$[81] $[XeF][BiF_6]$[81], and $[XeF][SbF_6]$[80,81] display similar $Xe\cdots F$ SBIs.

$Xe\cdots N$ SBIs have also been detected in the structures of several compounds, including $[F_4SNXeNSF_3][AsF_6]$[82], $[C_6F_5XeNCCH_3][BY_4]$ (Y= CN, CF_3, C_6F_5),[83] $O_3XeNCCH_3$ (Figure 1.12)[84], $O_3Xe(NCCH_3)_2$[84], $O_3XeNCCH_2CH_3$[84], and $O_3Xe(NCCH_2CH_3)_2$.[84] The positive electrostatic potential of the alkyl-nitrile adducts of XeO_3 is located on Xe trans to the Xe-O bond and further topological analysis was carried out to show the donation of the lone pair of the N atom to the Xe σ-holes.[84] All three phases of XeO_3 also display the Xe···O secondary bonds.

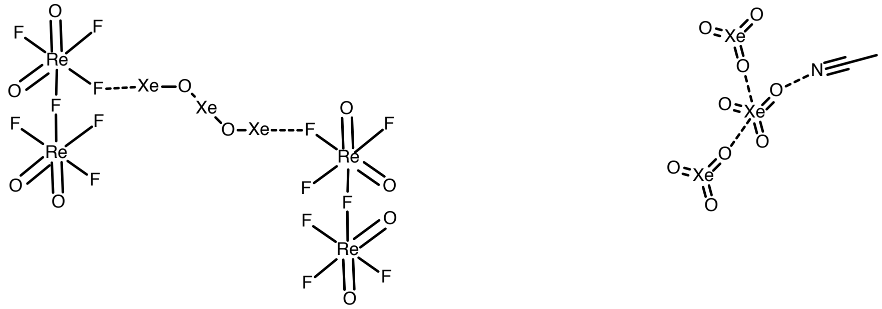

(a) (b)

Figure 1.12 Structures of (a) $[\mu\text{-}F(ReO_2F_3)_2]_2[XeOXeOXe]$ (b) $O_3XeNCCH_3$

Kr-centred SBIs in the $[HCN\text{-}KrF][AsF_6]$ salt has been characterized by low-temperature Raman spectroscopy and NMR (^{1}H, ^{13}C, ^{15}N and ^{19}F) spectroscopy.[85] Further theoretical investigation of the Kr···N secondary bond in the same salt. A contour map of the charge density displays a planarity for the Kr···N surface that resembles a characteristic feature of hydrogen bonding.[86]

1.5 Scope and Overview of the Thesis

The versatility of tellurium-centred SBIs is well exemplified by the derivatives of the 1,2,5-telluradiazole ring. However, their moisture sensitivity hinders more widespread applications. The selenium analogues are more stable, to the point that some can exist in aqueous solution. However, Se···N SBIs are much weaker than in the tellurium case and intermolecular association is much less common in the crystal structures of selenadiazoles.

The goals of the research described in this thesis are to:

1. Update the current understanding of the chalcogen-centred SBIs to include the

contribution of dispersion forces.

2. Establish a method to strengthen the supramolecular interactions of the selenadiazole heterocycles and identify suitable targets for synthesis.
3. Establish efficient and flexible methods for their synthesis.
4. Provide an understanding of their chemical properties including their ability to associate with other species such as anions, and solvents.
5. Define protocols for application of those compounds as supramolecular building blocks.

Based on observations such as the structures of the triphenylborane adduct of benzo-telluradiazole, the initial hypothesis was that electron withdrawing groups on one nitrogen atom of the selenadiazole heterocycle could achieve the desired effect on Se···N SBIs.

The findings of these investigations are arranged as follows. Chapter 2 compiles all experimental and computational details. Detailed computational studies of Lewis acidity and basicity of 1,2,5-chalcogenadiazoles are presented in Chapter 3. Chapter 4 presents synthetic and computational investigations of borane adducts of benzo-2,1,3-selenadiazolium cations. The synthesis and magnetic properties of coordination polymers of selenadiazoles are provided in Chapter 5. Chapter 6 discusses an effective synthetic method applicable to benzo-2,1,3-selenadiazolium cations. Chapter 7 presents the structural studies of dications bridged by organic molecules. Chapter 8 provides details of synthetic attempts to make foldamers based on Se···N SBIs. Chapter 9 provides the details of X-ray crystallographic work done for various *iso*-tellurazole *N*-oxides. Finally, Chapter 10 summarizes the significance of these findings and offers some suggestions for future work.

Chapter 2. Experimental

2.1 Instrumental Methods

2.1.1 Nuclear Magnetic Resonance Spectroscopy

Sample Preparation

All samples were prepared by dissolving approximately 15 mg of the compound in 0.5 mL of deuterated solvent.

Data Acquisition

The ^{19}F NMR spectra were acquired on a Bruker Avance 200 (200.13 MHz) spectrometer at ambient temperature. Chemical shifts were recorded using $CFCl_3$ as a reference for ^{19}F samples.

A Bruker 600 (600.13 MHz) spectrometer was used to acquire the high-field nuclear magnetic resonance spectra. A Bruker 5-mm broad-band inverse probe was used to acquire ^{1}H spectra and a 10-mm broad-band probe for the ^{13}C and ^{77}Se spectra. Chemical shifts are reported in δ values (parts per million) with respect to the resonances of tetramethylsilane for ^{1}H and ^{13}C and with respect to the resonance of Me_2Se (measured from a secondary reference of Ph_2Se, $\delta = 463$ ppm) for the chemical shift of ^{77}Se. Unless otherwise indicated, the spectra were obtained at 303 K. All data were processed using Bruker's TopSpin™ v2.1 software package.

2.1.2 Mass Spectrometry

Sample Preparation

All samples were dissolved in chloroform prior to introduction into the mass spectrometer.

Data Acquisition

Low- and high-resolution electrospray spectral analyses were performed using a Micromass GCT spectrometer and a Micromass Quattro Ultima for electron ionization spectra. In each case, the sample was introduced into the ionization chamber in a shortened borosilicate glass capillary on a probe rod. The samples were heated and the temperature range that displayed the most intense parent ion peaks was used for acquisition. A 70 eV electron stream ionized the sample and the positively charged ions were identified by a time-of-flight detector.

2.1.3 Single-crystal X-ray Diffraction

Sample Preparation

Samples were handled at room temperature coated in Paratone-n oil. Suitable crystals were mounted on a nylon loop.

Data Acquisition

X-ray data were collected on a Bruker SMART APEX II diffractometer equipped with an APEX II 4K CCD area detector, using either a graphite monochromator or a Bruker Triumph curved crystal monochromator Mo-Kα radiation (λ=0.71073) at 100(2) K.

Data Treatment

Once the data collection was completed, the structures were solved using the SHELXTL suite of programs and most structures were refined by full-matrix least square of all F^2 values with the WinGX package. The data was empirically corrected for absorption and other effects using SADABS.[87] The non-H atoms were refined anisotropically, while H atoms were constrained to idealized positions using appropriate riding models. Molecular graphics were produced using the Cambridge Crystallographic Data Centre's Mercury package versions 2.0-3.9.

2.1.4 IR Spectroscopy

Sample Preparation

Samples were compressed as polyethylene pellets and placed in a nitrogen purged sample housing. Samples of **20** were measured neat using the Bio-Rad FTS40 IR spectrometer.

Data Acquisition

The background spectra were recorded and subtracted from each spectrum acquisition. Each spectrum was then required with a resolution of 4 cm^{-1} in the region of 4000-400 cm^{-1} and were normalized using GRAMS/AI.

2.1.5 UV-Vis Spectroscopy

The salts were dissolved in buffer solutions at pH 2, 4, 7, and 11. Measurements were performed on a Cary 50 UV-vis spectrometer using Varian's Cary Win-UV software package. Additional processing was carried out using the GramsAI suite.

2.1.6 Magnetic Susceptibility

DC magnetization measurements were performed in a 100 Oe field over the temperature range of 2-300 K using a Quantum Design Magnetic Properties Measurement System with a 5.5 T magnet. The magnetic parameters and their standard errors were obtained by fitting the nonlinear models to experimental data before antiferromagnetic ordering with Mathematica® 8.0.4.0.

2.1.7 Elemental Analysis

Combustion elemental analyses were carried out by the London Metropolitan University Elemental Analysis Service (London, United Kingdom). Elemental analysis is not provided in the case of compounds for which HR-MS is an appropriate alternative or the samples were too unstable or hygroscopic to permit accurate measurement.

2.1.8 Melting Point

Melting points were measured on a Thomas-Hoover melting point apparatus and are reported uncorrected.

2.2 Computational Details

Density Functional Theory calculations were performed using the Software for Chemistry & Materials Amsterdam Density Functional package versions 2006.02 through 2017.01. The adiabatic local density approximation (ALDA) was used for the exchange-correlation kernel, and the differentiated static LDA expression was used with the Vosko-Wilk-Nusair parameterization. The calculations of model geometries were gradient corrected with the exchange and correlation functionals of the gradient correction proposed by Perdew and Wang (PW91).[105] Preliminary geometry optimizations were performed using a double-ζ basis set with frozen cores corresponding to the configuration of the preceding noble gas and no polarization functions; the resulting structures were refined by using a triple-all-electron basis set with one polarization function and applying the zeroth-order relativistic approximation (ZORA) with the specially adapted basis sets. The effect of dispersion forces was examined with the use of the Perdew-Burke-Ernzerhoff (PBE)[104,106] functional supplemented by Grimme's D3 correction.[113]

2.3 Materials and Methods

The manipulation of air-sensitive materials was carried out in a glovebox or standard Schlenk techniques under atmospheres of anhydrous nitrogen or argon. All glassware was dried at 200 ºC in an oven. Organic solvents were purified either by distillation over the appropriate dehydrating agents under nitrogen or using an Innovative Technologies purification system.

The following compounds were prepared following literature methods: benzo-2,1,3-selenadiazole[88], N-isopropyl 1,2,-phenyleneidamine, N-^{t}butyl 1,2-phenylendiamine, 1,2-di(o-nitrophenylamine)ethane[89], N,N'-bis(2-nitrophenyl)cyclohexane-1,2-diamine[90], 1-(α,β)-O-methyl-2-deoxy-D-ribose[91], 1-(α,β)-O-methyl-3,5-di-(O-p-toluoyl)-2-deoxy-D-ribose[92], and 1-(α)-chloro-3,5,-di-(O-p-toluoyl)2-deoxy-D-ribose[93].

The following compounds were used as received from the commercial suppliers: selenium dioxide (Sigma Aldrich), selenous acid (Sigma Aldrich), triphenylborane (Strem), boron trichloride (Sigma Aldrich), boron trifluoride etherate (Aldrich), boron tribromide (Sigma Aldrich), trifluoromethanesulfonic acid (VWR), cobaltous chloride hexahydrate (Anachemica), nickel chloride hexahydrate (Fischer), manganese chloride tetrahydrate (Merck), cadmium chloride (Fischer), iron chloride (Fischer), iodomethane (JT Baker), 1-fluoro-2-nitrobenzene (VWR), N-methyl-1,2-phenylenediamine (Sigma Aldrich), 10% Pd/C catalyst (Sigma Aldrich), hydrogen gas (Air Liquide), HCl (Sigma Aldrich), sodium iodide (JT Baker), sodium carbonate (EMD), $NOBF_4$ (VWR), fluoroboric acid (BDH Laboratory), 2-deoxy-D-ribose (ChemImpex), p-toluoyl chloride (Alpha Aesar), sodium suflate (Caledon). Deuterated solvents d_6-dimethyl sulfoxide (Aldrich), d_2-dichloromethane (Sigma Aldrich), $CDCl_3$ (Cambridge Isotope Laboratories), D_2O (Cambridge Isotope Laboratories). All organic solvents such as acetonitrile, dichloromethane, methanol, ethanol, chloroform, toluene, and THF were stored under nitrogen following distillation from molecular sieves (4 Å). Ortho-phenylenediamine (Aldrich) was recrystallized from ethanol.

2.4 Syntheses

($C_6H_4N(B(C_6H_5)_3NSe$) (12a): Freshly sublimed **3b** (0.1g, 0.54 mmol) was mixed with triphenylborane (0.13 g, 0.54 mmol) in anhydrous toluene (5 mL). The solution immediately became yellow upon mixing and was refluxed for 24h. After removing the solvent under vacuum, yellow microcrystals formed and were decanted. ^{1}H NMR (CD_2Cl_2, 600 MHz): δ (ppm) 7.84 (m, 1H, Ar-H), 7.47 (m, 1H, Ar-H). ^{13}C NMR (CD_2Cl_2, 600 MHz): δ (ppm) 137.83, 135.40, 131.19, 130.87, 128.86, 128.45 (Ar-C), 127.96, 127.49 123.96 ($B(C_6H_5)_3$). ^{1}H-^{77}Se HMBC NMR (CD_2Cl_2, 600 MHz): (δ ppm) 1501.01.

($C_6H_4N(BX_3)NSe$) (12b-d): The appropriate amount of BX_3 (X= Ph_3, F, Cl, Br) (0.27 mmol, 1 equiv.) was added to a solution of **3b** (0.27 mmol, 1 equiv.) dissolved in anhydrous dichloromethane under an inert atmosphere. The solution immediately became yellow and yielded crystals which were isolated for X-ray crystallography. **12b** ^{1}H NMR (CD_2Cl_2, 500 MHz): 7.84 (m, 1H, Ar-H), 7.55 (m, 1H Ar-H). ^{19}F NMR (CD_2Cl_2, 200 MHz): (δ ppm) -146 (s, 1F, B-F), -148 (s, 1F, B-F). ^{13}C NMR (CD_2Cl_2, 600 MHz): (δ ppm)

137.98 132.79, 126.49, 121.14 (Ar-C). **12c** ^{1}H NMR (CD_2Cl_2, 500 MHz): (δ ppm) 8.36 (s, 1H, Ar-H), 7.92 (s, 2H, Ar-H). 7.73 (s, 1H, Ar-H). ^{1}H-^{77}Se HMBC NMR (CD_2Cl_2, 600 MHz): (δ ppm) 1464.2. **12d** ^{1}H NMR (CD_2Cl_2, 500 MHz): (δ ppm) 8.61 (m, 1H, Ar-H), 8.06 (m, 1H, Ar-H), 7.22 (m, 1H, Ar-H), 7.16 (m, 1H, Ar-H). ^{13}C NMR (CD_2Cl_2, 500 MHz): (δ ppm) 136.94, 134.78, 129.35, 128.53, 134.78, 123.60 (Ar-C).

($C_6H_4N(BCl_3)N(BCl_3)Se$) (**13**): A solution of **3b** (0.125 mmol, 2 equiv.) in anhydrous dichloromethane was added to a solution of BCl_3 (0.25 mmol, 2 equiv.) in a dropwise fashion. Upon mixing the two reagents, the solution turned orange with crystalline materials which were isolated for X-ray crystallography. ^{1}H NMR (CD_2Cl_2, 500 MHz): (δ ppm) 8.44 (m, 1H, Ar-H), 8.05 (m, 1H, Ar-H). ^{13}C NMR (CD_2Cl_2, 500 MHz): (δ ppm) 137.83, 122.62 (Ar-C). ^{1}H-^{77}Se HMBC NMR (CD_2Cl_2, 600 MHz): (δ ppm) 1513.2.

[$MCl_2(C_6H_4N_2Se)_2$] (M= Mn, Cd) (**14, 15**) and [$MCl_2(Me_2SO)_2(\mu\text{-}C_6H_4N_2Se)_2$] (**16-18**): In a typical experiment, a solution of the **3b** (0.1 g, 0.5 mmol) in DMSO (0.5 mL) was slowly diffused into a solution of anhydrous MCl_2 (0.5 mmol) in absolute ethanol (0.9 mL). Crystals of the products usually formed over 24 hours and were isolated by vacuum filtration, washed with diethyl ether (5 mL) and dried under nitrogen. The materials obtained in this way were stored and handled under an atmosphere of dry nitrogen. The products are deliquescent, being easily hydrated while exposed to the atmosphere. Multiple attempts to perform combustion analysis of the sampled were thwarted by the sensitivity of the sample. Instead, the purity of the samples, especially those used for magnetic studies, was assessed by comparison of diffraction data obtained from single crystals with those from powders in sealed capillary tubes. Spectroscopic characterization was therefore limited to vibrational spectroscopy.

($C_6H_4N_2Se[C_6H_4NN(CH_3)Se]_2[I]_2$ (3b(19a)$_2$[I]$_2$): Benzo-2,1,3-selenadiazole (0.1 g, 0.547 mol) and iodomethane (0.35 mL, 0.602 mmol) were mixed neat with stirring under nitrogen. The mixture became purple and gave a microcrystalline red powder. Yield 60%. The product was washed with hexanes and dried under vacuum. Crystals suitable for single X-ray diffraction were grown by slow diffusion of the reagents dissolved in ethanol. ^{1}H NMR (d$_6$-DMSO, 600 MHz) (δ ppm): 4.13 (s, 3H, CH_3), 7.54, 7.82, 7.96 (m, 6Hs, Ar-CH) ppm. ^{13}C NMR (d$_6$-DMSO, 600 MHz): (δ ppm) 159.74 156.40 150.622 131.65 126.43 125.88 116.91 (Ar-C) 39.42 (CH_3) ppm.^{77}Se NMR (d$_6$-DMSO, 600 MHz) (δ ppm):1494.0 ($[C_6H_4N(NCH_3)\underline{Se}]^+$), 1529.7 ($C_6H_4N_2\underline{Se}$) ppm. IR (cm^{-1}): 3602 (m), 2854(b), 2341 (m), 2150 (vw), 2018 (w), 1982 (w), 1949 (w), 1812 (w), 1600 (w), 1529 (m), 1515 (m), 1464(sh), 1134 (vw), 1044(m), 905(vw), 730 (sh) 720 (sh). Mp. 148–150 °C (d). E.A. % calcd. for $C_{20}H_{18}I_2N_6Se_3$: C 28.83, H 2.18, N 10.09; found C 28.72, H 2.09, N 9.98.

$[C_6H_4NNCH(CH_3)_2Se]_2I$ ([19a][I]): Method A. A sample of **3b[19a]**$_2$[I]$_2$ (0.02 g, 0.109 mmol) was dissolved in methanol (1.6 mL) with stirring at 42-46 °C. The colour of the solution slowly changed from dark green to bright red. Cooling to room temperature produced red crystals which were recovered by filtration. Yield 17%. Method B. To a solution of N-methyl-phenylenediamine (0.11 mL, 1.023 mmol) and H_2SeO_3 (0.1319 g, 1.023 mmol) in anhydrous ethanol, trifluoroacetic acid (0.07 mL, 1.023 mmol) was added dropwise under nitrogen. The reaction mixture was allowed to stir at room temperature for 20 min, time after which a solution of NaI (0.1533 g, 1.023 mmol) in ethanol (10 mL) was added with vigorous stirring, a dark red solid precipitate formed and was separated by filtration, washed with hexanes, dried under vacuum and stored under nitrogen. Yield 22%. ^{1}H NMR (D_2O, 600MHz): (δ ppm) 4.60 (s, 3H, CH_3), 7.78, 7.96 (m, 4H, Ar-CH) ppm. ^{13}C NMR (d_6-DMSO, 600 MHz): (δ ppm) 156.36, 150.73, 136.53, 129.95, 125.02, 116.46 (Ar-C), 38.35 (CH_3) ppm. ^{77}Se NMR (d_6-DMSO, 600MHz): (δ ppm) 1490.4 ppm. LR ESI-MS: m/z 199.0 (M^+). HR ESI-MS: m/z 198.9774 (M^+) (Cf. calc. for $C_7H_7N_2Se$ 198.9774). IR (cm^{-1}): 3606 (m), 3219 (w), 2913 (s), 2866 (b), 2345 (m), 2018 (w), 1956 (w), 1811(w), 1536 (w), 1470 (m), 1305 (w), 1167 (vw), 1135(m), 807 (w), 744(sh), 730(sh), 720 (sh). UV-Vis λ_{max} = 345 nm, ε = 664.6 L mol^{-1}cm^{-3}. Mp. 184-188 °C (d).

[$C_6H_4N(NCH(CH_3)_2)Se]_2[I]$ ([19b][I]): To a solution of N-isopropyl-benzene-1,2-diamine and H_2SeO_3 in anhydrous ethanol, trifluoroacetic acid was added. The reaction mixture was allowed to stir at room temperature for 20 min under nitrogen. Upon the addition of NaI, the product immediately precipitated. The dark red solid was washed with hexane, dried and stored under a nitrogen atmosphere. Yield 30%. ^{1}H NMR (CD_2Cl_2, 600 MHz): (δ ppm) 7.99 (dd, 1H, J= 6, 12Hz, Ar-CH) 5.60 (sept, J= 6Hz, 1H, NH-CH) 1.87 (d, 6H, J= 7 Hz, CH_3) ppm. ^{13}C NMR (CD_2Cl_2, 600 MHz): (δ ppm) 138.18, 131.42, 125.34, 115.71 (Ar-C) 57.87 (NH-CH), 24.22 (CH_3) ppm. ^{77}Se NMR (d_6-DMSO, 600MHz): (δ ppm) 1459.5 ppm. LR ESI-MS: m/z 227.0 (M^+). HR ESI-MS: m/z 227.0095 (Cf. calc. for $C_9H_{11}N_2Se$ 227.0088). IR (cm^{-1}): 3605 (w), 3374 (m), 2848 (b), 2329 (w), 2010 (vw), 1952 (w) 1980 (vw), 1842 (vw), 1896 (vw), 1809 (vw), 1720 (vw), 1523 (w), 1473 (sh), 1369 (m), 1314 (m), 1176 (sh), 1164 (sh), 1142 (m), 1121 (m), 823 (w), 757 (vs), 730 (vs), 719 (vs). UV-Vis λ_{max} = 343 nm, ε = 428.5 L mol^{-1}cm^{-3}. Mp. 165-168 °C (d).

$[C_6H_4N(NC(CH_3)_3)Se][I]$ ([19c][I]): Using the procedure above described for **[19a]**[I] and **[19b]**[I], the compound was obtained as a dark red crystalline material. ^1H NMR (d_6-DMSO, 600MHz) (δ ppm): 8.30 (d, 1H, Ar-CH) 8.08 (d, 1H, Ar-CH) 7.97 (dd, 1H, Ar-CH) 7.79 (dd, 1H, Ar-CH) 1.97 (9H, $(CH_3)_3$). ^{13}C NMR (d_6-DMSO, 600 MHz): (δ ppm) 158.46 148.03, 136.44, 129.5,1 126.17, 118.40 (Ar-C) 67.28 (N-CH) 29.66 $(CH_3)_3$. ^{77}Se NMR (d_6-DMSO, 600MHz): (δ ppm) 1454.7 ppm. LR ESI-MS: m/z 241.0 (M^+) HR ESI-MS: m/z 241.0248 (M^+) (Cf. calc. for $C_{10}H_{13}N_2Se$ 241.0244). IR (cm^{-1}) 3647 (vw), 3604 (w), 2793 (b), 2340 (w), 2150 (vw), 2108 (w), 1859 (vw), 1602 (w), 1526 (w), 1472 (sh), 1371 (m), 1302 (m), 1180 (w), 1132 (w), 954 (vw), 872 (vw), 844 (vw), 744(sh), 719 (sh). UV-Vis $\lambda_{max} = 330$ nm, $\varepsilon = 282.5$ L $mol^{-1}cm^{-3}$. Mp. 130–132 °C (d).

$[1,2-(C_6H_4N_2Se)_2C_2H_4]X_2$ (20a), $[1,2-(C_6H_4N_2Se)_2C_3H_6]X_2$ **(20b)**, **$[R,R-1,2-C_6H_8(C_6H_4N_2Se)_2]X_2 \cdot H_2O$ (20c) (X= Cl, CF_3SO_3)**: Adapted from the literature procedure[94], a neat reaction mixture of 1-fluoro-2-nitrobenzene (2 equiv.) and appropriate diamine (1 equiv) was stirred vigorously for 1 h at 100°C and kept hot until work-up in order to keep the material molten. The molten mass was then washed with 25 mL ethanol and vacuum filtered (40% yield). Crystals of the nitro compound (1.66 mmol, 1 equiv.) was then dissolved in 30 mL absolute ethanol and Pd/C catalyst 10% (50 mg/mmol) was added to the stirring solution. The reaction was placed under a H_2 atmosphere and was allowed to stir until no starting material was detected by TLC (10% ethyl acetate in hexanes). The final solution was filtered through Celite to remove any precipitate and concentrated under reduced pressure to yield a brown, sticky residue.

a) **X=Cl, (2[20a]$Cl_2 \cdot 8H_2O \cdot HCl$ and [20c]$Cl_2 \cdot H_2O$)**: Freshly synthesized tetramine was dissolved in anhydrous THF, and HCl gas was bubbled through the reaction flask at 0 ºC. After 15 mins, the light purple powder was filtered and washed with hexanes. The product was then dried under vacuum for 3 h and kept under nitrogen. The hydrochloride salt dissolved in 5 mL $HCl_{(aq)}$ was mixed with a solution of SeO_2 (2.19 mmol. 4 equiv.) in ethanol. Recrystallization from $HCl_{(aq)}$ gave needles which were isolated for characterization.: 2[**20a**]$Cl_2 \cdot 8H_2O \cdot HCl$ ^1H NMR (d_6-DMSO): δ (ppm) 7.96(m, 2Hs, Ar-H), 7.85(m, 2Hs, Ar-H), 7.83 (m, 2Hs, Ar-H), 7.69 (m, 2H, Ar-H), 5.45 (s, 4H, CH_2). ^1H-^{77}Se HMBC NMR (d_6-DMSO, 600 MHz): (δ ppm) 1444.9. ^{13}C NMR (d_6-DMSO): δ (ppm) 156.97, 149.52,138.34, 136.69, 129.31,128.30, 116.68(Ar-C), 52.60 (CH_2). HR ESI-MS: *m/z* $[M]^{2+}$ 197.9325 (*Cf.* calc. for $C_{14}H_{10}N_4Se_2^{2+}$ 197.9320). [**20c**]$Cl_2 \cdot H_2O$ ^1H NMR (d_6-DMSO): δ (ppm) 7.76 (bs, 1H, Ar-H), 7.63 (m, 2H, Ar-H), 7.43 (bt, 1H, Ar-H), 6.21(m, 1H Ar-H), 2.43(m, 2H, Ar-H), 1.96(m, 1H, Ar-H), 1.83(m, 1H, Ar-H). ^{13}C NMR (d_6-DMSO): δ (ppm) 156.25, 150.52, 136.43, 128.82, 125.00, 117.28 (Ar-C), 66.33, 24.12, 36.49 ($(CH_2)_3$) HR ESI-MS: *m/z* $[M]^{2+}$ 225.3829 (*Cf.* calc. for $C_{14}H_{10}N_4Se_2^{2+}$ 225.3820).

b) **X= CF_3SO_3, ([20a]$(CF_3SO_3)_2$ and [20b]$(CF_3SO_3)_2$)**:To the solution of tetramine in anhydrous ethanol, triflic acid was added in a dropwise fashion. The mixture was stirred for 24 hours and red powder was filtered and recrystallized in acetonitrile. ([**20a**]$(CF_3SO_3)_2$**)** ^1H NMR (d_6-DMSO): δ (ppm) 8.15 (d, 1H, C_{Ar}-H) 8.08 (pt, 2H, C_{Ar}-H), 7.87 (dt, 1H, C_{Ar}-H), 5.54 (bs, 2H, (CH_2)). ^{13}C NMR (d_6-DMSO) δ (ppm): 156.57, 151.11, 137.35. 130.35, 125.53, 116.33 (Ar-C), 51.30 (CH_2). ^1H-^{77}Se HMBC NMR (d_6-DMSO, 600 MHz): δ (ppm) 1490.0. ([**20b**]$(CF_3SO_3)_2$**)**: ^1H NMR (d_6-DMSO): δ (ppm) 8.07 (dd, 3H, Ar-CH), 7.83 (dq, 1H, Ar-CH), 5.20 (t, 2H, CH_2). 2.60 (p, 1H, CH_2). ^{77}Se NMR (d_6-DMSO, 600 MHz) δ (ppm) 1486.3. ^{13}C NMR (d_6-DMSO) δ (ppm): 206.48, 156.65, 150.63, 137.11, 130.23, 125.0 (Ar-C), 116.15, 48.68 (CH_2), 33.77 (CH_2), 30.06 (CH_2).

X= BF_4, ([20a](BF_4)$_2$): ^{1}H NMR (d_6-DMSO): δ (ppm) 8.05 (bs, 1H, C_{Ar}-H), 7.94 (m, 1H, C_{Ar}-H), 7.77(m, 1H, C_{Ar}-H), 7.50(m, 1H, C_{Ar}-H), 6.26 (bs,1H, CH_2) . ^{77}Se NMR (d_6-DMSO, 600 MHz) δ (ppm): 1481.6. ^{13}C NMR (d6-DMSO): δ (ppm) 156.93, 150.07, 137.93, 130.29, 125.57, 116.42 (Ar-C), 53.5 (CH_2).

$[1,2\text{-}(C_6H_4N_2Se)_2C_6(CH_2)]_2H_4]Cl_2$ ([20d]Cl_2): *p*-xylylenediamine (1 g, 3.79 mmol) was dissolved in 35mL CH_3CN with *o*-phenylenediamine (2.05 g, 18.9 mmol) and refluxed for 4 h under N_2. White precipitate was formed upon reflux. Solvent was removed under reduced pressure and 10^{-5} M NaOH was added followed by extraction with CH_2Cl_2 until the pH of the aqueous layer remained constant. The organic layer was dried using Na_2SO_4 and concentrated. The crude material was sublimed at 100°C under reduced pressure. The diamine was a viscous dark orange oil (82% yield). ^{1}H NMR (CD_3OD, 200MHz): (δ ppm) 7.36 (s, 4H, Ar-H), 6.61, 6.55 (m, 4H, Ar-H), 4.32 (s, 4H, CH_2) ppm. LR ESI-MS: *m/z* 319.2 (M+H) (*Cf.* calc. for $C_{20}H_{22}N_4$ 319.2). The diamine (0.989 g, 3.11 mmol) was dissolved in 20 mL anhydrous CH_2Cl_2 under N_2 and reacted with HCl (g) for 15 min until precipitation was complete. A purple precipitate was formed upon reaction and remaining solvent was allowed to evaporate under nitrogen atmosphere. The resulting product was a light purple powder (93% yield). Composition was determined via acid-base titration with 0.05 M NaOH and KHP as the primary standard. IR: 3377.21, 2871.60, 2603.85, 2090.36, 2011.76, 1633.05, 1561.82, 1510.17, 1461.45, 1322.50, 1155.30, 1137.52 cm^{-1}. HR ESI-MS: *m/z* 319.1923 (M+H) (*Cf.* calc. for $C_{20}H_{22}N_4$ 319.1916). The hydrochloride salt (0.409 g, 0.96 mmol) was dissolved in 40mL 1:1 v/v 10% HCl/EtOH. H_2SeO_3 (0.308 g, 2.39 mmol) dissolved in 4 mL of the same solvent, and added, turning the solution red and producing a yellow precipitate. The mixture was vacuum filtered and the final product was a yellow powder (61% yield). The product was then dehydrated with Al_2O_3 in 20 mL of ternary azeotrope with water, ethanol, and toluene. ^{1}H NMR (d$_6$-DMSO, 600MHz): (δ ppm) 7.95 (d, 2H, Ar-H), 7.83 (m, 4H, Ar-H), 7.67 (m, 2H, Ar-H), 7.48 (s, 4H, Ar-H), 6.14 (s, 4H, CH_2) ppm. ^{13}C NMR (d$_6$-DMSO, 600MHz): (δ ppm) 52.60, 116.68, 125.40, 128.73, 129.31, 136.32, 136.69, 149.53, 158.98 (Ar-C). ^{1}H-^{77}Se HMBC NMR (d$_6$-DMSO, 600MHz): (δ ppm) 1445.8 ppm. IR: 3055.60, 2970.40, 2937.30, 2793.36, 2721.35, 2637.11, 1977.05, 1955.18, 1837.26, 1810.53, 1714.29, 1607.43, 1530.10, 1504.74, 1423.52, 1323.22, 1163.82 cm-^{1}. LR ESI-MS: *m/z* 235.7 (M^{2+}) (*Cf.* calc. for $C_{20}H_{16}N_4Se_2^{2+}$ 236.5), 506.9 (M-Cl) (*Cf.* calc. for $C_{20}H_{16}N_4Se_2Cl^+$ 506.9).

[1,2-($C_6H_4N_2Se$)$_2C_6$(CH_2)]$_2H_4$]Cl_2]BF_4 (**[20d]BF_4**): N,N'-bis(2-aminophenyl)-p-xylenediamine (0.234 g, 0.735 mmol) was suspended in 9 mL of CH_3OH in a polypropylene test tube. 48% wt. HBF4 in water (1.15 mL, 7.17 mmol) was added to the suspension, immediately dissolving all solids into a brown solution. H_2SeO_3(0.235 g, 0.185 mmol) dissolved in 2 mL of CH_3OH was added and the solution turned red and a red-orange precipitate was produced and allowed to react for 1 h. The mixture was then centrifuged, the liquid decanted, and the solid was washed with saturated $NaBF_4$ in EtOH solution until the pH of the solution was no longer acidic, followed by a wash with EtOH, then a final wash with anhydrous ether and allowed to dry under atmosphere, resulting in an orange powder. The powder was recrystallized with CH_3CN and the final product consisted of orange needle-like crystals (66% yield). ^1H NMR (d_6-DMSO, 600 MHz): (δ ppm) 8.05 (d, 2H, Ar-H), 7.93 (m, 4H, Ar-H), 7.77 (m, 2H, Ar-H), 7.50 (s, 4H, Ar-H), 6.26 (s, 4H, CH_2) ppm. ^{13}C NMR (d_6-DMSO, 600MHz) (δ ppm): 53.45, 116.42, 125.57, 128.64, 130.29, 135.91, 137.39, 150.08, 156.93 (Ar-C). ^1H-^{77}Se HMBC NMR (d_6-DMSO, 600MHz): δ (ppm) 1481.5 ppm. ^{19}F NMR (d_6-DMSO, 200MHz) (δ ppm): -151.5. IR: 3606.23, 3519.00, 3104.46, 2045.80, 3022.69, 2384.48, 2106.00, 1969.36, 1822.20, 1606.87, 1532.31, 1396.54, 1319.03, 1115.62 cm-^{1}. LR ESI-MS: *m/z* 236.2 (M^{2+}) (*Cf.* calc. for $C_{20}H_{16}N_4Se_2^{2+}$ 236.5), 559.3 (M-BF_4) (*Cf.* calc. for $C_{20}H_{16}N_4Se_2BF_4^+$ 559.0).

[1,2-($C_6H_4N_2Se)_2C_6(CH_2)]_2H_4]Cl_2]BF_4.CH_3CN$ (**[20d]BF_4·CH_3CN**): The solution of **[20d]BF_4** was allowed to slowly evaporate, resulting in a product that consisted of yellow crystals.

1-(α,β)-O-methyl-2-deoxy-D-ribose (**22**): 2-deoxy-D-ribose (0.5 g, 3.76 mmol) was dissolved in 80 mL of freshly distilled methanol. 1 mL of 1% solution of hydrogen chloride in methanol was added dropwise while stirring. Once the mixture became a thick yellow syrup, sodium bicarbonate was added to complete the reaction. The evaporation of the filtrate under vacuum at 60 °C gave dark yellow syrup. ^1H NMR ($CDCl_3$, 500 MHz): (δ ppm) 5.07-5.09 (m, H_1), 2.00-2.23 (m, H_2, H_3), 4.02-4.04 (m, H_4), 4.50 (m, H_5), 3.58-3.68 (m, H_6), 3.32-3.34 (d, 3H, methyl). HRMS-EI $[M-H]^+$ m/z = 147.0697 (*Cf.* calc. for $C_6H_{12}O_4$ 147.0658)

1-(α,β)-O-methyl-3,5-di- (O-p-toluoyl)-2-deoxy-D-ribose (**23b**): To a solution of **22** in 20 mL of pyridine, p-toluoylchloride (2 equivalents) was added and stirred at 0 °C for

24h. The reaction mixture was extracted with diethyl ether and water. The organic layer was washed with $NaHCO_3$, NaCl. It was then dried over anhydrous Mg_2SO_4 and filtered. The evaporation of excess pyridine gave an orange oil. ^{1}H NMR ($CDCl_3$, 500 MHz): (δ ppm) 5.58 (m, H_1), 2.85-2.91 (m, H_2, H_3), 4.58 (m, H_4), 4.91 (q, H_5), 4.66 (m, H_6), 7.24-7.29 (m, 4H, benzoyl), 7.89-8.01 (m, 4H, benzoyl), 3.42 (d, 3H, methoxy). HRMS-EI m/z = 384.1567 (Cf. calc. for $C_{22}H_{24}O_6$ 384.1573)

1-(α)-chloro-3,5,-di-(O-p-toluoyl)2-deoxy-D-ribose (**26b**): The orange oil **23b** was dissolved in dried diethylether, and HCl gas was bubbled through the reaction flask at 0 °C. After 15 min, the white powder was filtered and washed with diethyl ether. The product was then dried under vacuum for 3 h and kept in a freezer. ^{1}H NMR ($CDCl_3$, 500 MHz): (δ ppm) 6.46-6.48 (d, H_1), 2.83-2.91 (m, H_2, H_3), 5.55-.5.58(m, H_4), 4.85 (q, H_5), 4.57(m, H_6), 7.23 (m, 4H, benzoyl), δ 7.87(m, 4H benzoyl), 2.41(d, 3H, methyl). HRMS-EI calculated [M-Cl] m/z = 353.1371 (Cf. calc. for $C_{21}H_{21}ClO_5$ 353.1389)

1-(α,β)-O-(2-amino-phenyl-amino)-3,5-di-(O-p-toluoyl)-2-deoxy-D-ribose (**28b**)**:** A solution of 1,2,-phenylenediamine in chloroform (0.26 mmol) was added onto the solution of 22b (0.13 mmol) under nitrogen. The reaction was refluxed at 50 °C for 4 h. The progress of the reaction was monitored using TLC (1% methanol in chloroform). Once the reaction was complete, the crude product was dried, and washed with diethyl ether. HRMS-ES $[M-H]^+$ m/z = 459.1920 (Cf. calc. for $C_{27}H_{28}N_2O_5$ 459.1920).

2.5 Summary of Crystallographic Data

Table 2.1 Crystallographic and refinement data for all compounds.

Compound	**12a**	**12b**	**12c**	**12d**	**13**
Empirical formula	$C_{24}H_{19}BN_2Se$	$C_6H_4BF_3N_2Se$	$C_6H_4BCl_3NSe$	$C_6H_4BBr_3N_2Se$	$C_3H_2BCl_3N_2Se_{0.5}$
Crystal system	Monoclinic	Triclinic	Monoclinic	Monoclinic	Monoclinic
a [Å]	18.501(3)	6.243(1)	15.302(1)	7.566(0)	14.914(1)
b [Å]	11.075(1)	8.220(1)	7.259(6)	7.307(0)	11.574(1)
c [Å]	19.110(2)	8.683(1)	10.037(8)	19.026(1)	9.890(1)
α [°]	90	98.535(2)	90	90	90
β [°]	91.537(1)	107.446(2)	118.332(3)	100.257(2)	127.603(2)
γ [°]	90	103.446(2)	90	90	90
V [Å^3]	3914.1(8)	894.9(3)	981.23(14)	1035.08(5)	1352.56(2)
T [K]	296(2)	296(2)	296(2)	296(2)	296(2)
Space group	I 1 2/a 1	$P\bar{1}$	C 1 2/m 1	P 1 2_1/c 1	C 1 2/c 1
Z	8	2	4	4	8
No. of reflections measured	33798	7865	16584	34295	43233
No. of independent reflections	5638	1645	2529	5022	4574
No. parameters refined	329	134	76	118	78
Final R_1 values (I > 2σ(I))	0.0371	0.0177	0.0164	0.0249	0.0228
Final wR(F^2) values (I > 2σ(I))	0.0634	0.0403	0.0476	0.0568	0.0585
Final R_1 values (all data)	0.0371	0.0200	0.0191	0.0391	0.0286
Final wR(F^2) values (all data)	0.0678	0.0412	0.0614	0.0713	0.0603

Table 2.1 Crystallographic and refinement data for all compounds (continuation)

	3b[**19a**]$_2$[I]$_2$	[**19a**][I]	[**19b**][I$_3$]	[**19b**][I]	[**19c**][I$_3$]	[**19c**][I]
Chemical formula	$C_{20}H_{18}I_2N_6Se_3$	$C_7H_{10}N_2SeI$	$C_9H_{11}N_2SeI_3$	$C_9H_{11}N_2SeI$	$C_{10}H_{13}N_2SeI_3$	$C_{10}H_{13}N_2SeI$
Crystal system	monoclinic	monoclinic	monoclinic	monoclinic	monoclinic	orthorhombic
a [Å]	15.986(1)	6.471(1)	11.317(2)	16.084(1)	7.668(1)	11.668(1)
b [Å]	11.671(1)	13.216(2)	9.818(2)	10.525(1)	10.014(2)	7.699(1)
c [Å]	12.743(1)	10.474(2)	13.569(2)	6.597(1)	20.949(4)	13.253(1)
α [°]	90	90	90	90	90	90
β [°]	92.566(3)	92.426(4)	105.047(3)	90	95.631(3)	90
γ [°]	90	90	90	90	90	90
V [Å^3]	2375.2(2)	894.9(3)	1456.0(4)	1116.8(2)	1600.7(5)	1190.6(1)
T [K]	100.15	100.15	100.15	100.15	100.15	296
Space group	C 1 2/c1	P 2_1/n	P 1 2_1/n 1	P n a 2_1	P 21/c	P nma
Z	4	4	4	4	4	4
No. of reflections measured	2700	12698	19082	16547	8761	26960
No. of independent reflections	2213	2521	4908	3306	4094	3066
No. of parameters refined	147	101	136	120	146	82
Final R_1 values ($I > 2\sigma(I)$)	0.0404	0.0199	0.0261	0.0229	0.0381	0.0331
Final w$R(F^2)$ values ($I > 2\sigma(I)$)	0.0685	0.0385	0.0447	0.0419	0.0759	0.0828
Final R_1 values (all data)	0.0550	0.0262	0.0399	0.0276	0.0682	0.0413
Final w$R(F^2)$ values (all data)	0.0733	0.0404	0.0481	0.0434	0.0861	0.0847

Table 2.1 Crystallographic and refinement data for all compounds (continuation).

	14	**15**	**16**	**17**	**18**
Chemical formula	$C_{12}H_8Cl_2MnN_4Se_2$	$C_{12}H_8Cl_2CdN_4Se_2$	$C_{10}H_{16}$ Cl_2 $FeN_2O_2S_2Se$	$C_{10}H_{16}$ Cl_2 $CoN_2O_2S_2Se$	$C_{10}H_{16}$ Cl_2 $NiN_2O_2S_2Se$
Crystal system	Triclinic	Triclinic	Orthorhombic	Orthorhombic	Orthorhombic
a [Å]	3.720(1)	3.777(2)	8.4810(6)	8.5078(8)	7.668(1)
b [Å]	9.278(2)	9.284(4)	13.4884(9)	13.3811(12)	10.014(2)
c [Å]	10.769(3)	10.824(5)	14.3386(11)	14.384(13)	20.949(4)
α [°]	80.055(4)	78.814(7)	90	90	90
β [°]	81.254(4)	82.416(8)	90	90	95.631(3)
γ [°]	83.353(4)	82.514(7)	90	90	90
V [Å^3]	2375.2(2)	366.9(3)	1640.3(2)	1638.1(3)	1600.7(5)
T [K]	100(2)	100(2)	100(2)	100(2)	100(2)
Space group	$P\bar{1}$	$P\bar{1}$	$P\ 2_1\ 2_1\ 2_1$	$P\ 2_1\ 2_1\ 2_1$	$P\ 2_1\ 2_1\ 2_1$
Z	1	1	4	4	4
No. of reflections measured	4125	1495	2743	21854	14668
No. independent reflections	1447	1495	2743	6035	6049
No. of parameters refined	98	102	186	246	185
Final R_1 values ($I > 2\sigma(I)$)	0.0254	0.006	0.0366	0.0291	0.0325
Final $wR(F^2)$ values ($I > 2\sigma(I)$)	0.0595	0.1273	0.0732	0.0369	0.0496
Final R_1 values (all data)	0.0311	0.1061	0.0431	0.0264	0.0372
Final $wR(F^2)$ values (all data)	0.0618	0.1481	0.0761	0.0380	0.0524

Table 2.1 Crystallographic and refinement data for all compounds (continuation).

	2[**20a**]$Cl_2 \cdot 8H_2O \cdot HCl$*	[**20c**]$Cl_2 \cdot H_2O$	[**20a**] $(CF_3SO_3)_2$	[**20b**] $(CF_3SO_3)_2$	[**20d**] $(BF_4)_2$	[**20d**] $(BF_4)_2 \cdot (CH_3N)$
Chemical formula	$C_{14}H_{12}N_4Se_2Cl_{2.5} \cdot 4(H_2O)$	$C_{18}H_{18}N_4Se_2Cl_2 \cdot H_2O$	$C_{14}H_{12}N_4Se_2 (CF_3O_3S)_2$	$C_{15}H_{14}N_4Se_2 (CF_3O_3S)_2$	$C_{20}H_{16}N_4Se_2 (BF_4)_2$	$C_{20}H_{16}N_4Se_2 (BF_4)_2 \cdot (CH_3CN)$
Crystal system	Triclinic	Monoclinic	Triclinic	Monoclinic	Monoclinic	Monoclinic
a [Å]	7.624(2)	8.9756(3)	8.3966(16)	11.9799(2)	6.4979(3)	10.353(2)
b [Å]	7.942(2)	12.4952(4)	110.300(2)	29.5901(6)	11.9131(6)	7.3989(17)
c [Å]	18.270(5)	9.3428(3)	11.9466(19)	6.63540(10)	14.6745(8)	33.631(7)
α [°]	83.560(5)	90	90.953(3)	90	90	90
β [°]	77.649(5)	108.347(2)	90.846(4)	93.9400(10)	97.399(3)	93.4020(5)
γ [°]	71.357(4)	90	94.122(4)	90	90	90
V [Å^3]	1022.9(5)	994.55(6)	1130.3(4)	2370.39(7)	1126.50(10)	2571.5(10)
T [K]	296(2)	100(2)	296(2)	100(2)	100(2)	100(2)
Space group	$P\bar{1}$	P 1 2_1 1	$P\bar{1}$	P 1 2_1/c 1	P 1 2_1/n 1	P 1 2_1/n 1
Z	2	2	2	4	2	4
No. of reflections measured	16237	35869	22047	84681	27865	7012
No. independent reflections	4253	10311	4639	7255	4296	5030
No. of parameters refined	250	253	325	387	163	353
Final R_1 values (I > 2σ(I))	0.0691	0.0356	0.0256	0.0306	0.0293	0.0470
Final wR(F^2) values (I > 2σ(I))	0.1670	0.0584	0.0634	0.0843	0.0678	0.1168
Final R_1 values (all data)	0.0845	0.0602	0.0407	0.0363	0.0412	0.0882
Final wR(F^2) values (all data)	0.1731	0.0635	0.0899	0.0966	0.0750	0.1503

* Preliminary model, the positions of water hydrogen atoms require further refinement.

Table 2.1 Crystallographic and refinement data for all compounds (continuation).

	$3(\mathbf{30})\cdot(C_6H_6)$	**30**	$[12(\mathbf{30})\cdot 2(CH_2Cl_2)$	$3(\mathbf{30})\cdot(C_4H_8O)$
Chemical formula	$C_{12}H_{12}NOTe$	$C_{10}H_9NOTe$	$C_{61}H_{55}N_6O_6ClTe$	$C_{68}H_{70}N_6O_7Te_6$
Crystal system	Orthorhombic	Triclinic	Triclinic	Triclinic
a [Å]	8.6720(11)	14.457(3)	14.457(3)	21.706(4)
b [Å]	12.6535(17)	15.311(3)	15.311(3)	21.706(4)
c [Å]	31.538(4)	15.817(3)	15.817(3)	12.127(2)
α [°]	90	105.395(3)	105.395(3)	90
β [°]	90	102.892(3)	102.892(3)	90
γ [°]	90	103.246(3)	103.246(3)	120
V [Å^3]	3460.7(8)	3131.8(10)	3131.8(10)	4930.3(10)
T [K]	100.15	100.15	100.15	3
Space group	$P\ 2_1\ 2_1\ 2_1$	$P\bar{1}$	$P\bar{1}$	$R\bar{3}$
Z	4	1	2	3
No. of reflections measured	38614	53585	53585	84681
No. independent reflections	7931	12799	12799	7255
No. of parameters refined	409	736	736	94
Final R_1 values ($I > 2\sigma(I)$)	0.0266	0.0128	0.0259	0.0306
Final $wR(F^2)$ values ($I > 2\sigma(I)$)	0.0554	0.0315	0.0516	0.0843
Final R_1 values (all data)	0.0290	0.0135	0.0406	0.0363
Final $wR(F^2)$ values (all data)	0.0575	0.0318	0.0553	0.0966

Table 2.1 Crystallographic and refinement data for all compounds (continuation).

	$(0.86Pd\bullet 1.73BF_4)^{\cdot}4(\mathbf{30})$ $1.72(CH_2Cl_2)$	$(0.80Pd\bullet 1.59(BF_4)^{\cdot}4(\mathbf{30})^{\cdot}$ $1.41(CH_2Cl_2)$	$[12(\mathbf{30})^{\cdot}2(CH_2Cl_2)$
Chemical formula	$C_{41.72}H_{39.44}B_{1.73}N_4O_4$ $F_{6.92}Cl_{3.44}Pd_{0.86}Te_4$	$C_{41.41}H_{38.82}B_{1.59}N_4O_4F_{6.36}Cl_{2.82}Pd_{0.8}Te_4$	$C_{25}H_9NOTe$
Crystal system	Tetragonal	Tetragonal	Monoclinic,
a [Å]	11.2576(14)	11.2652(2)	23.9972(18)
b [Å]	11.2576(14)	11.2652(2)	13.2242(10)
c [Å]	40.011(5)	40.0616(9)	21.0668(16)
α [°]	90	90	90
β [°]	90	90	97.8540(10)
γ [°]	90	90	90
V [Å^3]	5070.7(14)	5084.0(2)	6622.7(9)
T [K]	100.15	100.15	100.15
Space group	$I4_1/a$	$I4_1/a$	C 2/c 1
Z	4	4	8
No. of reflections measured	9429	32559	31330
No. independent reflections	2277	2929	14335
No. of parameters refined	189	189	507
Final R_1 values (I > 2σ(I))	0.0486	0.039	0.0404
Final w$R(F^2)$ values (I > 2σ(I))	0.1306	0.1288	0.0793
Final R_1 values (all data)	0.0827	0.0432	0.0668
Final w$R(F^2)$ values (all data)	0.1428	0.1309	0.0862

$R_1 = \Sigma \,||F_o|-|F_c|| \,/\, \Sigma|F_o|$, $wR(F^2) = \{\Sigma[w(F_o^2-F_c^2)^2] \,/\, \Sigma w(F_o^2)^2\}^{½}$

Chapter 3. Computational Studies of the Structures and Energetics of Supramolecular Aggregates of Chalcogenadiazoles and their Derivatives

Portions of this chapter have been included in the following publications:

1. A. F. Cozzolino, G. Dimopoulos-Italiano, L. M. Lee, I. Vargas-Baca,* "Chalcogen-nitrogen secondary bonding interactions in the gas phase: spectrometric detection of ionized benzo-2,1,3-telluradiazole dimers", Eur. J. Inorg. Chem. **2013**, *15*, 2751-2756; DOI: 10.1002/ejic.201201439.[56]

2. A. F. Cozzolino, P. J. W. Elder, L. M. Lee, I. Vargas-Baca,* "The Role of the Lewis Acid-Base Properties on the Supramolecular Association of 1,2,5-Chalcogenadiazoles", Can. J. Chem. **2013**, *91*, 338-347; DOI: 10.1139/cjc-2012-0323.[95]

3. N. A. Pushkarevsky, P. A. Petrov, D. S. Grigoriev, A. I Smolentsev, L. M. Lee, F. Kleemiss, G. E. Salnikov, S. N. Konchenko, I. Vargas-Baca, S. Grabowsky, J. Beckmann, A. V. Zibarev. *Chem. Eur. J.* **2017**, DOI: 10.1002/chem.201703018.

3.1 Introduction

Earlier quantum mechanical studies of the supramolecular interactions of the 1,2,5-chalcogenadiazoles (**1**)[96] were concerned with identifying the most appropriate computational methods, considering both accuracy and expediency (computational cost). Given the need to include atoms as heavy as tellurium, only Density Functional Theory (DFT) methods were considered. It was established that the SBI distances within the [Ch-N]$_2$ supramolecular synthon are best modelled with all-electron basis sets, which were not available in GAUSSIAN; instead the Amsterdam Density Functional (ADF)[97-99] package was selected. One important feature of ADF is that it employs actual Slater-type orbitals, not approximations built from Gaussian functions. Relativistic effects were accounted for within the Scalar Zeroth Order Regular Approximation (ZORA).[100-104] Additional requirements imposed by the heavy atoms such as orbitals of triple-ζ quality and polarization functions favoured methods within the Generalized Gradient Approximation (GGA) over hybrids such as the popular B3LYP.[105] In particular, the exchange and correlation GGA functionals of Perdew and Wang (PW91) gave the smallest deviations from experimental values. PW91 had already an established reputation in modelling heavy main-group systems.[106] The exchange and correlation components of PW91 are now superseded by more modern functionals such as those of Perdew-Burke-Ernzerhof (PBE).[105,107] This functional was recently shown to produce some of the most accurate profiles of electron density for individual atoms.[108] This ability is critical to the application of supplemental methods such as the Theory of Atoms in Molecules (AIM)[109,110] for the characterization of interatomic interactions based on the features of the charge distribution in space.

It must be noted that the performance of the DFT methods was assessed using only structural parameters because there were no experimental determinations of SBI energies. Energy Decomposition Analyses (EDA)[111-113] parsed the results of those calculations into electrostatic, covalent and steric contributions but the evaluation of dispersion was only realistic for small molecules of sulfur and selenium[23] but not for tellurium compounds. Dispersion-corrections to some DFT methods became available only recently; Grimme's

D3[114] approach is one of the best established and is suitable for PBE calculations.

This chapter updates and expands the computational characterization of the auto-association of **1** through the $[Ch\text{-}N]_2$ supramolecular synthon using the PBE method and its dispersion-corrected version PBE-D3. These methods are then applied to adducts with Lewis bases, to interpret the results of mass spectrometric experiments intended to search for evidence of supramolecular association in the gas phase. Finally, these methods and supplemental analyses of the electronic structure and charge density are applied to the characterization of the Te-C bonding interaction in the recently isolated adducts of telluradiazoles and *N*-heterocyclic carbenes.

3.2 Results and Discussion

3.2.1 The Contribution of Dispersion to the Supramolecular Interactions of 1,2,5-chalcogenadiazoles

In order to make appropriate comparisons and an assessment of the dispersion contributions, PW91, PBE and PBE-D3 calculations were carried out for the dimers of the chalcogenadiazoles and their adducts with DMSO, pyridine and benzene. SBI distances and interaction energies are presented in Table 3.1 and Table 3.2. Actual examples of the adducts of chalcogenadiazoles with DMSO and pyridine have been structurally characterized[71,72] and interactions between the chalcogen atom and aromatic rings have been observed in the structures of the borane adducts **8a** and **9**.

Table 3.1 Calculated dissociation energies (kJ mol^{-1}) and secondary-bond lengths (Å) of the dimers(**$1a_2$-$1c_2$**).

Functional	**$1a_2$**	**$1b_2$**	**$1c_2$**
		Dissociation Energy	
PW91	11.23	27.16	67.10
PBE	9.88	24.99	75.77
PBE-D3	15.9	32.51	84.18
		d_{SBI} Ch-N	
PW91	3.201	2.869	2.554
PBE	3.201	2.869	2.579
PBE-D3	3.199	2.869	2.581

Calculated SBI distances for the dimers **$1a_2$-$1c_2$** are almost insensitive to the GGA functional; it is indeed known that PBE and PW91 yield very close bond distances. On the other hand, the interaction energies are more strongly affected. PBE estimates smaller interaction energies for Ch = S, Se and larger for Ch = Te; with differences up to 12%. Interestingly, the dispersion contributions increase with the weight of the chalcogen but their relative importance is greatest for the lightest element, Ch = S.

Table 3.2 Interaction energies of donor molecules and **1a-1c** (kJ mol^{-1}).

Functionals	**1a**	**1b**	**1c**
		DMSO	
PW91	15.3	25.9	39.9
PBE	13.8	24.3	37.8
PBE-D3	21.0	31.7	45.6
		Pyridine	
PW91	13.9	25.1	41.0
PBE	12.3	23.2	38.7
PBE-D3	19.1	31.2	47.4
		Benzene	
PW91	5.2	8.6	11.4
PBE	4.2	7.3	10.8
PBE-D3	12.9	17.3	21.1

For the adducts of the **1** with DMSO, pyridine and benzene SBI distances follow the same pattern as in the case of the dimers; for brevity only the interaction energies are given in Table 3.2. The SBI energies of the chalcogens with DMSO and pyridine are comparable in strength and much stronger than with benzene. The contribution of dispersion is important in all these structures and follows the overall trend of absolute and relative magnitudes found for the dimers. As can be expected from the polarizability of the aromatic ring and the poor donor ability of carbon, dispersion is the most significant contribution to the formation of adducts with benzene.

3.2.2 The Structures of Benzo-2,1,3-telluradiazole Dimers in the Gas Phase

The DFT studies summarised above suggest that the $[Ch\text{-}N]_2$ SBIs are strong enough to form supramolecular aggregates in gas phase or in solution.[66,67,72,115] Similar studies have suggested that modern spectroscopic methods should be able to detect SBI aggregates formed in gas phase. A fast-mixing nozzle in conjunction with a pulsed-jet Fourier-transform microwave spectrometer was used to monitor the formation of the donor-acceptor complexes of dihalogen-molecules in the gas phase prior to undergoing irreversible chemical reactions.[116]

Because chalcogenadiazoles are heavier and more stable, mass spectrometry was proposed as to conduct experiments to search for supramolecular aggregates. Also, these molecules are volatile enough to be amenable to purification by sublimation under modest vacuum and temperatures. The experimental results of laser desorption/ionization time-of-flight mass spectrometry (UV-LDI TOFMS) performed on several benzo-2,1,3-telluradiazoles (**3c**, **4**, **5**, **6**) showed the isotopic patterns that correspond to the ion of composition $[2M+H]^+$ (Figure 3.1). In the case of **5**, $[2M]^+$ was observed in the same spectrum. However, none of the selenium or sulfur compounds tested gave any supramolecular ions.[96] Dispersion-corrected DFT calculations were used to identify the most-likely interactions responsible for the assembly of the secondary ions.

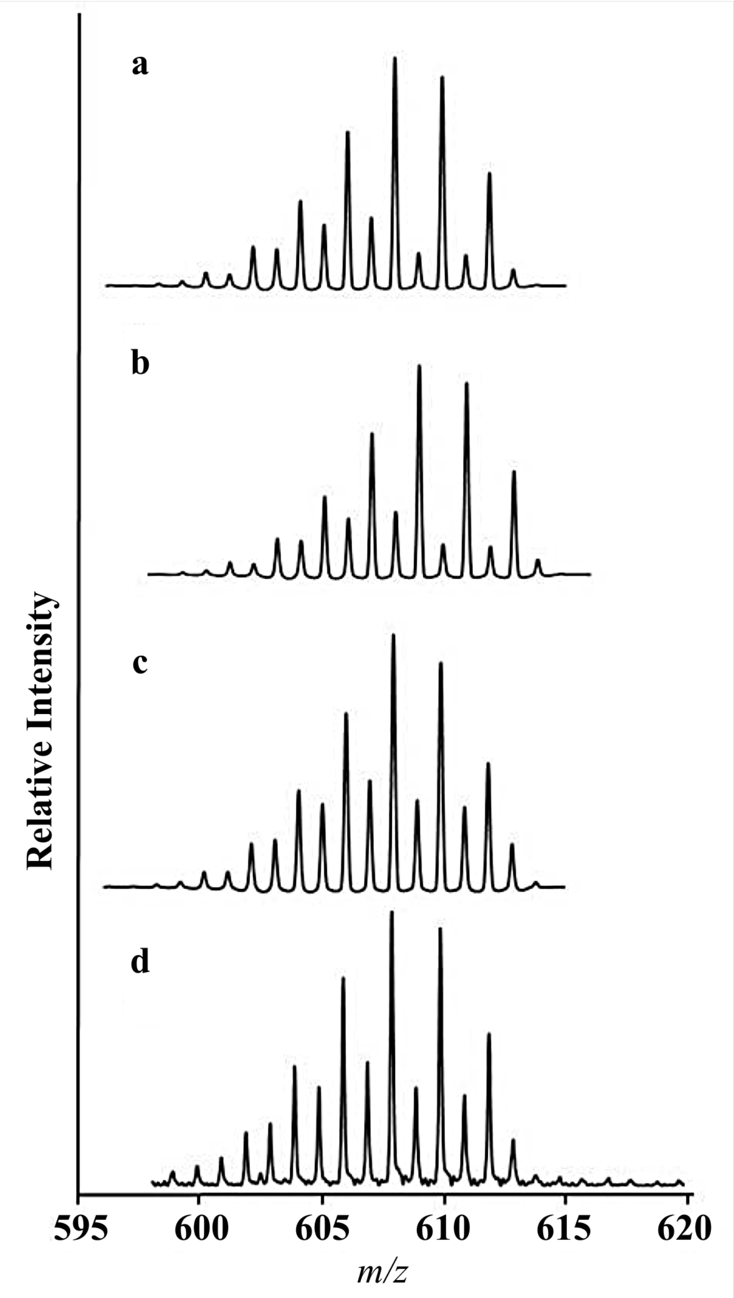

Figure 3.1 Isotopic distributions of the ionized supramolecular aggregates of **5.** Modeled: a) $[2M]^+$ b) $[2M+H]^+$, c) $[2M]^+ + [2M+H]^+$; d) experimental.

3.2.2.1 Analysis of Bonding Energies

PBE-D3 calculations were performed in order to identify the most-likely structures of the ions observed in the LDI mass spectra of the benzo-2,1,3-chalcogenadiazoles. The geometries of the primary ions were initially optimized and later used to build plausible models of the supramolecular ions that would result from the secondary ionization processes in Equations 3.1 and 3.2. Each model was fully optimized.

$$[\mathrm{M}\ +\ \mathrm{H}]^{+}\ +\mathrm{M}\ \rightarrow\qquad [2\mathrm{M}\ +\ \mathrm{H}]^{+}\qquad (3.1)$$

$$[\mathrm{M}\ ]^{+}\ +\mathrm{M}\ \rightarrow\qquad [2\mathrm{M}]^{+}\qquad (3.2)$$

The crystal structures of [**3b**H]$^{+}$ [117,118] and [$\mathbf{3c_2}$]$^{2+}$ as well as the proton affinity map of telluradiazoles[95] indicate that the N atom is the preferred site for proton attachment. From the calculations for this study, the proton affinities of **3a, 3b** and **3c** are, 886.9, 910.3, and 943.2 kJ mol^{-1}, respectively. These values are of the same order of magnitude as the proton affinities calculated for a series of pyrido-indoles, pyridylindoles, and pyridylpyrido-indoles that were investigated as matrices for UV MALDI-TOF MS; ions of composition [M+H]$^{+}$ were detected in all those cases.[28]

The [M]$^{+}$ ion results from the single ionization of the neutral molecule. The experimental vertical ionization energies for **3a, 3b** and **3c** determined by UV photoelectron spectroscopy are 866.4, 849.1 and 826.9 kJ mol^{-1}, respectively.[119] The DFT calculations reproduced the vertical ionization energies well and gave adiabatic ionization energies of 857.2, 844.5, and 820.8 kJ mol^{-1}, respectively. As the electron is removed from a π orbital with a modest bonding character, ionization only causes a small structural distortion.

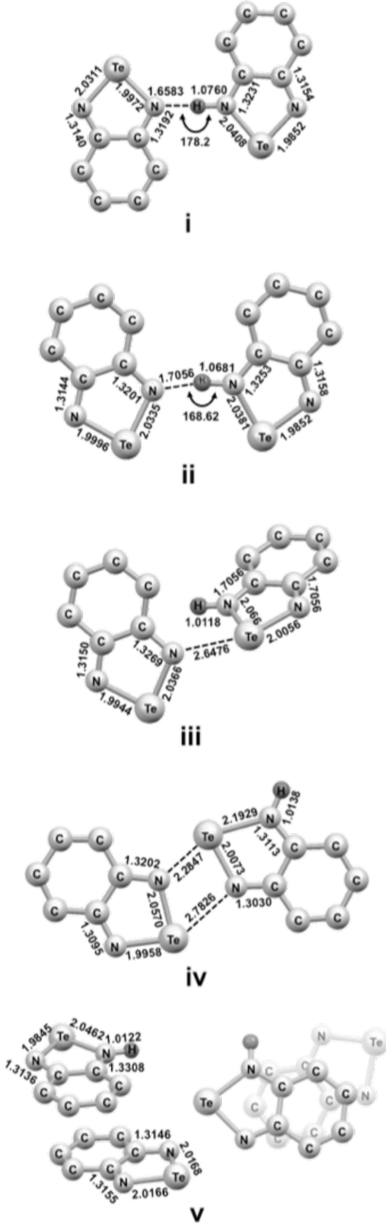

Figure 3.2 Optimized (PBE-D3) model structures for the $[2M+H]^+$ ion formed from **3c**, designated as i-v. Selected interatomic distances (Å) and angles (°). H atoms are omitted for clarity, two views are provided for v.

Table 3.3 Calculated gas-phase energetic and thermodynamic parameters (kJ mol^{-1}) for the assembly of structures **3c**(i-v) of the [2M+H]$^+$ ion.

	i	ii	iii	iv	v
ΔTBE	-78.6	-72.4	-100.5	-151.1	-49.1
ΔZPE	3.63	4.52	7.82	9.43	5.97
ΔU	-78.7	-71.6	-92.0	-141.4	-46.8
ΔH	-81.1	-74.1	-94.4	-143.9	-49.2
ΔS	-193.1	-192.2	-151.5	-165.9	-198.0
$\Delta G_{273.15}$	-28.4	-21.6	-53.0	-98.6	4.9

Five structures were identified as minima in the potential energy surface of the [2M + H]$^+$ system (Figure 3.2) The corresponding binding energies between M an 2[M + H]$^+$ can be estimated as the change of total bonding energy (TBE) for the addition reaction [Equation (3.1)], and follow-up vibrational calculations completed the analysis by providing the zero-point energies (ZPE), total internal energies (*U*), enthalpies (*H*), entropies (*S*), and Gibbs free energies (*G*). Structures i and ii feature a single H bond between coplanar molecules and their binding energies are close in magnitude and consistent with H bonding.[120] By using a combination of one H bond and one Te-Te contact for a planar starting point, geometry optimization led to structure iii, which features a single Te···N SBI and an interplanar angle of 59.67°. Of the geometries investigated, the most stable arrangement is iv, in which M and [M + H]$^+$ are linked by the [Te-N]$_2$ supramolecular synthon. However, in iv the SBIs are not equal; the Te···N SBI distance is shorter opposite to the protonated N atom. The long Te···N SBI (2.7826 Å) is longer than the average Te···N

SBI distance observed in the crystal structure of **3c** [2.701(7) Å], and the short SBI (2.2847 Å) is shorter than that observed in the crystal structures of the N-alkylated 1,2,5-telluradiazolium cations [2.417(3) and 2.301(5) Å].[75,121] Considering the dimerization energy of **3c** has been estimated as 68.8 kJ mol^{-1},[66] these results indicate that protonation of one N atom strongly stabilizes the $[Te\text{-}N]_2$ supramolecular synthon; this is in agreement with other computational studies on these systems.[95] Interestingly, structures i and iv resemble the links that alternate in the crystal structures of $\mathbf{3b_2}{\cdot}HI_3{\cdot}I_2$.[122] Modeling of π stacking between M and $[M + H]^+$ yielded structure v, in which there is considerable interaction between the aromatic rings. The centroids of the rings are separated by 3.497 Å, and the molecular planes define a 5.96° angle. The small interaction energy identifies structure v as the least stable option for the $[2M + H]^+$ ion: the inclusion of the entropic contribution indicates that association in such a fashion would not be thermodynamically favored at standard temperature.

Supplemental calculations for the S and Se $[2M + H]^+$ ions provided consistent energies for H bonding (76-86 kJ mol^{-1}) and π stacking (43-45 kJ mol^{-1}); model iii converged to a H-bonded structure with E = S; those observations and the weak SBI association (ΔTBE < 97 kJ mol^{-1}) appear to be consistent with the lack of supramolecular aggregates in the mass spectra of the S and Se compounds. (Table 3.4)

Table 3.4 Association energies for the assembly by the structures i-v of the $[2M+H]^+$ ion formed from **3b-c** in gas phase (Equation 3.1)

		Ch	
Structure		S	Se
i	ΔTBE (kJ mol^{-1})	-81.0	-81.2
	d N-H (Å)	1.0886	1.0867
	d H···N (Å)	1.6032	1.6014
	∡ N-H···N (°)	177.15	179.22
ii	ΔTBE (kJ mol^{-1})	-78.0	-76.2
	d N-H (Å)	1.0862	1.0759
	d H···N (Å)	1.6511	1.6571
	∡ N-H···N (°)	174.57	171.73
iii	ΔTBE (kJ mol^{-1})	-85.9	-78.0
	d N···Ch (Å)	-	2.7158
	d N-H (Å)	1.0854	1.0124
	d H···N (Å)	1.6119	2.3794
	∡ N-H···N (°)	168.43	106.19
	∡ interplanar (°)	56.81	72.42
iv	ΔTBE (kJ mol^{-1})	-57.3	-95.6
	d N···Ch (Å)	2.4475	2.2982
	d N···Ch (Å)	3.2293	3.0673
v	Δ_{TBE} (kJ mol^{-1})	-43.4	-45.3
	∡ interplanar (°)	10.40	6.44

The mass spectrum of **5** contains the ion $[2M]^+$, which would arise from the reaction of $[M]^+$ with M (Equation 3.2). According to the geometry optimization and maps of Lewis acidity and basicity[118], this reaction would likely lead to a structure assembled from the $[Te\text{-}N]_2$ supramolecular synthon (Figure 3.3). The calculated interaction energies for these structures are 149.3 kJmol^{-1} for **3c** and 137.5 kJmol^{-1} for **5**. In both instances, the SBI distances are more than 0.2 Å shorter than those in the supramolecular ribbons that the neutral heterocycles form in the solid state.[67,71]

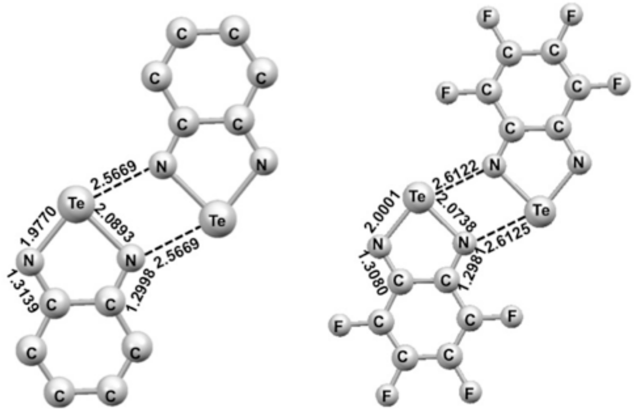

Figure 3.3 DFT-D3 optimized structures for the $[2M]^+$ ions formed from **3c** and **5**. Hydrogen atoms are omitted for clarity.

3.2.3 Analysis of Te-C bonding in the Adducts of 1,2,5-Telluradiazoles with a N-Heterocyclic Carbene

As noted in Chapter 1, 1,2,5-chalcogenadiazoles form adducts with a variety of neutral and anionic Lewis bases.[59,74] Amongst those species, those obtained from the reactions of 1,3-bis(mesityl)imidazol-2-ylidene (**10)** with 3,4-dicyano-1,2,5-telluradiazole (**2**) and 2,1,3-benzo-telluradiazole (**3c**), complexes **2·10** and **3c·10**, are especially interesting due to their long Te-C distances, 2.343(4) and 2.530(2) Å, respectively.

R= Ph

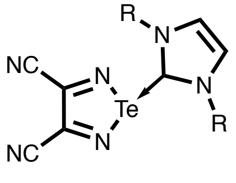

2·10

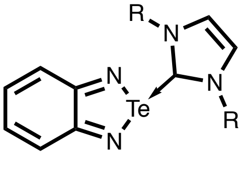

3c·10

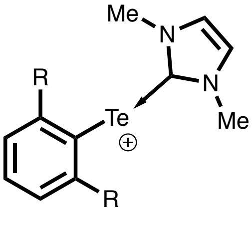

11

The DFT methods described above (ADF, GGA PBE-D3, triple-ζ double polarization all-electron basis sets) were used to characterize these Te-C interactions. For computational expediency, the model structures used phenyl groups on the carbene instead of mesityl. In addition, compound **11** (also a simplified model for an experimentally known compound[123]) was calculated as a point of reference**.** Their optimized geometries reproduced well the internal dimensions of the telluradiazoles and carbene moieties. Calculated C-Te bond distances decrease in the order **2·10** > **3c·10** >**11**, in agreement with the experimental observation. The free energies of interaction indicate that **2·10** and **3c·10** would be stable complexes in the gas-phase. (Table 3.5)

The electronic components of the interaction energy ($E_{\text{Total Electronic}}$) are exothermic and were analyzed under the Ziegler-Rauk transition-state formalism.[112,113,124] In this approach, aside from the geometric distortion that gives a preparation energy ($E_{\text{Preparation}}$), this “transition state” calculation evaluates the electrostatic interaction (E_{Elstat}) and Pauli repulsion (E_{Pauli}) (total steric interaction as their combination E_{Steric}), the orbital (E_{Orbital}) and the dispersion interaction energy ($E_{\text{Dispersion}}$). In both **2·10** and **3c·10** the electrostatic interaction is the major stabilizing factor, approximately in a ratio of 3:2 over the orbital interaction energy that represents covalent bonding (Table 3.5).

Table 3.5 Energy decomposition analysis for the C-Te interaction in the models **2·10**, **3c·10** and **11**. All values in kJmol^{-1} unless otherwise noted.

Contribution	**2·10**	**3c·10**	**11**
$E_{Preparation}$	9.2	3.5	34.6
E_{Elstat}	-269.5	-197.2	-561.0
E_{Pauli}	360.7	272.4	1696.6
E_{Steric}	91.2	75.2	1135.6
$E_{Orbital}$	-194.6	-132.0	-1423.5
$E_{Dispersion}$	-24.6	-22.0	-36.5
$E_{Total\ Electronic}$	-108.8	-70.7	-359.67
ΔZPE [eV]	0.042	0.040	0.112
ΔH	-106.5	-66.5	-318.7
ΔS [J mol^{-1}K^{-1}]	-211.1	-188.2	-193.9
$\Delta G_{273.15K}$	-43.6	-10.4	-260.9

Topological analysis of the electron density (as per the Quantum Theory of Atoms in Molecules / QTAIM)[109,110] confirms the existence of bond paths and bond critical points (BCPs) between the C and Te atoms in all model compounds (Figure 3.4). The BCP electron densities are the largest so far calculated between Lewis bases and telluradiazoles, this is in line with the calculated magnitudes of the interaction energies. However, the nature of the interacting orbitals could not be unambiguously assessed from the Kohn-Sham orbitals due to extensive mixing, but is clearly discernible through the Boys-Foster[125] localization method (Figure 3.5). In addition, the contour plots of the electron density for the C–Te interaction in **2**·**10** and **3c**·**10** are devoid of features that would be indicative of back-donation from Te to the carbene. (Figure 3.6)

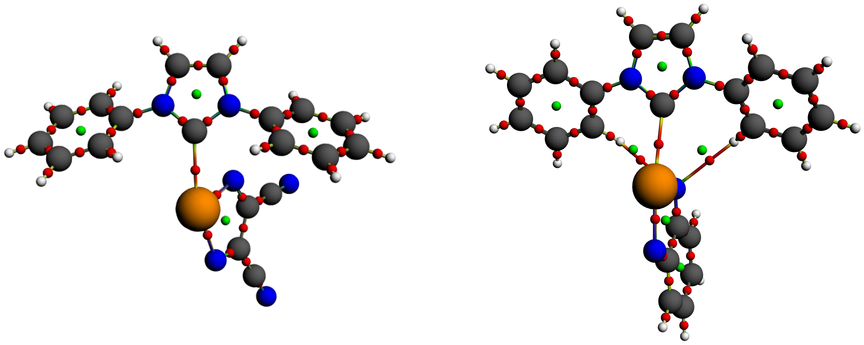

Figure 3.4 QTAIM analysis of bonding in **2**·**10** and **3c**·**10**. Bond critical points are shown in red, ring critical points in green. The H–N bond paths and critical points are the result of contacts generated by the geometry optimization of these models.

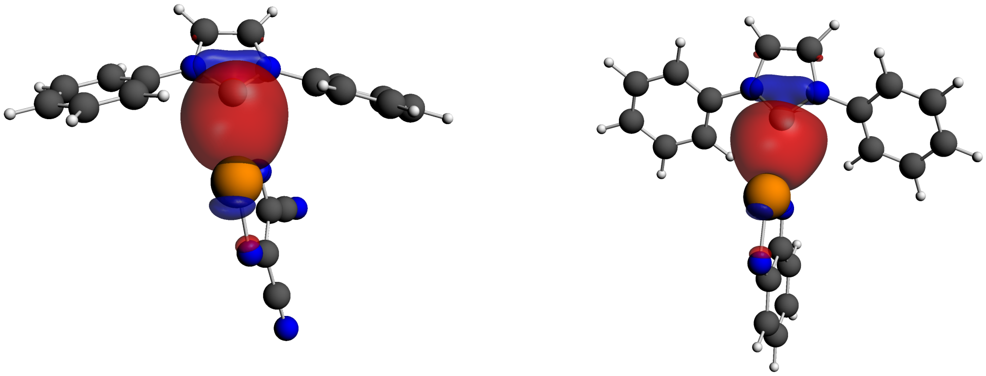

Figure 3.5 Boys-Foster localized molecular orbitals that correspond to the Donor–Acceptor interaction C–Te in in **2**·**10** and **3c**·**10**.

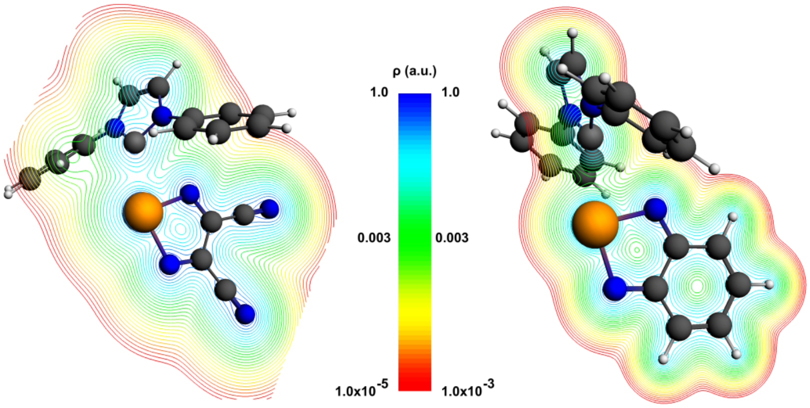

Figure 3.6 Contour plots of the electron density for the C–Te interaction in in **2**·**10** and **3c**·**10** in the plane perpendicular to the heterocyclic carbene.

All calculated C-Te bond orders are around 0.5, with those for **2**·**10** being slightly higher than those for **3c**·**10**, whereas the bond order for **11** is that of a single bond (Table 3.6). In each case, according to an ETS - Natural Orbital of Chemical Valence (NOCV)[126] analysis, the main contribution to $E_{Orbital}$ is a NOCV for which the deformation density corresponds to donation of the carbon LP orbital to the chalcogen ruling out partial double bond character through π-interactions (Figure 3.7).[127]

Table 3.6 Calculated bond orders for C-Te bonds in the models **2**·**10**, **3c**·**10** and **11**.

Method	**2**·**10**	**3c**·**10**	**11**
Mayer[128]	0.54	0.43	1.06
Nalewajski-Mrozek[129-133]	0.42	0.32	1.02
Wiberg[134]	0.35	0.31	0.96

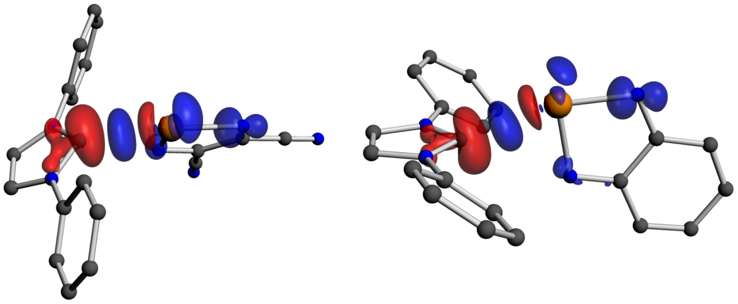

Figure 3.7 Deformation density derived from the NOCV that contributed to the largest extent to the orbital interaction energy **2·10** and **3c·10**. Electron depletion is shown in red while electron concentration is shown in blue.

The degree of charge transfer (CT) is consistent in all Mulliken, [135-138] NBO, [139,140] Hirshfeld and Bader[109,110,141] charge analyses, which denotes approximately even sharing of electrons between the NHC and tellurenyl cation in **11**, whereas for **2·10** and **3c·10** only a third of a charge has been transferred from the NHC onto the telluradiazole (Table 3.7).

Table 3.7 Calculated degree of charge transfer (a.u.) from carbene to telluradiazole

Method	**2·10**	**3c·10**	**11**
Mulliken	0.32	0.22	0.46
NBO	0.27	0.17	0.57
Hirshfeld	0.22	0.1	0.49
Bader	0.23	0.14	0.41

A striking consequence of the interaction of the NHCs with the telluradiazoles is the absence of solid-state dimerization through the $[Te–N]_2$ supramolecular synthon, such as present in the crystal structures of **4** with DMSO as well as **5** with pyridine.[65-67,71,73,115] The Te atom in both **2**·**10** and **3c**·**10** is not sterically shielded from the opposite side of the NHC ligand. Instead, this phenomenon appears to be an electronic effect. The optimized geometry of the hypothetical dimer (**2**·**10**)$_2$ features long (> 2.9 Å) secondary bonding distances and a rather small binding energy per Te···N interaction (41.3 kJ mol^{-1}). Similarly, models for (**2**·**10**)$_2$ and **2**·**10**·THF could not be optimized due to very shallow Te···N and Te···O potential well depths. Carbene coordination to tellurium increases the height of the acceptor $^*\sigma_{\text{Te-N}}$ orbitals to -2.49 eV and -0.73 eV in **2**·**10** and **3c**·**10**, respectively. There is also a significant polarization effect on the second, vacant, σ-hole of the chalcogen. The maximum of potential decreases to just 17 kJ mol^{-1} in **2**·**10** and becomes negative (-7.9 kJ mol^{-1}) in **3c**·**10** (Figure 3.8).

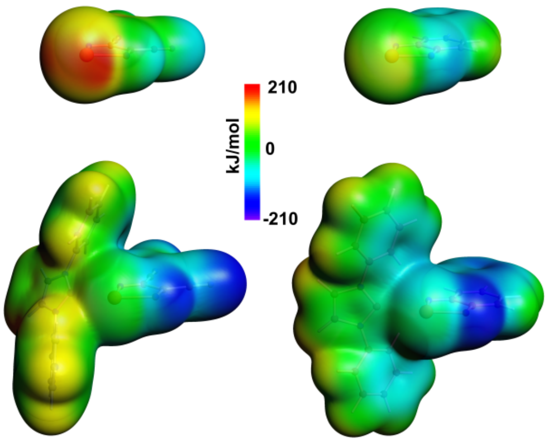

Figure 3.8 Electrostatic potential plotted over the 10^{-3} a.u. isodensity surface of **2**·**10** and **3c**·**10**.

3.3 Summary

DFT-D3 calculations indicate that the contribution of dispersion forces to the SBIs must not be neglected. The results show that, due to the great covalent and electrostatic character, the tellurium-centred SBIs are properly modeled without dispersion. However, the calculations for the S and Se systems must include dispersion corrections. Application of DFT-D3 to modeling the $[2M + H]^+$ secondary ion detected in the mass spectra of 1,2,5-telluradiazoles established that its most stable structure features the $[Te\text{-}N]_2$ supramolecular synthon and that hydrogen-bonded and π-stacked alternatives are much less stable. Lastly, the attractive C-Te interaction in adducts **2·10** and **3c·10** originates in a σ hole on Te and the donation of the carbene lone pair into a $\sigma^*_{Te\text{-}N}$ orbital. Bonding orders and the interaction energies indicate that these bonds are significantly weaker than classic single Te-C bonds.

Chapter 4. Structural and Synthetic Investigations of Borane adducts of Benzo-2,1,3-Selenadiazole

4.1 Introduction

The unusually short Te···N SBI distance in the DFT-D3 model of the $[2M+H]^+$ ion in the mass spectrum of **3c** strongly suggests that the Ch···N SBIs can be strengthened by attaching a Lewis acid to the nitrogen atom adjacent to the chalcogen. Calculations of the protonated chalcogenadiazoles ({**1a**-**c**}-H^+) and the borane adducts ({**1a**-**c**}-BH_3) did show a striking reorganization of electron density in the heterocycles, which is most noticeable on the chalcogen antipodal σ hole (Figure 4.1).[95]

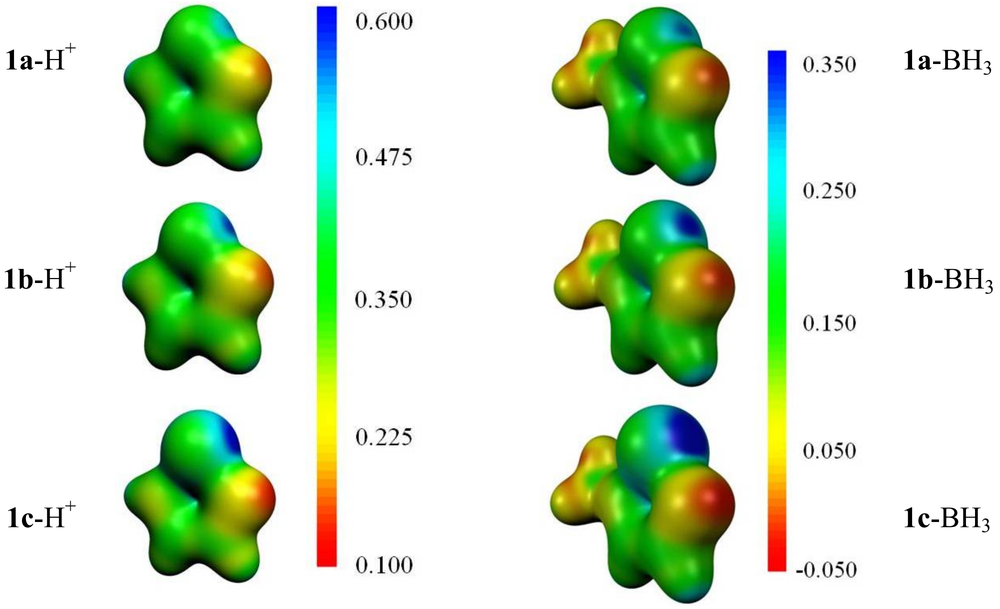

Figure 4.1 Maps of electrostatic potential (a.u.) on the 0.03-a.u. isodensity surfaces of {**1a**-**c**}-H^+ (left) and {**1a**-**c**}-BH_3 (right). Adapted from reference 95.

The crystal structure of **8a**, the 1:1 borane adduct of benzotelluradiazole, features a dimeric structure in which the $[Te\text{-}N]_2$ supramolecular synthon contains very short SBIs.[70] The Te···N SBI distances (2.593(1) and 2.578(7) Å) are shorter than the 2.688(1) Å observed in the crystal of the parent compound.

Those observations made it of interest to investigate the adducts of benzo-2,1,3-selenadiazole with Lewis acids such as triphenyl borane and boron trihalides (**12**). If these are acidic enough, they would strengthen the selenium-centred SBIs and induce dimerization of the adducts through the $[Se\text{-}N]_2$ supramolecular synthon.

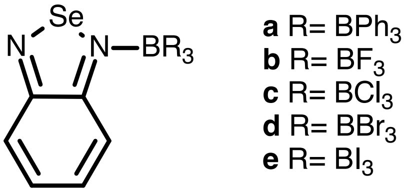

12

4.2 Results and Discussion

4.2.1 Synthesis

Slow addition of the boranes to benzo-2,1,3-selenadiazole in solution under an atmosphere of nitrogen yielded yellow-orange solutions from which crystalline materials were isolated and identified by single-crystal X-ray diffraction. The attempted synthesis of **12e** afforded elemental selenium, and the use of BI_3 was not pursued any further.

4.2.2 Crystal Structures

Crystallographic and refinement data for the borane adducts of the benzo-2,1,3-selenadiazole are presented in Table 2.1; selected distances and angles in each crystal structure are provided in Table 4.1.

The crystal structure of N-triphenylboryl-benzo-2,1,3-selenadiazole (**12a**) confirmed binding of triphenylborane to one nitrogen atom of the benzo-2,1,3-selenadiazole molecule. Unlike the telluradiazole analogue (**8a**)[70], the heterocycle does not dimerize through the formation of Se···N secondary bonds. Instead, one of the phenyl rings of a neighbouring molecule sits close to the chalcogen and the adjacent nitrogen atom, preventing such interaction. The structure features a short distance (3.448(2) Å) between the chalcogen and a carbon the ring located closest to the chalcogen, which is significantly shorter than the sum of the Se and C van der Waals radii (3.60 Å). The Se···Cπ interaction can also be assessed by comparing the N1-B1-C_{aryl} angles. The phenyl ring closest to the selenium atom defines an angle that is 3° smaller. Such an angle distortion is less pronounced than in the tellurium analogue.

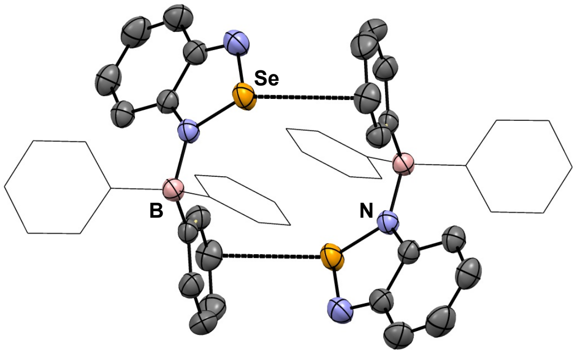

Figure 4.2 ORTEP (50% probability) of the asymmetric unit in the crystal of **12a**. Hydrogen atoms are omitted for clarity.

The crystal structures of **12b** and **12c** show binding of BX_3 to one nitrogen atom of the benzo-2,1,3-selenadiazole molecule and the adducts dimerize forming the $[Se\text{-}N]_2$ supramolecular synthon with SBI distances 2.782(2) and 2.865(3) Å, respectively (Figure 4.3a,b). These contacts are longer than those observed in the tetrafluoroborate (2.573(4) and 2.996(6) Å) and iodide (2.574(4) and 2.937(1) Å) salts of the **3b**[**19**]$_2$I$_2$ but much shorter than in the complexes of selenadiazoles with transition metal ions (**12**,**13**).[142] In contrast with the fluoride and chloride adducts, the bromide adduct (**12d**) does not dimerize.

In all cases, short contacts between the halogens and selenium are observed. Each selenium atom in **12b** engages in an intramolecular Se···F SBI (2.900(1) Å, Cf. $\sum r_{vdw} = 3.37$ Å); a second, longer (3.187(1) Å), contact to the F atom of another heterocycle above the plane would be a case of F···Se halogen bonding. The chlorine atom in **12c** engages in two distinct interactions with the selenium atom. (Figure 4.3c) The shortest (3.070(1) Å, Cf. $\sum r_{vdw} = 3.65$ Å) is intramolecular. Above and below the heterocycle plane, the Cl1 and Cl2 of neighbouring molecules sit at 3.521(4) Å, Cf. the sum of van der Waals radii 3.65 Å. In the case of **12d**, the shortest Se⋯Br SBI (3.109(3) Å) is again intramolecular, an intermolecular Se⋯Br SBI (3.276 (3) Å) is nearly coplanar and the same bromine atom is engaged in a 3.565(1) Å Br⋯Br SBI (Cf. $\sum r_{vdw} =$ 3.70 Å).

Table 4.1 Selected bond distances (Å) and angles (°) for **12b, 12c, 12d** and **13**

Compound	**12a**	**12b**	**12c**	**12d**	**13**
Se-N1	1.817(1)	1.814(2)	1.821(1)	1.840(2)	1.810(1)
Se-N2	1.770(1)	1.777(2)	1.766(1)	1.768(2)	1.810(1)
N1-C1	1.340(2)	1.335(2)	1.345(2)	1.344(3)	1.340(1)
N2-C2	1.334(2)	1.334(2)	1.343(2)	1.338(3)	1.340(1)
C1-C2	1.446(2)	1.448(3)	1.447(2)	1.449(3)	1.446(2)
C2-C3	1.428(2)	1.431(2)	1.420(2)	1.429(3)	1.421(1)
C3-C4	1.354(2)	1.356(2)	1.366(2)	1.361(4)	1.368(2)
C4-C5	1.428(2)	1.436(3)	1.438(2)	1.435(4)	1.4399(2)
C5-C6	1.360(2)	1.363(3)	1.364(2)	1.366(3)	1.368(2)
C1-C6	1.426(2)	1.422(2)	1.422(2)	1.428(3)	1.421(1)
B1-N1	1.631(2)	1.613(3)	1.564(2)	1.553(3)	1.585(2)
N1-B1-R1	103.6(1)	104.9(2)	106.8(1)	107.0(1)	103.92(7)
N1-Se-N2	92.0(1)	90.68(8)	90.62(1)	90.9(1)	87.1(1)
Se-N1-C1	108.7(1)	109.9(1)	110.39(1)	109.7(2)	113.4(1)
Se-N2-C2	109.0(1)	110.5(1)	110.47(1)	109.9(2)	113.4(1)

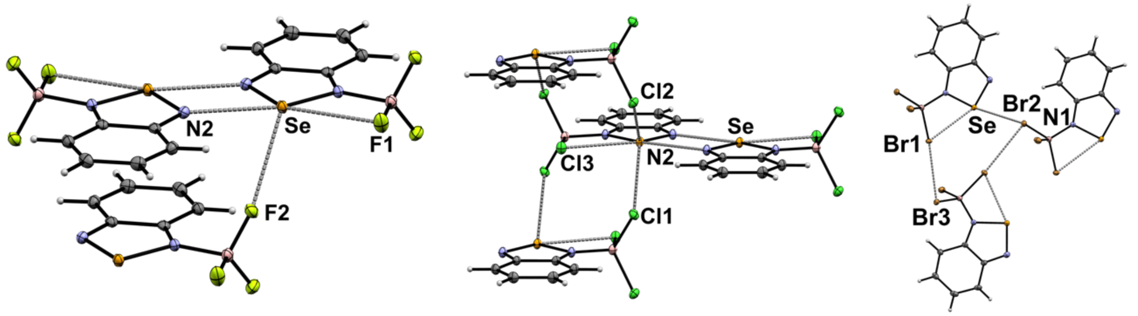

(a) (b) (c)

Figure 4.3 ORTEP and short contacts in the crystal structure of (a) **12b** (b) **12c,** and (c) **12d**. Displacement ellipsoids are shown at the 50% probability level.

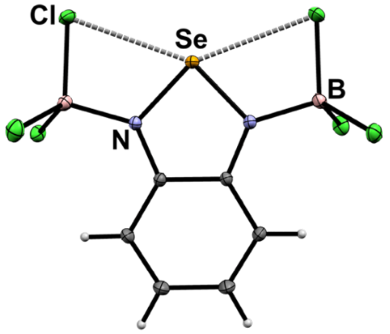

Figure 4.4 Molecular structure in the crystal of **13.** Displacement ellipsoids are shown at the 50% probability level.

Initial attempts to synthesize **12c** yielded the 1:2 adduct **13**. The molecule cannot dimerize because both nitrogen atoms are bound to BCl_3 (Figure 4.4). However, the structure features intramolecular Se···Cl SBIs with both distances at 2.865(1) Å (Cf. the Se-Cl SBI in **12c**, 3.065(5) Å). A small Se-N-B-Cl torsion angle of 3.010° indicates that N-

B-Cl plane molecule is nearly co-planar with the selenadiazole ring. These features result from the enhanced electrophilicity of the selenium atom. The structure is analogous to that of **6,** which features Te-Cπ SBIs.

4.2.3 NMR Spectroscopy

The resonances of the aromatic protons of the selenadiazole in adducts **12b-12d** occur at 7.16 to 8.61 ppm, the most deshielded signal belongs to the BBr_3 adduct. The ^{77}Se NMR chemical shifts of **12c** and **13** were obtained by ^{1}H-^{77}Se heteronuclear multiple bond correlation (HMBC) experiments. Their chemical shifts appear at lower frequency than those of the **3b** molecule (1528.4 ppm) and higher frequency than the monocations $[C_6H_4N(NR)Se][I]$ (R= Me, iPr, ^{t}Bu) (**6.1**). The HMBC experiment for **12a** and **12d** was unsuccessful due to the low solubilities of the compounds. All ^{13}C NMR spectra show 6 aromatic carbons located in the region of 120.7 – 136.9 ppm, which are lower than those observed for **6.1**.

4.2.4 DFT Calculations

The effect of the boranes on the stability of the $[Se\text{-}N]_2$ supramolecular synthon in the dimers of **12b-12d** was examined by use of DFT-D3 calculations. Models of **12b**$_2$ and **12c**$_2$ were optimized starting from the coordinates from the crystallographic determinations, the hypothetical dimer **12d**$_2$ was also minimized without convergence problems. Optimized Se···N SBI distances and energetic contributions are summarized in

Table 4.2. For **12b** and **12c,** the calculated Se···N SBI distances are respectively underestimated by 0.005 and 0.115 Å. A greater deviation in the latter case is not

unexpected given the heavier halogen atoms in the model. However, the calculation gives shorter Se···N SBIs for **12c**$_2$ than for **12b**$_2$, contrary to the experimental result. The longest Se···N SBI was calculated for **12d**. The calculated total energies of dimerization change very slightly, they are ca. 9 kJ mol^{-1} larger than for **1b**$_2$ but ca. 13 kJ mol^{-1} smaller than in the pseudotrimer **3b**[**19**]$_2$I$_2$ (Chapter 6). Contributions to the total interaction energy (E_{Int}) of dimerization, evaluated with the Ziegler-Rauk transition state formalism,[124] are all greater in magnitude for **12c**$_2$. In all three cases the covalent contribution (E_{Orb}) is dominant over the combination of the electrostatic interactions (E_{Elstat}) and Pauli repulsion (E_{Pauli}).

Table 4.2 Se···N SBI distance (Å) and contributions to the binding energies (kJ mol^{-1}) of the [Se-N]$_2$ supramolecular synthon in the dimers of **12b-12d**.

R	F	Cl	Br
Dimer	**12b**$_2$	**12c**$_2$	**12d**$_2$
$d_{Se...N}$	2.778	2.750	2.822
E_{Elstat}	-90.80	-98.16	-82.24
E_{Pauli}	118.68	133.09	106.03
E_{Steric}	27.87	34.93	23.79
E_{Orb}	-58.92	-65.26	-53.4
E_{Disp}	-10.36	-11.97	-12.4
E_{Int}	-41.41	-42.31	-42.02

In contrast with the apparent lack of a trend in the energetic contributions to the SBIs, the electron density and its Laplacian at the bond critical point (BCP) calculated with

Bader's Theory of Atoms in Molecules (AIM)[141] decrease with the mass of the halogen (Table 4.2) and are intermediate with respect to the values calculated for $\mathbf{1b}_2$ and $\mathbf{3b}[\mathbf{19}]_2I_2$ (Chapter 6, Table 6.5)[143].

4.2.5 Summary

The benzo-2,1,3-selenadiazole adducts of four boranes were prepared and characterized by NMR spectroscopy and single-crystal X-ray diffraction. The products from the most electron-withdrawing boranes dimerize through the $[Se\text{-}N]_2$ supramolecular synthon. Similar to the **8a** and **9**, the trihaloborane adducts of benzo-2,1,3-selenadiazole could not be easily used as supramolecular building blocks due to their moisture sensitivity but these compounds do demonstrate the enhancement of the Se···N SBIs.

Chapter 5. Structure and Magnetic Properties of the Coordination Polymers of Benzo-2,1,3-Selenadiazole.

5.1 Introduction

Intermolecular interactions between ligands can be used to tailor the structure and properties of a metal-organic framework.[144,145] An interesting example of this concept is given by the structures of trans-[$CoCl_2L_2$] [L=3,5-$X_2C_5H_3N$] (Figure 5.1) which feature arrays of parallel $[Co(\mu\text{-}Cl)_2]_\infty$[146] chains running perpendicular to the average plane of the $[X]_4$ supramolecular synthon (Figure 5.1) assembled by the dihalopyridine axial ligands. Although the halogen-halogen SBIs (clear examples of halogen bonding) favour organization of the cobalt(II) parallel chains in a tetragonal lattice, the size of the ligands keeps them 9.7 Å from each other. Because of the long distance between the $(MX_2)_\infty$ chains and the C-X···X angle, spin-spin interactions are weak and overall ferromagnetism is observed at low temperatures. This is in sharp contrast with the antiferromagnetic behaviour of materials with shorter distances between the $[Co(\mu\text{-}Cl)_2]$ chains.

(a) (b)

Figure 5.1 (a) Pyridine-based building block (where X= Cl, Br) and (b) the halogen bonding of the ferromagnetic chains based on Co(II) coordination polymers

There are several examples of structures containing the $[M(\mu\text{-}Cl)_2]_\infty$ arrangement, but such long interchain (M···M) distances are rare. One notable case is that of the crystal structure of $[HgCl_2(\mathbf{3b})_2]$[147]. In that lattice, a $[Hg(\mu\text{-}Cl)_2]_\infty$ chain is flanked by N-coordinated molecules of **3b**, which complete an octahedral coordination sphere. Each heterocycle is, in turn, linked to the selenadiazole of a neighbouring chain by the Se-N SBIs. The result is a layered arrangement with parallel metal chains separated by 9.7 and 11.2 Å. Therefore, it was of interest to explore whether such crystal structures can be obtained from light *d*-block metal ions with a high-spin configuration and if so, examine the magnetic properties of such materials.

As the nitrogen atoms of the heterocycle have the competing roles of coordinating the metal ion and forming SBIs, the overall structure would depend on the relative strengths of M-N and Se···N interactions. In addition, stoichiometry could also influence the overall arrangement. The structure $[HgCl_2(C_6H_4N_2Se)_2]$ obtained from mixing only one equivalent of selenadiazole with $HgCl_2$ features each heterocycle bound to two metal ions.[148] The M-M distances are 7.3 and 9.2 Å. Similarly, the size of the metal ion can limit the coordination number; the structure of $[ZnCl_2(C_6H_4N_2Se)_2]$ forms the $[Se\text{-}N]_2$ supramolecular synthon but with the metal in a tetrahedral geometry. This is in sharp contrast with the Zn(II), Cd(II) and Hg(II) complexes of 3,5-dihalopyridines which constitute an isostructural family. Rather, the Zn structure is related to chains observed in the two polymorphs of $[Ag(NO_3)(C_6H_4N_2Se)_2]]\cdot 1/2K(C_6H_4N_2Se)$.[149]

5.2 Results and Discussion

When two equivalents of **3b** were combined with MCl_2 (M= Mn, Fe, Co, Ni and Cd) in anhydrous DMSO, solid microcrystalline products separated within seconds. Single crystals of each material were grown by slow diffusion of the ligand into a solution of the metal salt. However, no solid product could be obtained from Cr(II) or Zn(II) chloride with this method.

Details of the crystallographic determinations are compiled in Table 2.1, and selected bond distances and angles are listed in Table 5.1. Two distinct families were observed for these products. The first is isostructural with $[HgCl_2(C_6H_4N_2Se)_2]$ and was formed when M = Mn (**14**) and Cd (**15**). The $[M(\mu\text{-}Cl)_2]_\infty$ chains (Figure 5.2) are parallel to the *a* axis while the coordinated benzoselenadiazoles extend the structure along the *ac* diagonal by formation of the $[Se\text{-}N]_2$ supramolecular synthon, and the layers defined in this way stack along the *b* axis. The interchain M···M distance ranges correspond to the lengths of *b* and *c* axes (ca. 9.3 and 10.8 Å, respectively).

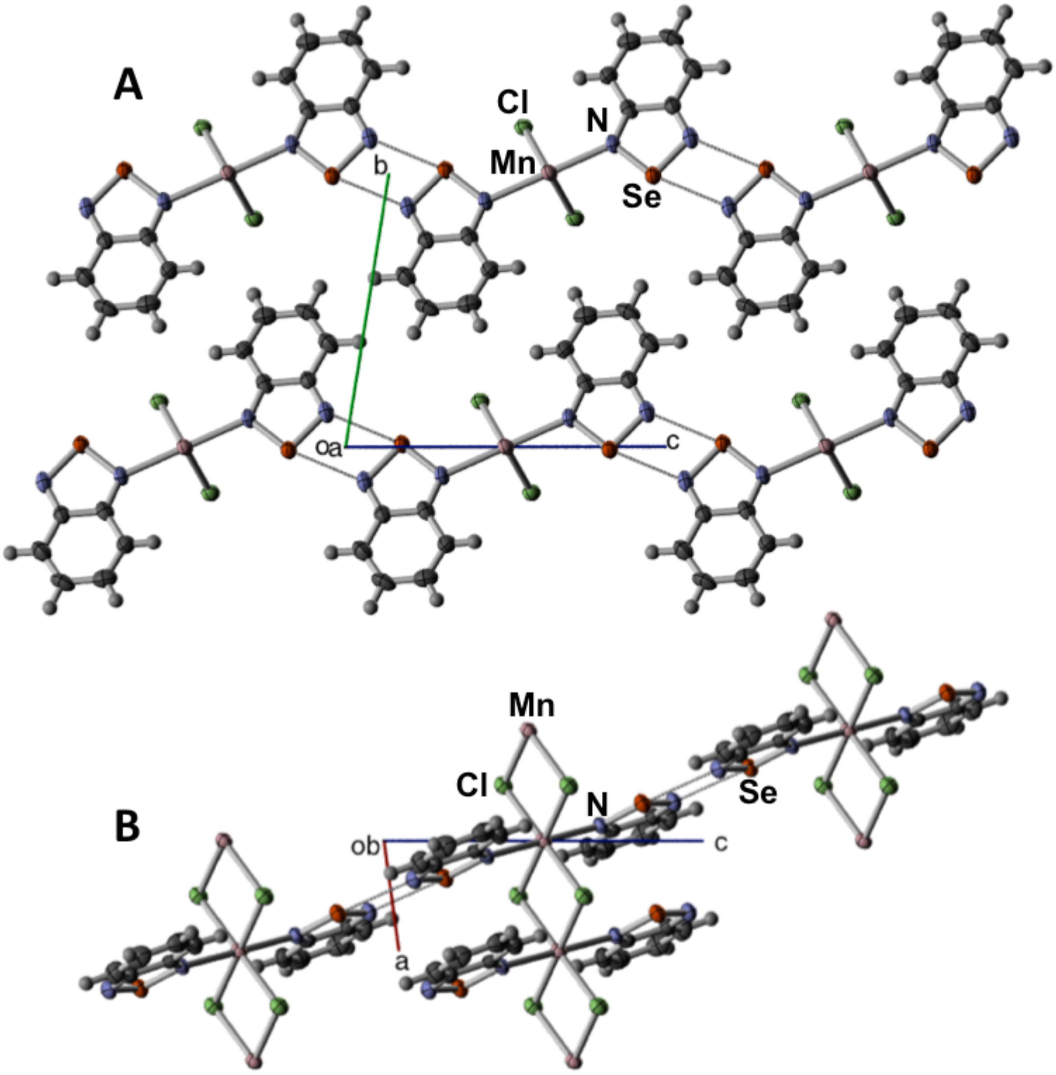

Figure 5.2 Two views of the crystal structure of [$MnCl_2(C_6H_4N_2Se)_2$] (**14**). **A**: along a; **B**: along b. Displacement ellipsoids are shown at the 50% probability level.

Table 5.1 Selected bond distances (Å) and angles (°).

	$[MCl_2(C_6H_4N_2Se)_2]$		
Compound Reference	**14**	**15**	
M	Mn	Cd	
M1-Cl1	2.5479(8)	2.617(3)	
M1-Cl2	2.5379(8)	2.603(3)	
M1-N1	2.324(2)	2.407(9)	
Se1-N1	1.782(3)	1.77(1)	
Se1-N2	1.803(2)	1.816(8)	
C1-N1	1.324(1)	1.32(1)	
C6-N2	1.333(4)	1.32(2)	
C1-C6	1.452(4)	1.46(2)	
Se1···N1	2.865(2)	2.849(1)	
N1-Se1-N2	92.9(1)	92.5(4)	
M1-N1-Cl1	135.5(2)	136.0(7)	
Se1-N2-C6	107.8(2)	107.5(7)	
N1-C1-C6	116.2(3)	115(1)	
N2-C6-C1	115.0(3)	116(1)	

	$[MCl_2(Me_2SO)_2(\mu\text{-}C_6H_4N_2Se)]$		
Compound Reference	**16**	**17**	**18**
M	Fe	Co	Ni
M1-Cl1,	2.456(1)	2.4155(1)	2.3838(7)
MCl2	2.472(1)	2.4365(1)	2.4029(7)
M1-O1	2.080(3)	2.075(1)	2.085(2)
M1-O2	2.093(4)	2.104(1)	2.065(2)
M1-N1	2.202(4)	2.179(1)	2.120(2)
Se1-N1	1.792(4)	1.791(1)	1.788(2)
C1-N1	1.345(6)	1.336(2)	1.332(3)
C1-C6	1.447(6)	1.455(2)	1.452(3)
M---M	6.755(1)	6.6979(6)	6.5599(9)
N1-Se1-N2	92.8(2)	92.58(6)	92.33(8)
C1-M-Cl2	177.60(5)	177.37(2)	177.86(2)
Cl1-M-N1	87.4(1)	87.78(3)	88.63(5)
M1-N1-Cl1	134.9(3)	135.1(1)	135.4(1)
Se1-N2-C6	108.1(3)	108.7(1)	108.8(1)
N1-C1-C6	114.9(4)	115.1(1)	115.0(2)
N2-C6-C1	115.8(4)	115.0(1)	114.9(2)

The second family of composition [$MCl_2(Me_2SO)_2(\mu\text{-}C_6H_4N_2Se)$], was obtained with M = Fe (**16**), Co (**17**), Ni (**18**). This new structural motif (Figure 5.3) consists of $MCl_2(Me_2SO)$ coordination centres bridged by selenadiazole molecules forming infinite chains along the *b* axis; each metal ion is in a distorted octahedral environment. The M-L bond distances suggest that the smaller ions prefer the second structural type.

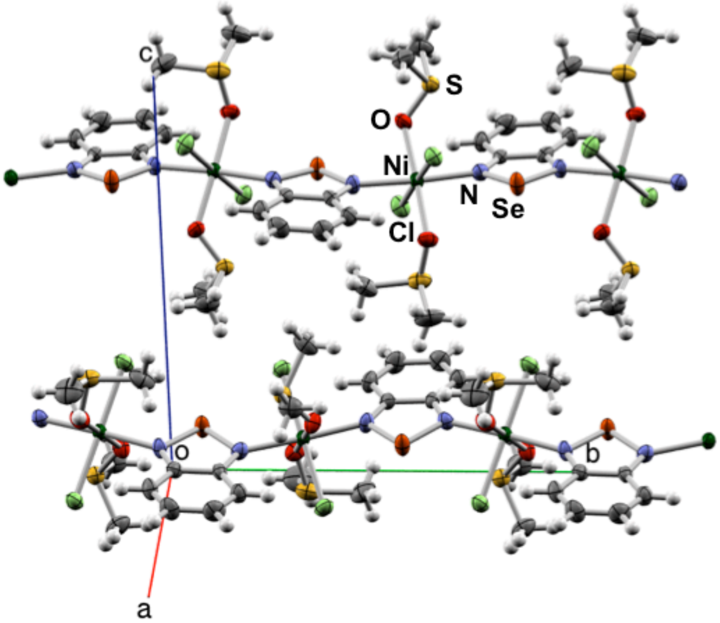

Figure 5.3 Crystal structure of [$NiCl_2(Me_2SO)_2(\mu\text{-}C_6H_4N_2Se)$] (**18**). Displacement ellipsoids are shown at the 50% probability level.

The benzoselenadiazole molecule is little affected by coordination of the metal ions. The similarity of the bond distances and angles with the dimensions of the free molecule indicate there is no electron transfer between the metal and the ligand. In apparent agreement, the room-temperature magnetic susceptibilities of the open-shell species are consistent with the number of unpaired electrons of each ion.

The magnetic susceptibilities of **14** and **16-18** were measured between 2 and 300 K and the data are presented in Figure 5.4. As the temperature decreases, the magnetic susceptibility of **14** and **16-18** increases. At higher temperatures, all these compounds obey the Curie-Weiss law. At the lowest temperatures, such behaviour was strictly followed only by **14**, and **17** displayed small deviations attributable to single-ion effects. In the latter case, while the Curie-Weiss fitting above 100 K provides a reliable measurement of the powder-averaged effective magnetic moment, the interpretation of the Curie-Weiss constant could be ambiguous as it is not purely due to exchange.

Moreover, in the cases of **16** and **18**, clearly-defined maxima (Figure 5.4), indicative of short-range ordering, appeared below 20 K before the onset of long range antiferromagnetic ordering at 7 K and 4 K, respectively. The profiles for **16** and **18** were therefore modeled assuming coupling between neighbours (Equation 5.1) using the Fisher classical model[150] based on one-dimensional antiferromagnetically coupled Heisenberg chains, which at high temperatures converges with the Curie-Weiss law (Equation 5.2) Fitting all data to the respective non-linear models are compiled in Table 5.2. Plots of χT revealed deviations from the model for **18** over 60 K.

$$H = J\sum_{i} S_i \bullet S_{i+1} \tag{5.1}$$

$$\chi_M = \frac{N_A g^2 \mu_B^2 S(S+1)}{3k_B(T-\theta)} \bullet \frac{1-u}{1+u} \tag{5.2}$$

where

$$u = \frac{T}{JS(S+1)/k_B} - \coth\frac{JS(S+1)/k_B}{T}$$

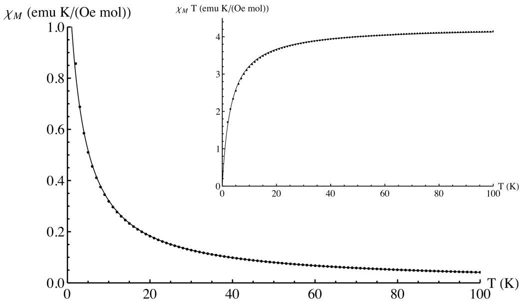

14, M = Mn

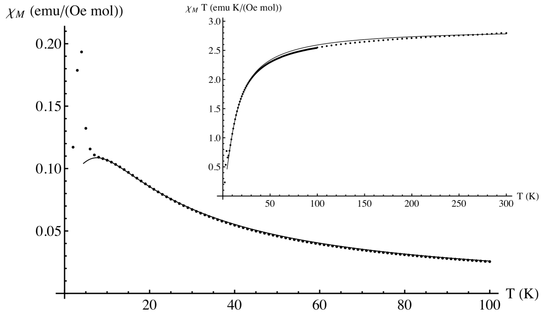

16, M=Fe

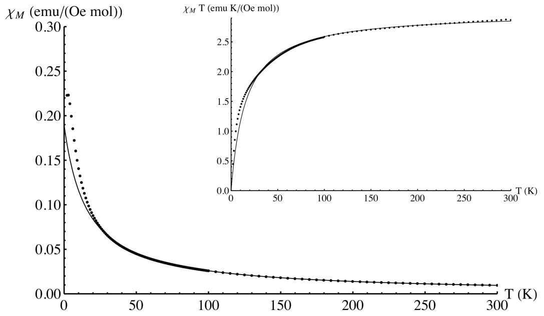

17, M = Co

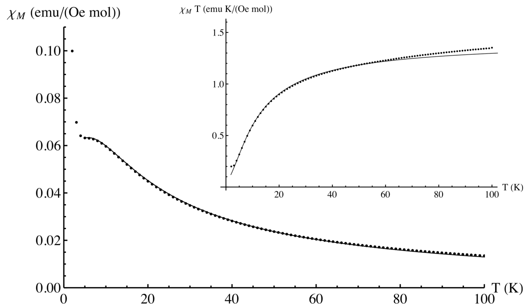

18, M = Ni

Figure 5.4 Temperature dependence of the molar magnetic susceptibilities of **14, 16-18**. Each continuous line is calculated by the corresponding fitted nonlinear model.

Table 5.2 Fitted magnetic parameters

Compound	**14**	**16**	**17**	**18**
M	Mn	Fe	Co	Ni
g	1.94±0.01	1.962±0.002	2.42±0.01	2.384±0.003
J (K)*		-2.64±0.01		-7.12±0.08
C (cm^3 K mol^{-1})	4.10±0.02	2.90±0.01	2.74±0.02	1.43±0.01
θ (K)	-2.85±0.03	0	-9.9±0.2	0.32±0.02

*1 kK = 1000 cm^{-1}

Hybrid UDFT calculations (ADF, B3LYP/ZORA) with all-electron basis sets of triple-ζ quality and two sets of polarization function were performed to analyze the spin-spin interactions in the crystals. The analyses were based on the model fragments shown in Figures 5.5-5.8). The resulting molecular orbitals were employed in Broken-Symmetry calculations in order to evaluate the J coupling constants without spin projection[151] using equation 5.3, where E_{HS} and E_{BS} are the high-spin and broken-symmetry energies.

$$E_{HS} - E_{BS} = -J(2S_1S_2 + S_2) \qquad (5.3)$$

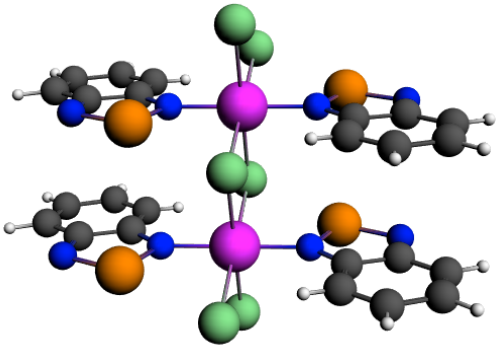

Figure 5.5 Model used for the calculation of the coupling constant between two Mn (II) ions along the $[MnCl_2]_\infty$ chains of compound **14** (*J* = 0.4 K).

The *J* values calculated in this way are shown in the caption of each figure. The serious disagreement between calculation and experiment indicates that the properties of these materials cannot be accounted from simplistic models for one pair of atoms at a time.

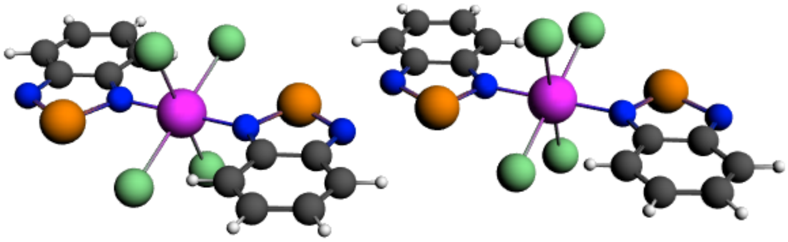

Figure 5.6 Model used for the calculation of the coupling constant between two Mn (II) ions through two molecules of benzoselenadiazole and the $[Se\text{-}N]_2$ supramolecular synthon of compound **14** (*J* = 4,377 K).

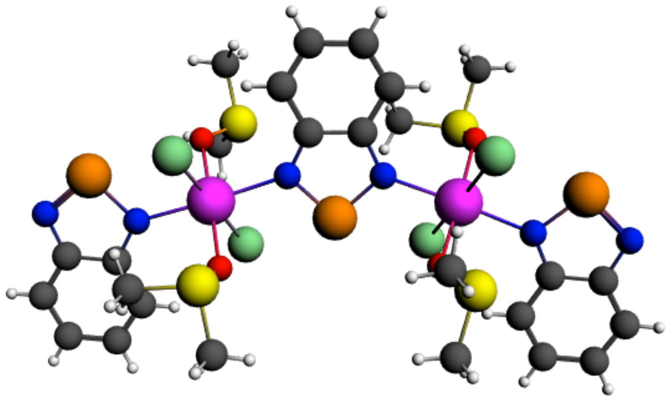

Figure 5.7 Model used for the calculation of the coupling constant between two M(II) ions through one molecule of benzoselenadiazole in compounds **16** (M = Fe, J = -216 K), **17** (M = Co, J = 4.2 K), and **18** (M = Ni, J = 5.6 K).

In the case of Mn (II), the coupling constant along $[\mathrm{MnCl_2}]_\infty$ chains is small, as expected from the nearly 90° Cl-Mn-Cl bond angles. The large coupling constant through the ligands (including the $[\mathrm{Se\text{-}N}]_2$ supramolecular synthon) suggests that there is spin delocalization on the heterocycles. Calculations for a $[(\mathrm{C_6H_4N_2Se})\mathrm{MnCl_4}(\mathrm{C_6H_4N_2Se})]^{2-}$ model afforded a map of spin density (Figure 5.8) which supports such interpretation. The spin density is heavily localized around the metal ion, however there is some delocalization in the ligand, suggesting there is a spin-communication through the Se-N secondary bonds. Delocalization of spin into the heterocycle would be enabled by molecular orbitals in the σ and mostly the π frameworks (Figure 5.9).

This is of special case that demonstrate the ability of Se-N secondary bonds to modulate the electronic properties of metal complexes, similar to Cozzolino's design of

NLO materials by manipulating the distortion of the $[Te\text{-}N]_2$ supramolecular synthon in **2** and **6**. This strategy has also been applied in the cationic complex of [Fe(N-(8-quinolyl)salicylaldimine)]$^+$, in which halogen bonding is used to induce the spin crossover behavior.[152]

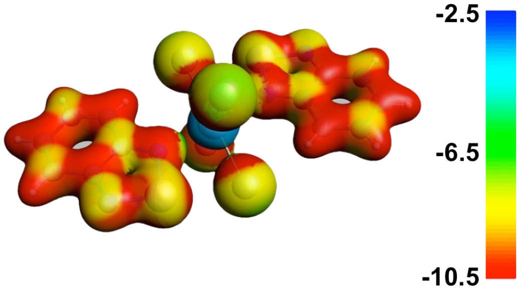

Figure 5.8 Spin-density (Log$_{10}$ scale of the magnitude in a.u.) of **14** model projected over the 0.03-a.u. electron density isosurface.

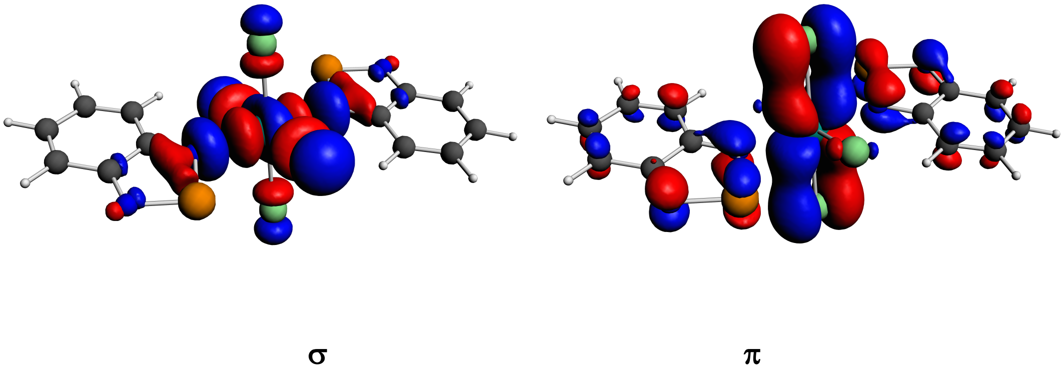

Figure 5.9 Kohn-Sham molecular orbitals that delocalize spin density from the metal ion into the selenadiazole ring of compound **14**.

5.3 Summary

Reaction of benzo-2,1,3-selenadiazole and chloride salts of divalent Mn, Fe, Co, Ni, and Cd from DMSO gave two different structural family of complexes. Crystal structures bearing smaller ions (Fe, Co, Ni) display infinite chains of metal atoms N,N'-bridged by the heterocycle. The larger ions, however, stabilize chains of metal atoms bridged by μ^2 halide ions and can establish a link to the next chain in the lattice through the Se-N SBIs.

Chapter 6. N-substituted Selenadiazolium Cations

The contents of this chapter have been published in:

L. M. Lee, V. C. Corless, M. Tran, H. Jenkins, J. F. Britten, I. Vargas-Baca. *Dalton Trans.* **2016**, *45*, 3285 – 3293. DOI: 10.1039/c5dt04314j

6.1 Introduction

The crystallographic evidence presented in Chapters 4 and 5 confirms that attachment of a Lewis acid such as a transition metal ion or a borane to one nitrogen atom of the heterocycle strengthens the secondary interactions made by Se, shortening the corresponding distances. Such an effect is also strong in the cations formed by *N*-alkylation and is consistent with the explanation for the peculiar trend in reduction potentials of the **8b** cations in acetonitrile.[153] Chapter 3 also discussed that such evidence of molecular association in solution through SBIs is consistent with the observation of $[M_2H]^+$ supramolecular aggregates in the mass spectrum of **3c**.[73]

N-alkyl substituted chalcogenadiazolium cationic rings could therefore be a convenient alternative to telluradiazoles in supramolecular architecture, provided that they are reasonably stable and their preparation methods are flexible enough to accommodate multiple variations in the structure. The most straightforward synthetic method would be the direct alkylation of the heterocycle. However, early reports of this approach describe very inefficient reactions plagued by multiple by-products with most common alkylating reagents.[154,155] Clean and efficient alkylations were reported more recently using very reactive agents such as Me-OS(O)$_2$-R' (R' = OMe, $C_6H_2(NO_2)_2$-2,4),[154] F_3C-SO_3-CH_3[75] or $(CH_3)_3O^+BF_4^-$[156]; but these methods are applicable with only a handful of alkyl groups. Alternatively, the alkyl group could be attached to nitrogen before formation of the heterocycle. This approach was actually claimed in an early publication[154,155] but its products were not structurally authenticated. A third route to N-alkyl telluradiazolium cations, also limited in flexibility, consists of the spontaneous de-alkylation of one N nitrogen atom during the reaction of N,N'-bis(tert-butyl)-diazabutadiene with $SeCl_4$.[157]

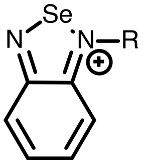

19

19a = CH_3
19b = $CH(CH_3)_2$
19c = $C(CH_3)_3$

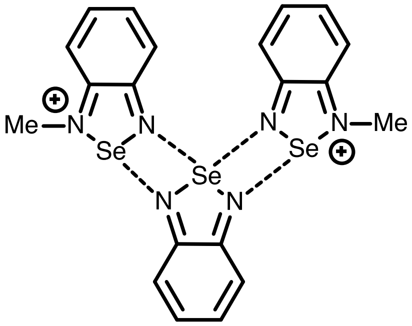

3b·19a$_2$

In this chapter, we compare the two most flexible synthetic methods for the preparation of the derivatives with primary, secondary and tertiary alkyl groups (**19**). We examine the crystal structures of their iodide salts, the affinity of the cations for halide anions, and spectroscopic properties useful for the characterization of these species in solution.

6.2 Results and Discussion

6.2.1 Crystal Structures of N-alkyl Benzoselenadiazolium iodides

Benzo-2,1,3-selenadiazole is a weak base which is readily protonated by strong acids.[117] For this reason, the purported inefficiency[154,155] of its reaction with primary alkyl-iodides is unusual and merited reinvestigation using a more reactive tertiary iodide. Initial attempts at atmospheric alkylation with $(CH_3)_3CI$ in a hot toluene solution yielded a complex mixture, as made evident by the ^{1}H NMR spectrum. Slow evaporation of the solution yielded a mixture of crystals having several morphologies; three of which were identified by single-crystal X-ray diffraction: [**19c**][I_3], [**3b**]$_2$[**3b**-H]$_2$[I][I_3] and [**3b**]$_2$($C_6H_4(NH_2)_2H^+$)$_2$][I]$_2$. The first species does contain the *N*-*tert*-butyl benzoselenadiazolium cation (**19c**), which demonstrates that the alkylation reaction does proceed. However, the presence of the triiodide anion, plus protonated phenylenediamine and benzoselenadiazole point to the actual problem with this experiment: the iodide ion is likely oxidized by atmospheric oxygen to I_3^- which then halogenates the solvent or benzoselenadiazole to generate HI. Crystals of [**19c**][I] were obtained when the reaction was carried out under an atmosphere of nitrogen, albeit in low yield. Similarly, the alkylation reaction proceeded with neat CH_3I in anaerobic conditions, however, in this case the alkylation is incomplete due to the formation of the crystalline **3b**[**19a**]$_2$[I]$_2$, which was identified by X-ray diffraction. The salt [**19a**][I] was obtained from **3b**[**19a**]$_2$[I]$_2$ by recrystallization from dilute solutions. Interestingly, *iso*-propyl iodide was completely unreactive towards benzoselenadiazole under the same conditions. While the reaction of *tert*-butyl iodide is likely to proceed by a S_N1 mechanism, it is likely that the primary and secondary iodides prefer a SN_2 mechanism but steric hindrance prevents the reaction of the *iso*-propyl halide.

Even in aqueous medium, benzoselenadiazole is readily formed by the reaction of H_2SeO_3 and phenylenediamine. *N*-substituted *ortho*-diamino benzenes were reported to undergo an analogous reaction in glacial acetic acid producing the benzoselenadiazolium cations, which are isolated by precipitation with sodium halide.[158,159] This procedure works as expected but it was found to be more convenient to carry out the reaction in a mixture of ethanol and trifluoroacetic acid in order to avoid using the less volatile acetic acid. Structural characterization by X-ray diffraction did confirm the identity of the products. In addition, the exposure of the cations in solution to the atmosphere resulted in iodide oxidation and crystallization of the corresponding triiodide salts, which was verified by the strong scattering band[160] at 111 cm^{-1} in the Raman spectrum or crystallographic analysis. Crystallographic and refinement data for the salts of the three cations are presented in Table 2.1; selected distances and angles in each crystal structure are provided in Table 6.1.

Table 6.1 Selected bond distances (Å) and angles (°) for **3b[19a]**$_2$[I]$_2$ and **19a-c**.

Compound	**3b**[**19a**]$_2$[I]$_2$	[**19a**][I]	**19b**[I$_3$]	[**19b**][I]	[**19b**][I$_3$]	**19c**·I
Se-N1	1.856(5)	1.785(2)	1.766(3)	1.774(3)	1.742(5)	1.749(2)
Se-N2	1.777(5)	1.875(2)	1.857(3)	1.881(2)	1.841(4)	1.864(2)
N1-C1	1.339(7)	1.327(3)	1.333(4)	1.333(4)	1.349(8)	1.343(3)
N2-C6	1.336(7)	1.329(3)	1.338(4)	1.338(4)	1.347(6)	1.339(3)
C1-C6	1.443(7)	1.440(3)	1.444(4)	1.439(4)	1.414(7)	1.442(4)
C1-C2	1.432(8)	1.431(3)	1.355(5)	1.428(6)	1.414(7)	1.421(4)
C2-C3	1.366(8)	1.351(4)	1.426(5)	1.355(6)	1.342(9)	1.361(3)
C3-C4	1.428(8)	1.431(4)	1.426(5)	1.360(4)	1.400(9)	1.417(4)
C4-C5	1.371(8)	1.359(3)	1.353(4)	1.427(5)	1.345(9)	1.368(4)
C5-C6	1.428(8)	1.422(3)	1.422(5)	1.425(5)	1.418(1)	1.421(3)
N1-Se-N2	88.7(2)	88.16(9)	89.6(1)	88.6(2)	90.4(4)	90.2(1)
Se-N1-C1	111.3(4)	111.2(2)	110.7(2)	111.0(3)	109.7(7)	110.3(2)
Se-N2-C6	111.6(4)	111.4(1)	110.6(2)	111.0(3)	109.8(7)	110.2(2)
Se-N2-C7	124.0(4)	124.9(2)	124.4(2)	124.7(3)	122.4(6)	122.4(2)
C6-N2-C7	124.4(5)	123.7(2)	125.1(3)	124.3(3)	127.8(8)	127.5(2)

The crystal structure of **3b**[**19a**]$_2$[I]$_2$ consists of a molecule of **3b** bound to two **19a** conforming a pseudo-trimer assembled by two asymmetric [Se–N]$_2$ supramolecular synthons with asymmetric SBI distances of 2.573(4) and 2.937(1) Å. This aggregate is analogous to the product formed by the reaction of **3b** with [(CH$_3$)$_3$O][BF$_4$],[156] in which the Se···N and Se···F secondary bonding distances are 2.573(2) and 2.966(6) Å and 2.970(4) Å respectively. In this arrangement, the molecules of **3b** and **19a** are nearly coplanar with a deviation angle of 5.06 °. This structure also features Se···I contacts at 3.528(1) Å and 3.831(1) Å. Both iodides sit out of the average plane of the aggregate forming a virtual four-membered ring (*i.e.* the [Se I]$_2$ supramolecular synthon) with the Se atoms of the **19a** molecules of two neighbouring pseudotrimers.

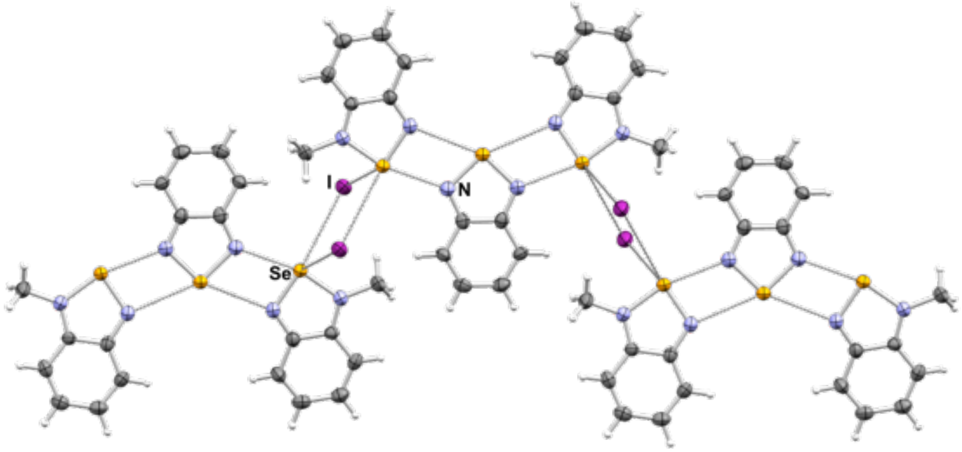

Figure 6.1 Arrangements of molecules and ions in the crystal **3b[19a]**$_2$[I]$_2$. Selected distances: Se···N1: 2.573(4) Å and 2.937(1) Å. Displacement ellipsoids are shown at the 50% probability level.

In clear contrast with the structures of the pseudo-trimers,[156] and the dimers observed for [**19a**][CF_3SO_3][75] and [$C_2H_2N(NC(CH_3)_3)Se$][Ga Cl_4],[121] the crystal structures of the iodide and triiodide salts of the alkylated cations **19a–c** feature no association of the heterocycles to each other. In all cases, strong Se–anion interactions prevent formation of the Se···N SBIs (Figure 6.2 and Figure 6.3).

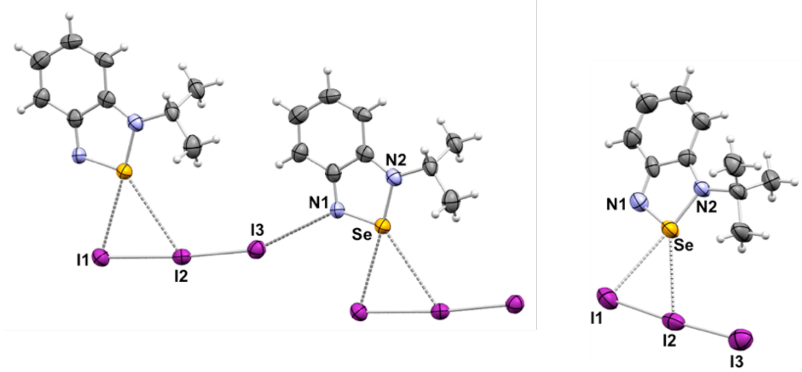

(a) **(b)**

Figure 6.2 Crystal structures of (a) **[19b]**[I_3] and (b) **[19c]**[I_3]. Displacement ellipsoids are shown at the 50% probability level. Selected bond distances (a) Se···I1: 3.249(1) Å, Se···I2: 3.626(4) Å; (b) Se···I1: 3.309(1) Å, Se···I2: 3.727(1) Å.

The triiodide anions in the crystals of [**19b**][I_3] and **[19c]**[I_3] engage in two interactions with the selenium atom. The shortest (3.249(1), 3.309(1) Å, respectively) is with the terminal iodine atom I1; the contact to the middle I2 atom is longer (3.626(1), 3.727(1) Å, respectively), *Cf.* the sum of van der Waals radii 3.88 Å. In the case of [**19b**][I_3] the terminal iodine atom I3 is in close proximity (3.491(3) Å, *Cf.* the sum of van der Waals radii 3.53 Å) to the nitrogen atom of a neighbouring **19b** cation, the nearly linear geometry of this arrangement is indicative of a halogen bond. Consequently, the I2–I3 bond is longer (2.879(1) Å) in [**19b**][I_3] than in [**19c**][I_3] (2.829(1)).

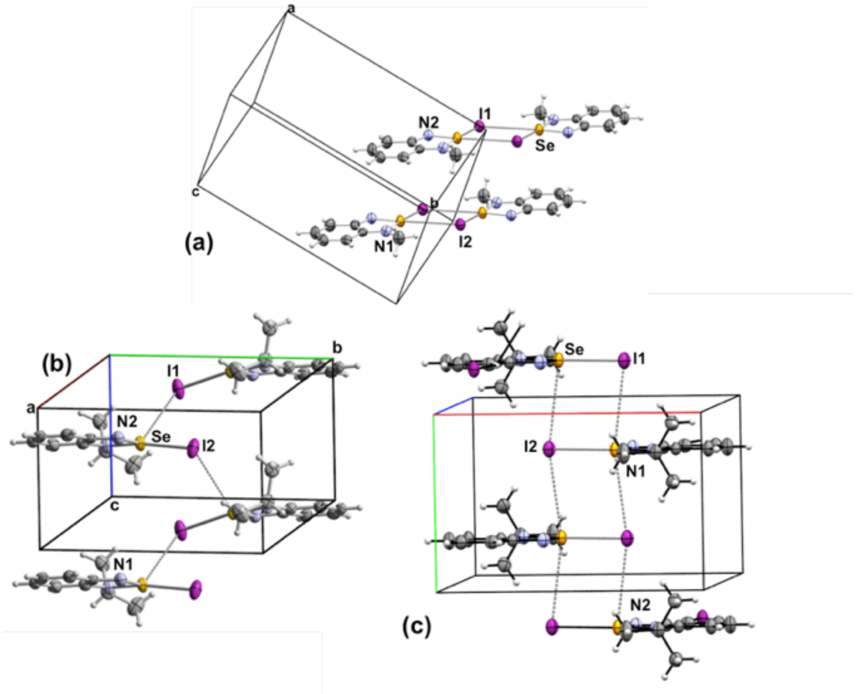

Figure 6.3 Packing arrangements in the crystal structures of the iodide salts of (a) **19a** (b) **19b** and (c) **19c**. Displacement ellipsoids are shown at the 50% probability level.

The arrangement of the ions and the Se···I interactions in the [**19a–c**][I] lattices are influenced the size of the alkyl group (Figure 6.3). The small methyl group in [**19a**][I] confines the Se···I interactions to the plane of the cation forming iodide-bridged dimers that form the $[Se\ I]_2$ supramolecular synthon with short (3.178 (1) Å) and long (3.610 (1) Å) SBIs. Similar binding of anions to Se has been observed in related species. For example, a virtual four-membered ring consisting of Se and Cl atoms is formed in the crystal structure of [$C_2H_2NN(H)Se$][Cl] (2.900(1) Å and (3.075 (1) Å).[117] The structure of

$[C_2H_2N(NC(CH_3)_3)Se][Cl]$ also features a planar selenadiazole ring with one Se–Cl bond distance of 2.605 (1) Å.[157] In contrast, the $GaCl_4^-$ salt of the same selenadiazole heterocycle does not display any Se–Cl short interactions, instead it contains the $[Se–N]_2$ supramolecular synthon.[121] The larger alkyl groups favour interlayer interactions (eminently electrostatic) in $[Se\ I]_\infty$ supramolecular chains. The Se–I distances are 3.043 (1) Å and 3.696 (1) Å in the structure of [**19b**][I] and 3.147 (1) and 3.880 (1) Å in [**19c**][I].

6.2.2 UV-vis Spectroscopic Studies

The iodide salts of **19a–c** are stable in air. The compounds are slightly soluble in water at room temperature, their solubility decreases with the size of the R group. In fact, it is possible to recrystallize **19a** from hot water. Aqueous solutions of the cations have a characteristic red-brown colour, their UV-vis absorption spectrum displays prominent maxima in the range of 330–343 nm and a weaker band between 440–460 nm. These spectra are in excellent agreement with the TD-DFT calculation for the **19a**, which attributes the bands to the LUMO ← HOMO and LUMO ← HOMO−1 excitations (Figure 6.4). The UV-vis spectra do not change from neutral to acidic pH, but hydrolysis ensues in basic medium. Given the modest solubility of the **19a–c** iodides, their ^{77}Se NMR chemical shifts are best obtained through $^1H–^{77}Se$ heteronuclear multiple bond correlation (HMBC) experiments. The ^{77}Se δ values (1455–1490 ppm) appear at slightly lower frequency than the 1515 ppm reported for $[C_6H_4N(NCH_3)Se][CF_3SO_3]$ in acetonitrile.[75] This difference in chemical shifts is small considering the range of resonances observed for other cationic selenium compounds,[161] this observation suggests anion binding in solution. For the pseudo-trimer **3b**[**19a**]$_2$[I]$_2$, two resonances were observed with frequencies that correspond to those of the constituting neutral and cationic molecules, suggesting that the aggregate dissociates in solution.

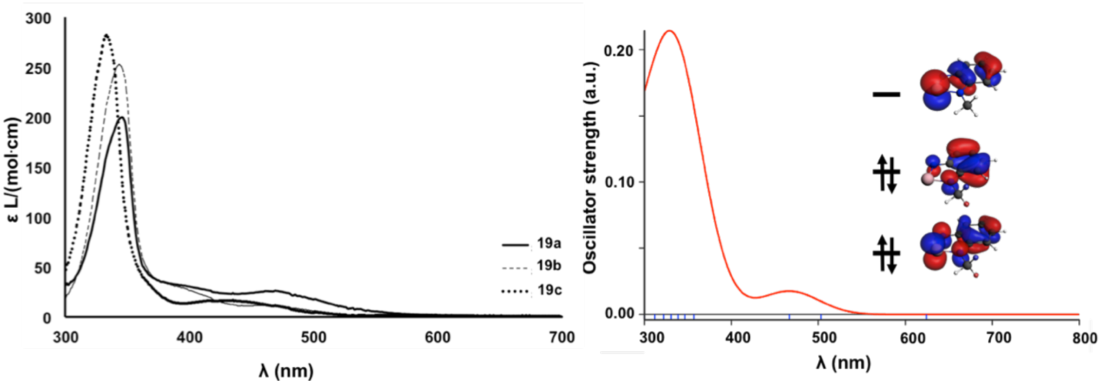

Figure 6.4 Experimental (left) and calculated (right) UV-vis spectra of [**19a**][I]. Frontier orbitals shown as inset in the calculated spectrum.

6.2.3 DFT Studies

As the crystal structures show there is competition between the formation of the [Se–N]$_2$ supramolecular synthon and binding of the anion to selenium, the relative strengths of these interactions were evaluated using DFT and were extended to include the chloride and bromide salts. For computational expediency, GGA calculations were performed with the PBE functional, supplemented by dispersion and relativistic corrections. Model structures were optimized from the crystallographic coordinates and expanded to include hypothetical isomers and the analogues with chloride and bromide anions. Whenever an experimental structure was available, bond lengths were reproduced within 0.01 Å, the largest deviations correspond to the intramolecular Se–N distances. Selenium-centred secondary bond distances were reproduced within 0.01 Å to nitrogen and 0.50 Å to iodide.

The large deviation in the latter case is likely due to the additional interactions of the anion in the lattices. Interaction energies were evaluated using the transition-state method[124] that partitions the energy of interaction between two molecules or fragments in a hypothetical process in which the constituting units are first calculated individually, brought to their equilibrium positions without orbital mixing, and finally the electron density is relaxed by the interaction of fragment orbitals. The change from the first to the second step is regarded as the total steric interaction that results from the sum of the electrostatic (E_{Elstat}) and Pauli-repulsion (E_{Pauli}). The third step gives the orbital interaction energy (E_{Orb}). Dispersion is treated as a separate contribution (E_{Disp}). The total interaction energy is given by the sum of all contributions (Equation 6.1).

$$E_{\mathrm{Interaction}} = E_{\mathrm{Elstat}} + E_{\mathrm{Pauli}} + E_{\mathrm{Orb}} + E_{\mathrm{Disp}} \qquad (6.1)$$

Three partitioning schemes (Figure 6.5) were used to evaluate the secondary interactions within the pseudo-trimer **3b**[**19a**]$_2$[I]$_2$ the results are summarized in Table 6.2. In this analysis, the average interaction energy of the [Se–N]$_2$ supramolecular synthon was 56.4 kJ mol^{-1}. Formation of the interactions in iii and ii could be regarded as steps in the assembly of the pseudotrimer and the calculations show that the interaction energies are nearly additive.

Table 6.2 Contributions to the energies (kJ mol^{-1}) of fragment interaction in [**3b**][**19a**]$_2$[I]$_2$ calculated under partition schemes i-iii.

Partition Scheme	E_{Int}	E_{Elstat}	E_{Pauli}	E_{Orb}	E_{Disp}
i	-112.05	-294.18	416.15	-203.76	-30.26
ii	-55.54	-145.38	209.63	-102.26	-17.54
iii	-57.65	-147.58	208.39	-103.30	-15.16

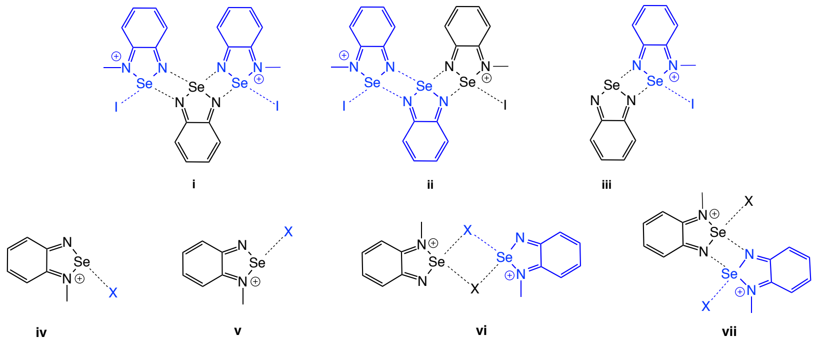

Figure 6.5 Partition schemes used in the DFT-D3 fragment interaction analyses. Each fragment (region) is identified with a distinct colour.

In the case of the [**19a**][X] (X = Cl, Br, I) ion pairs, two geometries were considered, *cis* and *trans* to the alkylated nitrogen atom (Figure 6.5). The results, summarized in Table 6.3, indicate that in all three cases the *trans* structure is preferred. This is consistent with the results of previous calculations of the electrostatic potential maps of the borane adducts of chalcogenadiazoles which showed that the most prominent σ hole on the chalcogen is opposite to the substituted nitrogen.[95]

Table 6.3 Contributions to the energy of interaction (kJ mol^{-1}) between the halide anions and **19a** in *cis* and *trans* geometries of [**19a**][X] (X = Cl, Br, I) ion pairs.

Partition Scheme	X	E_{Int}	E_{Elstat}	E_{Pauli}	E_{Orb}	E_{Disp}
iv	Cl	-520.8	-545.8	284.0	-255.2	-3.8
	Br	-492.8	-512.0	263.2	-239.6	-4.4
	I	-461.4	-470.7	232.7	-217.7	-5.7
v	Cl	-543.1	-558.9	375.5	-357.2	-2.5
	Br	-516.1	-521.0	345.1	-337.3	-2.9
	I	-487.5	-475.8	310.8	-319.1	-3.4

The dimerization energies the [**19a**][X] ion pairs were evaluated in two possible geometries (Figure 6.5, vi and vii), the results are compiled in Table 6.4. While dimer vi is formed from the *cis* (iv) structures and contains the $[Se–N]_2$ supramolecular synthon, the *trans* (v) models form the $[Se X]_2$ supramolecular synthon in dimer vii. The energy of interaction is more negative in latter case, which indicates that the structure of the dimer of the methyl cation experimentally observed in the crystal of [**19a**][I] salt is favoured by the greater stability of the *trans* geometry of the ion pair. The results also show that the dimerization of the ion pairs [**19a**][I] is stronger than the interaction of the ion pair with the neutral molecule of **3b**; however, the overall sum of interactions favours the formation of the pseudo-trimer.

Table 6.4 Calculated contributions to the binding energies for the dimers of the [**19a**][X] (X= Cl, Br, I) ion pairs

Partition Scheme	X	E_{Int}	E_{Elstat}	E_{Pauli}	E_{Orb}	E_{Disp}
	Cl	-61.2	-60.5	51.4	-39.6	-12.3
vi	Br	-64.3	-68.2	66.23	-48.6	-13.7
	I	-63.7	-75.2	87.1	-61.0	-14.7
	Cl	-57.2	-172.6	242.3	-110.7	-16.2
vii	Br	-65.4	265.1	-187.8	-124.8	-17.8
	I	-71.6	298.5	-206.8	-144.0	-19.3

The pseudo-trimer structures **3b**[**19a**]$_2$[X]$_2$ (X = I, BF_4) are especially interesting because of their two distinct Se···N SBI distances. In order to assess the relative strength of each SBI, a bond-energy decomposition analysis was performed using the extended-transition-state method from the natural orbitals for chemical valence (ETS-NOCV).[126] In this method the orbital component to the total bonding energy between fragments is calculated as in Equation 6.2.

$$\Delta E_{Orb} = \sum_k \Delta \mathrm{E}^{\mathrm{k}}_{\mathrm{orb}} = \sum_{k=1}^{M/2} \upsilon_k[-F^{TS}_{-k,-k} + -F^{TS}_{k,k}] \qquad (6.2)$$

The terms $-F^{\mathrm{TS}}{}_{-k,-k}$ and $F^{\mathrm{TS}}{}_{k,k}$ are diagonal transition-state Kohn–Sham matrix elements corresponding to NOCV's with eigenvalues $-\upsilon_k$ and υ_k respectively. This particular orbital interaction term provides both a qualitative and quantitative picture of the electron density reorganization in the [Se–N]$_2$ supramolecular synthons. Each of the fragment interaction calculations (i–iii) shows that the shorter Se···N SBI, that opposite to the quaternary nitrogen, is stronger (−13.0 to −16.9 kcal mol^{-1}) than the longer (−2.4 to −7.5 kcal mol^{-1}).

The Se···N interactions in **3b[19a**]$_2$[I]$_2$ were also examined through Bader's theory of Atoms in Molecules (AIM).[141] Previous studies[95] applied AIM to the examination the Lewis acidity and basicity of **1–3**; their results highlighted the ambiphilic character of the chalcogenadiazoles molecules and showed that the attachment of a Lewis acid to one nitrogen of the heterocycle strengthens the [E–N]$_2$ supramolecular synthon formed by the other nitrogen. The calculated electron density ($\rho(r)$) and its Laplacian ($\nabla^2\rho(r)$) at the bond critical points (BCPs) of **3b**[**19a**]$_2$[I]$_2$ are given in Table 6.6. Although the difference of Se···N distances is small, the AIM parameters suggest that they are very different in strength as there is indication that the energy of interaction scales linearly with the BCP density.

Table 6.5 Electron density and its Laplacian at the bond critical points of the Se···X and Se···N supramolecular interactions in **3b**[**19a**]$_2$[I]$_2$

	Se···N		
AIM parameter at BCP	long	short	Se···I
ρ (e/Å^3 x 10^2)	3.81	8.24	3.69
$\nabla^2\rho$ (e/Å^5 x 10^2)	2.38	6.67	4.67

Table 6.6 Electron density and its Laplacian at the bond critical points of the Se⋯X interactions in the dimers of the [**19a**][X] (X = Cl, Br, I) ion pairs

		AIM Parameter at BCP	
Structure	X	ρ (e/Å^3 x 10^2)	$\nabla^2\rho$ (e/Å^5 x 10^2)
vi[a]	Cl	6.67	7.95
		1.11	2.91
	Br	5.73	5.93
		1.82	2.51
	I	4.79	4.13
		1.19	2.37
vii	Cl	3.45	8.07
	Br	3.71	8.41
	I	3.91	8.67

For comparison, the corresponding BCP parameters of the Se···I interaction in the pseudo-trimer are included in Table 6.5. It is interesting that while the BCP electron density is smaller, the its Laplacian is intermediate between the values for the Se···N SBIs. The comparison was further extended by calculating the BCP parameters of the dimers of [**19a**][X] (X = Cl, Br, I) in the two possible conformations considered under partition schemes vi and vii. The results are compiled in Table 6.6. All these values suggest that the Se···X and Se···N interactions are of similar strength. In some cases, the calculated BCP parameters approach those of the Te···N SBI in the neutral dimer of 1,2,5-telluradiazole (4.20 e Å^{-3} × 10^{-2} and 10.9 e Å^{-5} × 10^{-2}).[95]

6.3 Summary

Despite the difficulties reported in earlier literature regarding the synthesis of alkylated chalcogenadiazoles, methyl, *iso*-propyl, and *tert*-butyl benzo-2,1,3-selenadiazolium cations were conveniently prepared by direct alkylation or cyclo-condensation of the alkyl-phenylenediamine with selenous acid. The former synthetic route only proceeds with the primary and tertiary alkyl iodides, the latter is very efficient for all derivatives. The solution chemistry of these cations confirmed their resiliency towards oxidation, and stability in acidic to neutral aqueous medium. X-ray crystallographic data showed the formation of Se-N secondary bonds was only observed in the pseudo trimer structure as anion binding to selenium is a strong competitor. The relative strengths of those forces and structural preferences they enforce were assessed with DFT-D3 calculations supplemented by AIM analysis of the electron density.

Chapter 7. Synthesis and Structures of Bis(benzo-2,1,3-selenadiazolium) Cations

7.1 Introduction

The results presented in Chapters 4, 5 and 6 demonstrate that the SBIs formed by the 1,2,5-selenadiazole ring are strengthened by increasing the electron-withdrawing ability of the nitrogen atom in the antipodal position. This was achieved by attachment of Lewis acidic groups such as electron-deficient boranes, transition metal ions, or alkyl groups (formally carbocations). In the first two cases, the lability of the bond between the nitrogen and the acidic group limits the application of this approach as a general strategy in the construction of supramolecular structures. On the other hand, nitrogen-carbon bonds usually are kinetically stable (inert). Furthermore, the stability towards hydrolysis of the cationic derivatives described in Chapter 6 makes them very attractive as supramolecular building blocks.

However, in comparison to **1c**, the auto-association of **19** is limited to dimers in the best case (Figure 6.3). Pseudo-trimers can be formed with the introduction of the neutral heterocycles (Figure 6.1). In order to favor the formation of a supramolecular polymer, dicationic molecules could be built by linking two N-alkyl selenadiazolium cations with an organic bridge (Scheme 7.1).

A wide variety of linking structures is conceivable, from saturated linear or cyclic hydrocarbons to phenylene or xylene bridges (Scheme 7.2). A cyclohexane bridge would be of special interest due to its chirality.

This chapter explores that concept. In addition to the synthesis of selected bis(N-substituted benzoselenadiazolium) dications, these investigations include the use of tetrafluoroborate and trifluoromethanesulfonate as counterions. As shown in Chapter 6, the Se-halide interaction strongly competes with the Se···N SBIs, which will likely interfere with the auto-association of the dications.

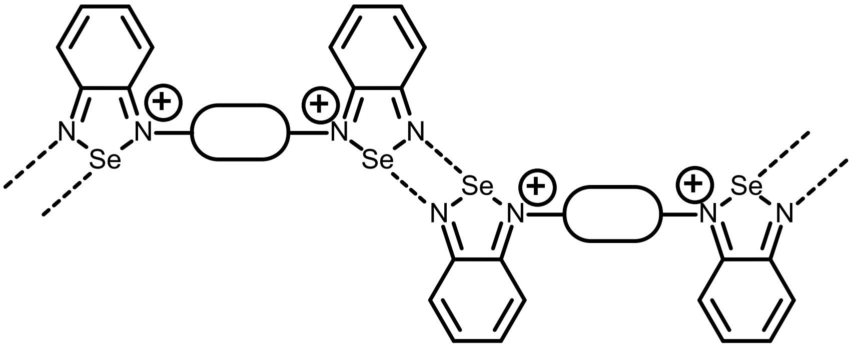

Scheme 7.1 Proposed supramolecular arrangement of bis(benzo-2,1,3-selenadiazolium) dications

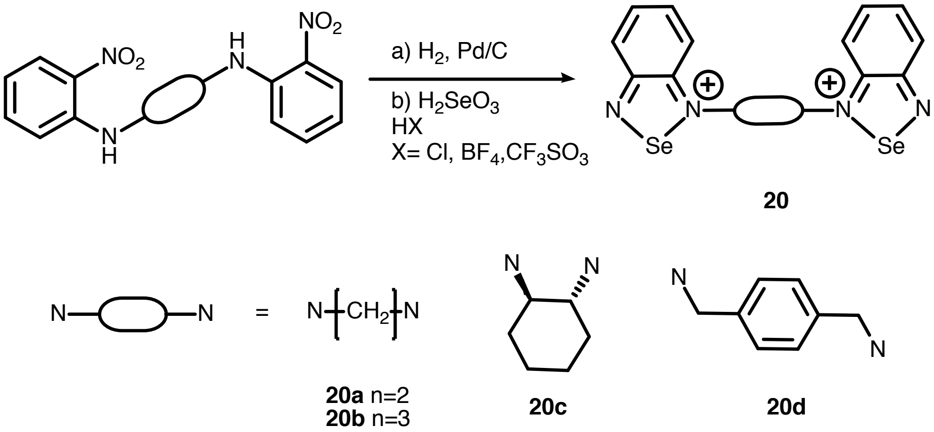

Scheme 7.2 Proposed structures of bis(benzo-2,1,3-selenadiazolium) dications (**20**)

7.2 Results and Discussion

7.2.1 Syntheses

7.2.2 Formation of the Chloride salts

The synthetic methods described in Chapter 6 for the synthesis of the N-alkyl benzo-2,1,3-selenadiazolium cations were readily applicable to the synthesis of bridged dications (Scheme 7.2) The key intermediates in these syntheses are bridged bis(*ortho*-phenylene diamines), for which the most efficient published preparation procedures are based on nucleophilic aromatic substitution reactions on 1-fluoro2-nitrobenzene, followed by catalytic hydrogenation.[94] In all instances, the precursor tetramines were easily oxidized upon exposure to air and ambient light; they were most conveniently isolated, purified and stored as their hydrochlorides after treatment with anhydrous hydrogen chloride gas. These intermediates easily reacted with H_2SeO_3 to produce the corresponding salts of the dications.

More specifically, the hydrochloride salt of 1,2-di(o-aminophenylamino)ethane reacted with a warm solution of selenous acid in aqueous HCl yielding a dark red precipitate. Recrystallization from ethanol gave pure 2[**20a**]$Cl_2 \cdot 8H_2O \cdot HCl$. The chloride salts of the cyclohexane- and *p*-xylene-bridged dications **[20c]**$Cl_2 \cdot H_2O$ and [**20d**]Cl_2 were prepared in a similar manner. However, the low solubility of the latter product precluded complete purification by recrystallization. The actual composition of the materials isolated in each case was established by single-crystal X-ray diffraction and is discussed in Section 7.2.3. The ^1H NMR spectrum of all dications is characterized by the resonances of the aromatic protons of the benzoselenadiazolium that range from 7.49–7.96 ppm. These signals are comparable to the N-methyl cations, and slightly lower relative to those observed for the *iso*-propyl and *tert*-butyl monocations. The same aromatic protons are shifted to lower frequency by 0.15 ppm from that of **3b**. The ESI mass spectra clearly display the dications (Figure 7.1) and the dication plus one chloride anion.

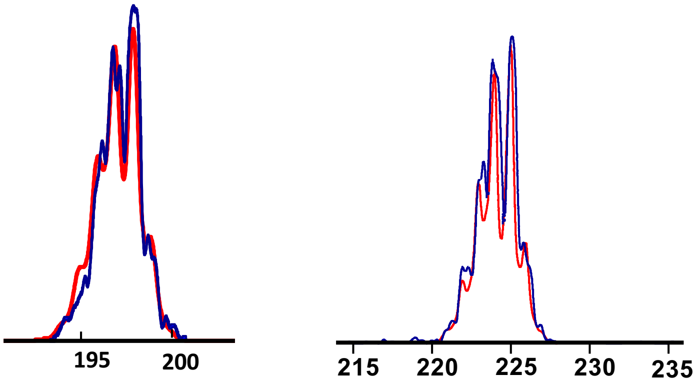

(a) (b)

Figure 7.1 Experimental ESI-HR mass spectrum (blue) and calculated pattern (red) for: (a) $[C_{14}H_{12}N_4Se]^{2+}$ of 2[**20a**]$Cl_2 \cdot 8H_2O \cdot HCl$ and (b) $[C_{18}H_{16}N_4Se]^{2+}$ of [**20c**]$Cl_2 \cdot H_2O$.

7.2.2.1 Syntheses of BF_4^- and $CF_3SO_3^-$ salts

Given the strength of binding of halide anions to the chalcogen atom in the selenadiazolium cation, attempts were made to replace the chloride with less coordinating species such as tetrafluoroborate and trifluoromethanesulfonate with the intention to promote the formation of intermolecular Se-N SBIs. Preliminary precipitation attempts with $AgBF_4$ failed to produce solid AgCl. This is likely due to coordination of Ag^+ despite the charge of the dication. Coordination of transition metal ions to cations is rare but has been observed with organic ligands that contain nitrogen donors.[162] Successful anion replacement was achieved in the reaction of 2[**20a**]$Cl_2 \cdot 8H_2O \cdot HCl$ and $NOBF_4$ under anhydrous conditions. The by-product, NOCl, is a gas at ambient temperature which obviates the need for purification workup. The $NOBF_4$ reactions produced yellow precipitates which were collected and characterized by ^1H and ^{19}F NMR spectroscopy. The aromatic proton resonances observed for the tetrafluoroborate salt appear at higher frequency (7.85-8.12 ppm) than those for the chloride salt (7.69-7.96 ppm). The protons on the ethylene bridge are found at 5.54 ppm, which is 0.09 ppm above the resonance of that in the chloride salt. The mass spectra of the chloride and tetrafluoroborate salts of **20d** are characterised by the presence of the isotopic patterns of the $[M]^{2+}$ and $[M]X^+$ ($X = Cl^-$, BF_4^-) ions (Figure 7.2).

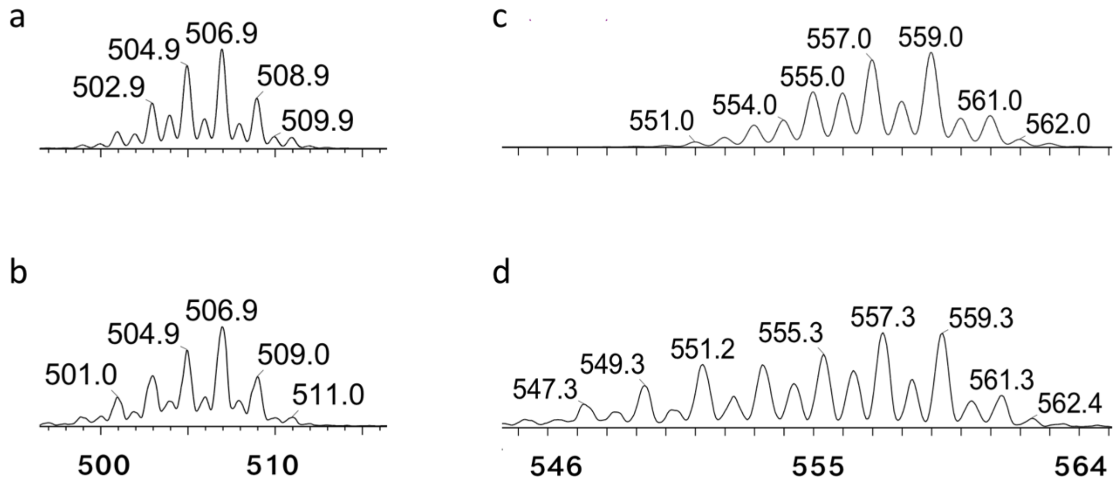

Figure 7.2 ESI-HR mass spectra of [**20d**]Cl^+ a) calculated, b) experimental; and [**20d**]$(BF_4)^+$ c) calculated, d) experimental.

The above anion replacement method is very efficient but unsuitable for a large-scale synthesis due to the cost of $NOBF_4$. For the preparation of *p*-xylene derivative [**20d**]$(BF_4)_2$, the appropriate tetramine was directly added to a stoichiometric amount of HBF_4 and H_2SeO_3 in solution. The resulting red-orange precipitate was washed with a saturated solution of $NaBF_4$ in ethanol until the remaining acid was removed. Recrystallization from acetonitrile gave two polymorphs of [**20d**]$(BF_4)_2$, depending on the concentration of the solution. Trifluoromethanesulfonate salts were prepared in an analogous way. The reaction of 1,2-di(*o*-aminophenylamino)ethane and selenous acid in trifluoromethanesulfonic acid yielded [**20a**]$(CF_3SO_3)_2$. Similarly, 1,2-di(*o*-aminophenylamino)propane was used to prepare [**20b**]$(CF_3SO_3)_2$.

7.2.3 Crystal Structures

Full crystallographic data are compiled in Table 2.1 and the selected bond distances and angles are compiled in Table 7.1. The crystal of 2[**20a**]$Cl_2 \cdot 8H_2O \cdot HCl$ displays a unique molecular arrangement. The dications feature the heterocycles in a *syn* orientation and are organized in pairs bridged by Se-Cl secondary bonds (2.803(2), 2.682(2) Å) forming a macrocycle-like structure with a third chloride anion at the centre making longer (3.313 and 3.647 Å) contacts with the four chalcogens (Figure 7.3). The two other chloride anions sit in the lattice without meaningful interatomic contacts.

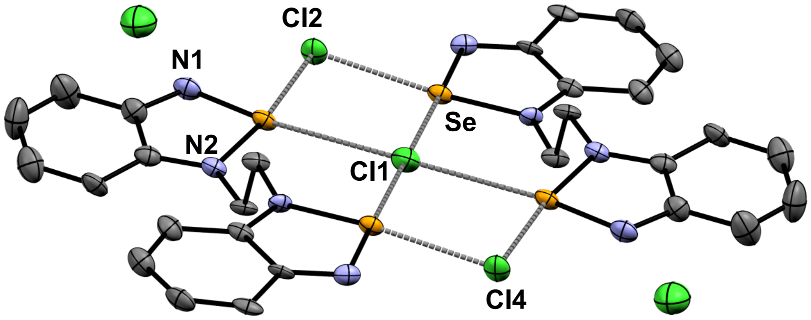

Figure 7.3 ORTEP and numbering scheme for the asymmetric unit in the crystal structure of 2[**20a**]$Cl_2 \cdot 8H_2O \cdot HCl$. Displacement ellipsoids are shown at the 50 % probability level.

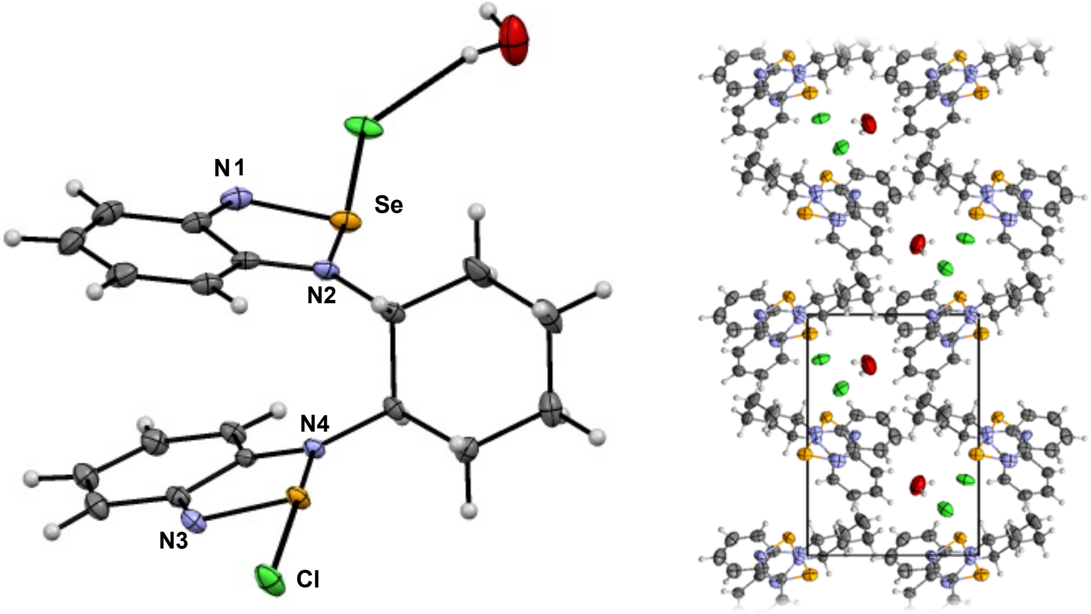

(a) (b)

Figure 7.4 (a) ORTEP and numbering scheme for the asymmetric unit and (b) packing in the crystal structure of [**20c**]$Cl_2 \cdot H_2O$. Displacement ellipsoids are shown at the 50 % probability level.

Table 7.1 Selected distances (Å) and angles (°) for 2[**20a**]$Cl_2 \cdot 8H_2O \cdot HCl$ and [**20c**]$Cl_2 \cdot H_2O$

Compound	2[**20a**]$Cl_2 \cdot 8H_2O \cdot HCl$	[**20c**]$Cl_2.H_2O$
Se1-N2	1.879(6)	1.892(3)
Se1-N1	1.793(6)	1.769(2)
Se2-N4	1.867(6)	1.888(2)
Se2-N3	1.778(6)	1.768(2)
N2-C6	1.340(8)	1.333(3)
N2-C7	1.456(8)	1.475(3)
N1-C1	1.329(9)	1.332(4)
C1-C6	1.442(8)	1.439(3)
C1-C2	1.442(9)	1.433 (4)
C2-C3	1.352(10)	1.352(4)
C3-C4	1.407(11)	1.432(4)
C4-C5	1.374(9)	1.356(4)
C5-C6	1.422(10)	1.424(4)
N2-Se1-N1	88.4(2)	88.4(1)
Se1-N2-C6	111.8(4)	110.8(2)
Se1-N1-C1	110.6(4)	111.1(2)
N1-C1-C6	118.5(6)	118.1(2)
N2-C6-C1	110.7(6)	111.3(2)

The asymmetric unit of [**20c**]Cl_2 (Figure 7.4a) shows two heterocycles bridged by a 1-(R),2-(R)-substituted cyclohexane ring featuring short selenium-chloride contacts with distances of 2.731 Å, which are shorter than that found in the monocation, N-hydro-benzo-2,1,3-selenadiazolium chloride. (2.901(1) and 3.075(1) Å) The chirality of the cyclohexane bridge leads to the formation of helical assemblies with a 9° deviation from the normal of the C1, C2, C3, C4 plane in the cyclohexane. (Figure 7.4b) The angle between two cation planes is much larger (25.5°) than that in the ethylene-bridged dication. (4.36°)

In the case of the chloride salt of the *p*-xylene-bridged dication [**20d**]Cl_2, it was not possible to obtain single crystals of the compound because of its low solubility. Attempts to grow crystals by diffusion under several conditions yielded dendrites, unsuitable for crystallographic determination.

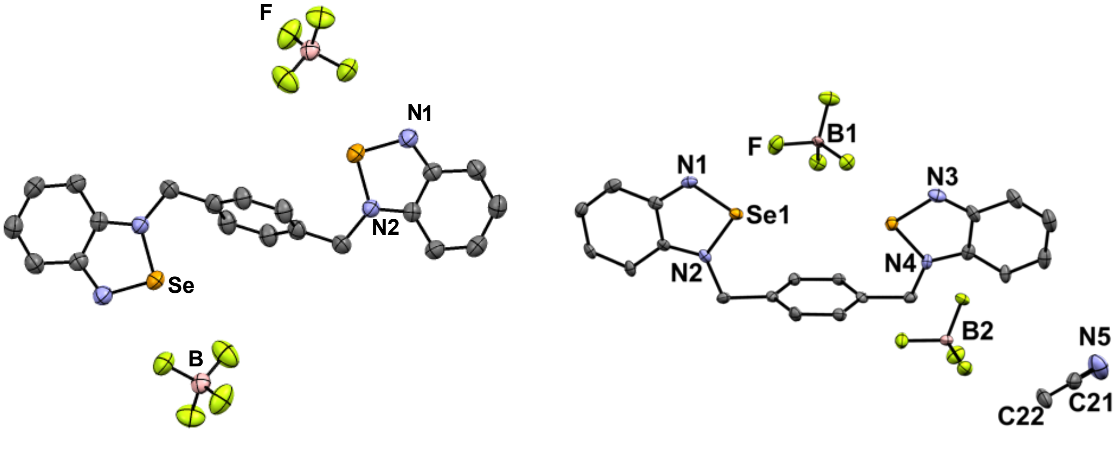

(a) (b)

Figure 7.5 Molecular structures in the crystals of (a) [**20d**]$(BF_4)_2$ and (b) [**20d**]$(BF_4)_2 \cdot CH_3CN$. Displacement ellipsoids are shown at 50% probability level. Hydrogens are omitted for clarity.

The first polymorph of [**20d**]$(BF_4)_2$ belongs to the $P12_1/n1$ space group and was obtained from acetonitrile. Its asymmetric unit features the dication with an *anti* conformation. Each selenium atom is engaged in a short contact with a BF_4^- anion (Figure 7.5a), the shortest Se-F distance is 2.769(1) Å is shorter than the sum of the van der Waals radii (3.37 Å). The second crystalline phase is a pseudopolymorph (Figure 7.5b) obtained from a dilution solution in acetonitrile, that includes solvent in the lattice

([**20d**]$(BF_4)_2 \cdot CH_3CN$). The molecular structure displays a *syn* conformation that appears to chelate the BF_4^- anion. The Se-F distances are 3.005(8), and 2.914(7) Å.

The asymmetric unit of [**20a**]$(CF_3SO_3)_2$ includes two heterocycles bridged by one ethylene molecule and two units of trifluoromethanesulfonate anions. (Figure 7.6) The selected distances and angles are compiled in Table 7.2. One heterocycle in the dication forms the $[Se\text{-}N]_2$ supramolecular synthons with a neighbouring dicationic unit with Se-N distances of 2.588(2) Å. The same selenium atom is also in close contact with the oxygen atoms of the trifluoromethanesulfonate anions sitting above and below the plane of the dication. (3.295(3), 3.319(3), 3.357(3) Å) The selenium atom of [**20b**]$(CF_3SO_3)_2$ features much shorter Se-O secondary bonds (2.665(1), 2.808(2), 3.137(2) Å) and does not form Se-N SBIs as the trifluoromethanesulfonate anion blocks this site.

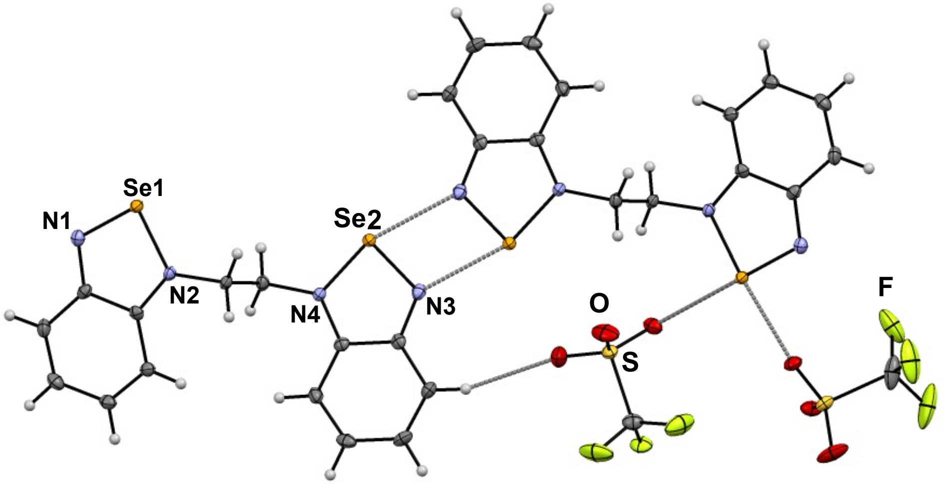

Figure 7.6 ORTEP and numbering scheme for the asymmetric unit in the crystal structure of [**20a**]$(CF_3SO_3)_2$. Displacement ellipsoids are shown at the 50 % probability level

Table 7.2 Selected distances (Å) and angles (°) for [**20d**](BF_4)$_2$, [**20a**](CF_3SO_3)$_2$ and [**20b**](CF_3SO_3)$_2$ and [**20d**](BF_4)$_2$·CH_3CN

Compound	[**20a**](CF_3SO_3)$_2$	[**20b**](CF_3SO_3)$_2$	[**20d**](BF_4)$_2$	[**20d**] (BF_4)$_2$·CH_3CN
Se-N1	1.768(2)	1.758(2)	1.768(2)	1.759(4)
Se-N2	1.850(3)	1.835(2)	1.832(1)	1.820(5)
Se-N4	1.838(3)	1.843(2)	1.832(1)	1.833(4)
Se-N3	1.778(3)	1.769(2)	1.768(2)	1.760(5)
N2-C6	1.339(4)	1.344(3)	1.341(2)	1.333(7)
N2-C7	1.469(4)	1.478(3)	1.485(2)	1.480(7)
N1-C1	1.324(4)	1.338(3)	1.332(2)	1.344(8)
C1-C6	1.443(5)	1.444(3)	1.445(2)	1.448(7)
C1-C2	1.426(5)	1.430(3)	1.434(2)	1.421(7)
C2-C3	1.343(5)	1.364(4)	1.363(2)	1.353(9)
C3-C4	1.440(5)	1.438(4)	1.433(3)	1.433(7)
C4-C5	1.361(5)	1.366(3)	1.369(2)	1.363(8)
C5-C6	1.415(5)	1.420(3)	1.418(2)	1.400(8)
N2-Se1-N1	89.3(1)	90.3(1)	90.4(6)	90.5(2)
Se1-N2-C6	110.7(2)	110.7(1)	110.4(1)	111.3(3)
Se1-N1-C1	111.0(2)	110.4(2)	109.9(1)	109.9(4)
N1-C1-C6	117.09(3)	116.9(2)	117.1(2)	116.7(5)
N2-C6-C1	111.84(3)	111.7(2)	112.0(1)	111.6(4)

The asymmetric unit of [**20b**](CF_3SO_3)$_2$ contains a two selenadiazolium heterocycles linked by a –(CH_2)$_3$– chain. (Figure 7.7) The trifluoromethanesulfonate anions are bound to the chalcogen, precluding the Se-N SBIs. The oxygen atoms display short distances to Se (2.685(1), 2.808(2) and 3.137(2) Å), all shorter than the sum of Se and O van der Waals radii (3.47 Å). Similar Se-O distances were observed in the dimer of the N-methyl-benzoselenadiazolium cation (2.823(8) Å).[143]

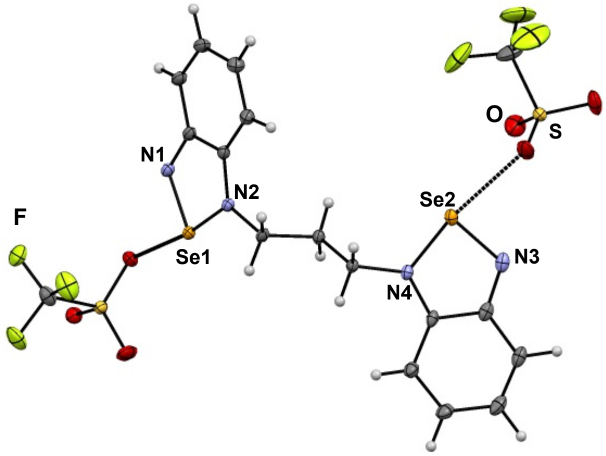

Figure 7.7 ORTEP and numbering scheme for the asymmetric unit in the crystal structure of (a) [**20b**](CF_3SO_3)$_2$. Displacement ellipsoids are shown at the 50 % probability level.

7.3 Summary

The synthetic route developed for mono N-alkylated benzo-2,1,3-selenadiazolium cation was used to prepare a variety of bis(benzoselenadiazolium) dications bridged by cyclohexane, alkyl chains, and xylene moieties. The chloride salts of the dications showed the strong affinity for the halide anions. The anion replacement for weakly coordinating anions such as tetrafluoroborate and trifluoromethanesulfonate were used in an attempt to suppress the competition between Se-Cl and Se-N SBIs. However, the formation of Se-N SBIs was only observed in [**20a**](CF_3SO_3)$_2$ as selenium showed strong affinity for fluorine atoms in the tetrafluoroborate and the oxygen atoms of the trifluoromethanesulfonate anions.

Chapter 8. Studies Towards the Construction of Foldamers Based on Selenadiazolium Cations

8.1 Introduction

DNA provides one of the most remarkable examples of self-assembly. Its double helical structure results from precise pairings of nucleic acids through a combination of hydrogen bonding, π-stacking, electrostatic interactions and the hydrophobic effect. Inspired by the cooperative interplay of these factors, DNA has been used as a template for the development of *self-programming* nanomaterials.[3]

The field of structural DNA nanotechnology aims to dictate the precise positioning of materials and molecules into any desirable structure at nanoscale. An initial challenge was to convert the one-dimensional primary structure of the DNA molecule into 2D and 3D structures. Seeman's group introduced a method in which branched DNA structures are used to generate rigid and well-defined 2D DNA assemblies. Using this construction principle, various types of structural motifs have been designed and used to access a rich number of 2D DNA architectures and refine DNA materials assembly. The development of precisely controlled nanoparticle assemblies substantially affects components in both biotechnology and materials science including genomics proteomics, diagnostics and tissue engineering. *DNA origami*, where a single strand of DNA is folded using a large number of smaller DNA strands, has been useful for constructing larger and complex DNA shapes with highly *addressable* surfaces. Three-dimensional structures have great potential for application in drug delivery, selective encapsulation of proteins and nanomaterials, 3D network assembly for catalysis and biomolecule crystallization.[3]

A new area of research termed *supramolecular DNA assembly* has recently emerged. The combination of DNA building blocks with synthetic organic, inorganic and polymeric structures provides a precise method to engineer both structural and functional components. The incorporation of synthetic insertions into DNA strands can alter the its hybridization and control its self-assembly outcome bringing highly ordered construction motifs for nanotechnology. DNA *foldamers*, synthetic, discrete chain molecules or oligomers that adopt a particular secondary structure due to noncovalent interactions have received great attention in DNA nanotechnology. Insertion of hydrophobic perylene units into a hydrophilic DNA chain can yield folded structures through π- stacking interactions. The ability to control the selective self-assembly can lead to highly stable hybrid structures that can mimic biologically folded and functional proteins.[3,4]

Many foldamers have been developed using hydrogen bonding and the coordination of transition metal ions. One early objective of this thesis was to incorporate into this area heavy main-group elements taking advantage of our experience constructing supramolecular structures with SBIs. This chapter provides an account of the research carried out in this area.

8.2 Design of an Oligonucleotide Analogue Based on Se-N SBIs

As noted above, the specific pairing of nucleobases and control of hybridization allow a remarkably precise control of structure and organization of the products. However, a limitation of developing self-assembled structures based on nucleic acids is that the materials are vulnerable to microorganisms and the functional groups that form hydrogen bonds preclude any chemistry that is sensitive to acidic hydrogens. As a means to circumvent such limitations, we proposed the development of foldamers analogous to nucleic acids in their ability to undergo self-assembly but through the formation of chalcogen-nitrogen SBIs instead of hydrogen bonds. As a first step in that direction, the incorporation of building blocks based on benzo-2,1,3-selenadiazole (**3b**) into the natural base sequence of an oligonucleotide would result in a unique structure with foldamer properties thanks to the formation of the $[Se\text{-}N]_2$ supramolecular synthon. A convenient approach to enable that concept would take advantage of established methods for the automated synthesis of oligonucleotides (Scheme 8.1).

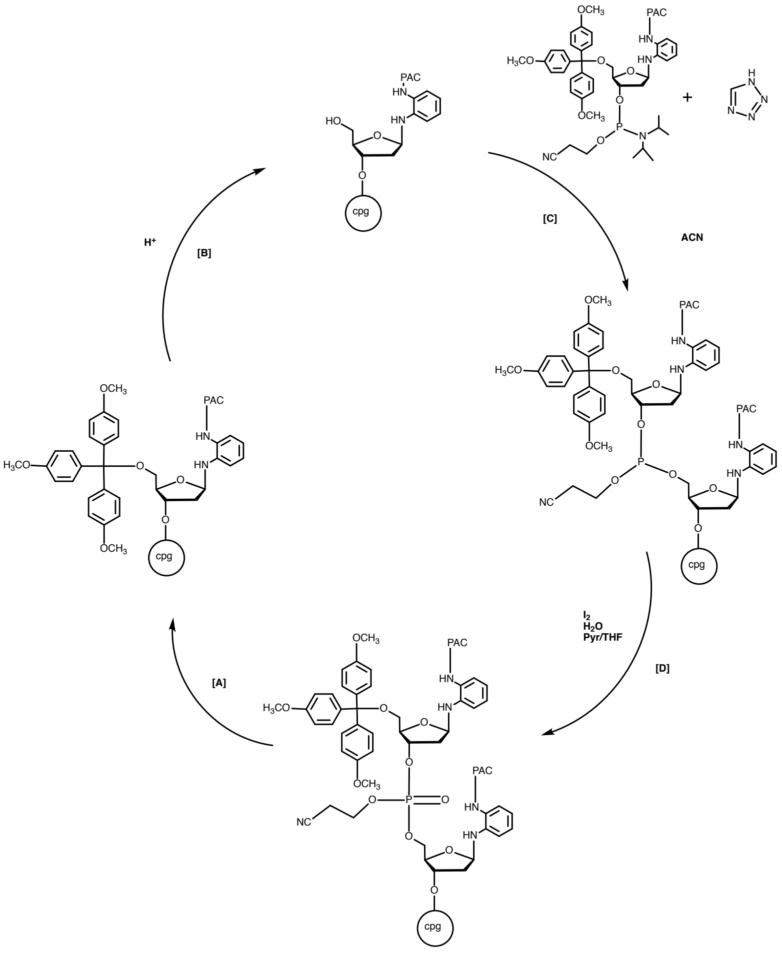

Figure 8.1 Proposed synthetic cycle for the synthesis of oligonucleotide SBI analogues.

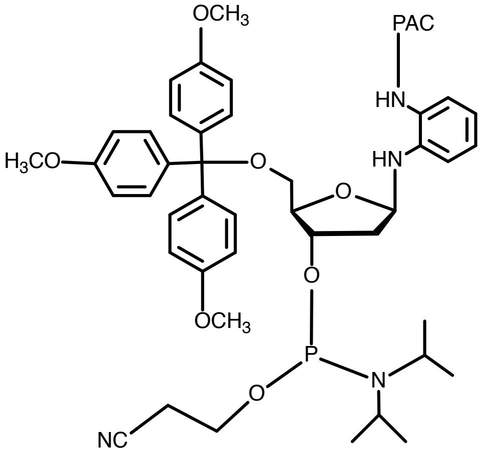

21

The synthesis of precursor **21** would be essential to construct an oligomer chain. After the first unit is attached to a *controlled-pore glass* (cpg) solid support, the 5' hydroxyl group would be deprotected in order to add the next base through condensation. The deprotection and coupling of the phosphorus group using tetrazole would result in a formation of a new phosphite linkage joining the two bases together. In order to stabilize such linkage, the phosphite group can be oxidized using iodine. The cycle would be repeated until all desired bases have been added to the oligonucleotide. The final steps involve the assembly of the cationic heterocycle on each of the phenylenediamino groups by reaction of each deprotected diamine with $Se_2O_3^{2-}$ in acidic medium. Secondary bonding would then lead to hybridization of two oligomer chains.

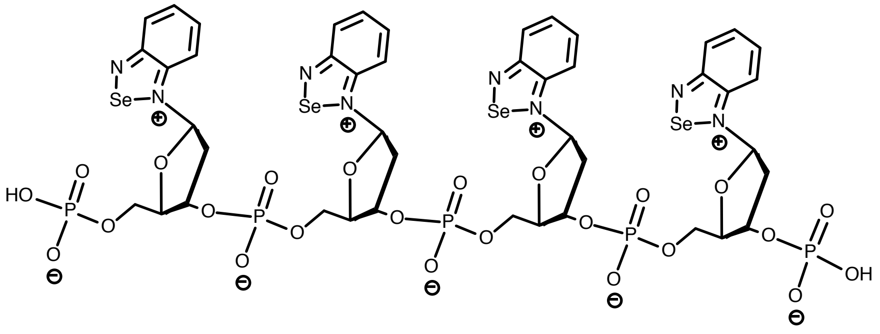

Scheme 8.1 Idealized structure of an oligonucleotide analogue based on the use of benzo-2,1,3-selenadiazolium cations in place of the natural nucleobases.

As a first step towards in this project, the goal was to prepare precursor **21** and to establish the optimum conditions for its application in the automated synthesis of the oligomer.

There are two compounds that are frequently used in the synthesis of building blocks for oligonucleotides, 1,3,5-tri-O-acetyl-2-deoxy-α,β-D-erythropentofuranoside (**24a**) and 2-deoxy-3,5-di-O-*p*-toluoyl-α-D-ribofuranosyl chloride **26b**. Based on each compound, two synthetic routes were proposed to make the intermediates **28a** and **28b** through **23a** and **23b**. (Equation 8.1)

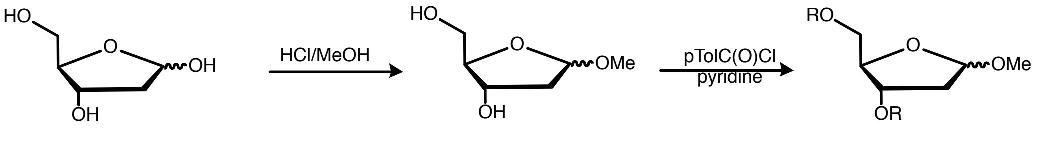

22

23a R= Ac
23b R= pTolC(O)

(8.1)

The first approach will require the reaction of **23a** with an azide (Equation 8.2), acetylation of **23a** and further reaction $TMSN_3$. The analog **25b** requires first replacing the methoxide group of **23b** with Cl and a subsequent reaction with CsN_3 (Equation 8.3). A selective reduction of the azide in **25a** and **25b** and coupling of 1-fluoro-2-nitrobenzene would lead to the synthesis of **28a** and **28b** (Equation 8.4).

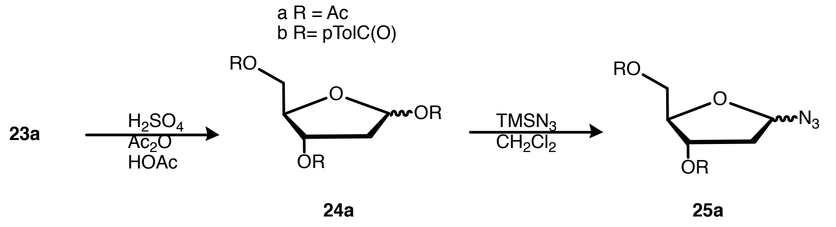

(8.2)

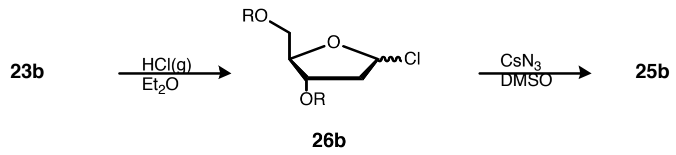

(8.3)

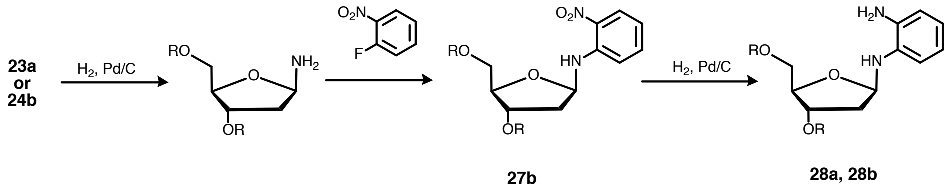

(8.4)

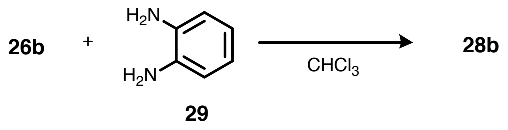

(8.5)

Reports of similar reactions involving **25a** and **25b** as intermediates quote overall low yields of the final products.[91-93] An alternative approach (Equation 8.5) would consist of the direct reaction of **26b** with o-phenylenediamine (**29**). Once the target molecule **28b** is obtained, the protecting groups would be introduced or replaced to finally produce **21.** (Scheme 8.2)

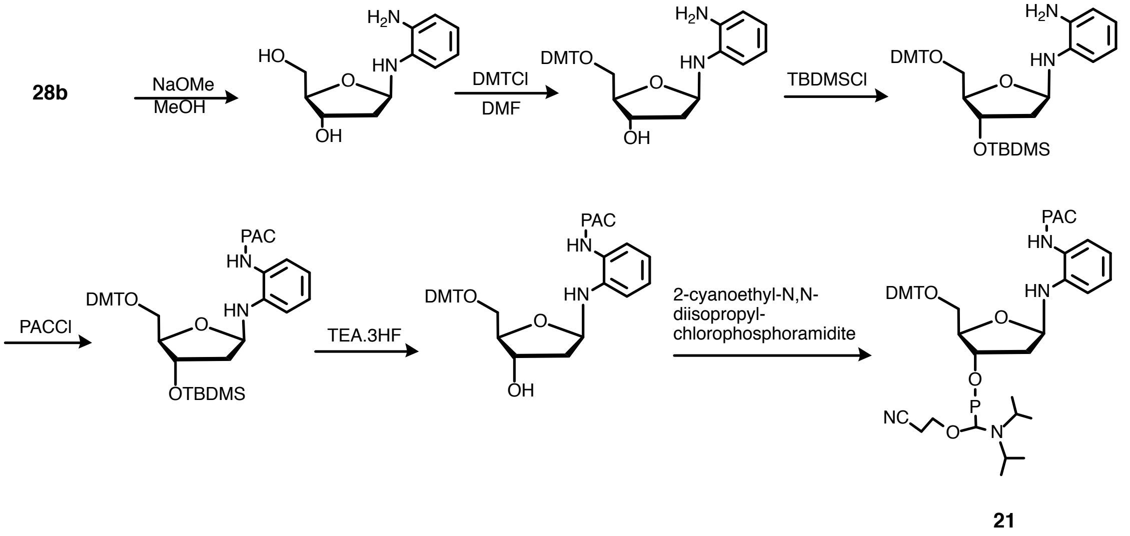

Scheme 8.2 Proposed synthesis of **21** using **28b** as a starting reactant

8.3 Results and Discussion

8.3.1 Synthesis of 1-(α,β)-O-methyl-2-deoxy-D-ribose (22)

There are two literature methods for methylation of 2-deoxy-*D*-ribose.[91-93] One technique uses H_2SO_4 as a catalyst and results in partial methylation. The alternative method proceeds in milder conditions and was used instead; quantitative methylation was accomplished by generating HCl *in situ* as a catalyst. 2-deoxy-*D*-ribose was dissolved in methanol and enough acetyl chloride was added to yield a 1% hydrogen chloride solution. (Equation 8.1) After 1 h, the reaction was completed and the acid was neutralized with sodium bicarbonate. The identity of the product was confirmed using ^{1}H NMR (Figure 8.1) and mass spectrometry. Two anomeric methoxy methyl signals are displayed at 3.36 and 3.37 ppm. The multiplet at 5.10 ppm corresponds to H_1 and signals at 2.22, 3.62 ppm are assigned to H_2, H_3, H_4 and H_6 respectively. Another multiplet at 4.08 represents H_5. The high-resolution electrospray ionization mass spectral analysis detected the [M-H] ion m/z = 147.0697 (Cf. calc. 147.0658)

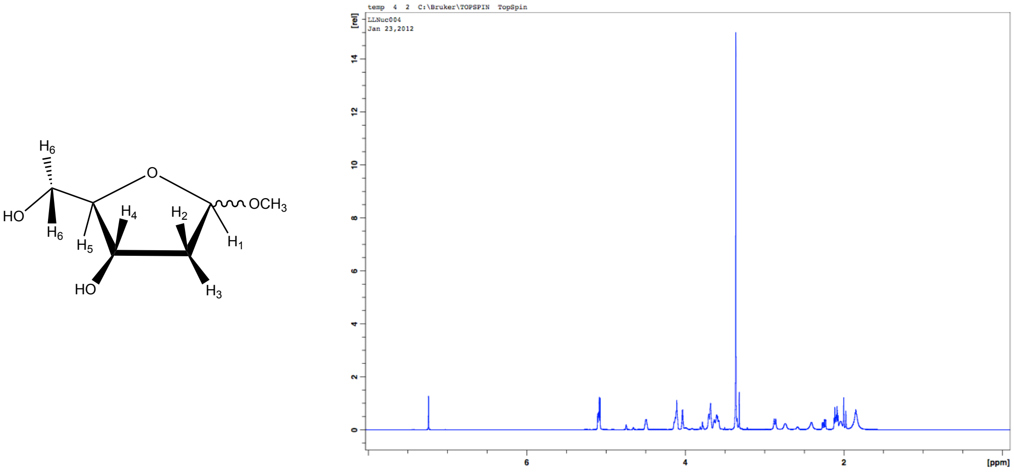

Figure 8.1 ^{1}H NMR spectrum of **22** acquired in $CDCl_3$.

8.3.2 Synthesis of 1-(α,β)-O-methyl-3,5-di- (O-p-toluoyl)-2-deoxy-D-ribose (23b)

The protected sugar was prepared by addition of p-toluoyl chloride to a solution of **22** in pyridine. The resulting mixture was stirred at room temperature for 6 h under nitrogen. The solvent was removed under vacuum at 60 °C. The presence of a mixture of anomers was confirmed by ^{1}H NMR (Figure 8.2). The multiplets observed at 5.58, 2.85, 4.58 and

4.66 ppm represent H1, H2, H3, and H4 and the quartet at 4.91 ppm corresponds to H5. The introduction of p-toluoyl group increased the deshielding of electrons so the signals for protons on the ribose structure are found at higher frequency. When compared to the ^{1}H NMR spectrum of **22**, the most significant difference consists of new signals at 7.95 and 3.42 due to the aromatic and the methyl protons respectively. The mass spectral analysis showed the molecular ion at m/z = 384.1567 (*Cf.* calc. 384.1573)

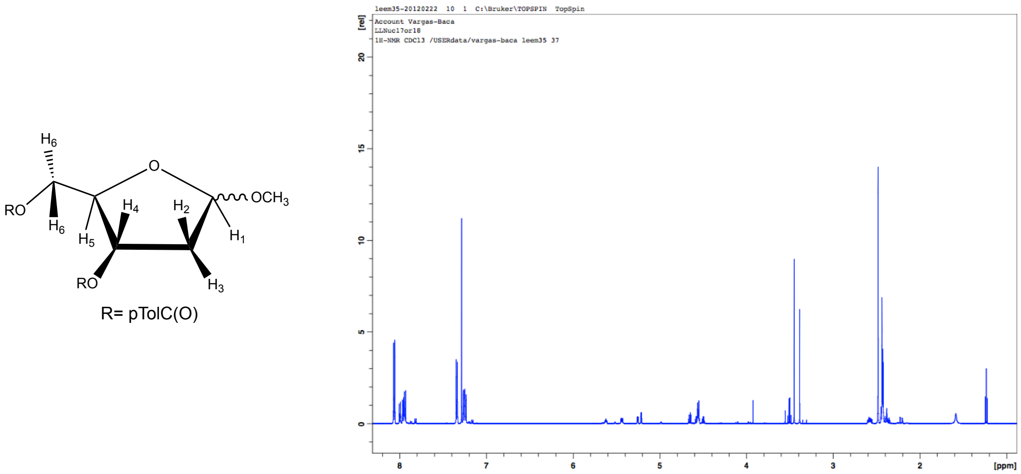

Figure 8.2 ^{1}H NMR spectrum of **23b** acquired in $CDCl_3$.

8.3.3 Synthesis of 1-(α)-chloro-3,5,-di-(O-p-toluoyl)2-deoxy-D-ribose (26b).

Two solvents, acetic acid and diethyl ether were considered for the chlorination of **23b**. Diethyl ether was chosen because the work up process would be more convenient. **23b** was treated with hydrogen chloride gas for 12 min until the product **26b** separated forming a thick mass. The solid was filtered and thoroughly washed with ether. It was then stored at -30 °C under nitrogen. (Figure 8.3) The multiplets at 6.46, 2.83, and 4.57 ppm were assigned to H1, H2, H3 and H6. The quartet at 4.85 ppm corresponds to H5 is assigned to H1 and the doublet of doublet of doublet at 5.55 ppm represents H4. A set of multiplets observed at 7.87 and 7.21 ppm corresponding to 8 protons and doublets at 2.41 ppm are characteristic of the p-toluoyl group. The high-resolution electron ionization mass spectral analysis detected the [M-Cl] fragment m/z = 353.1371 (Cf. calc. 353.1389).

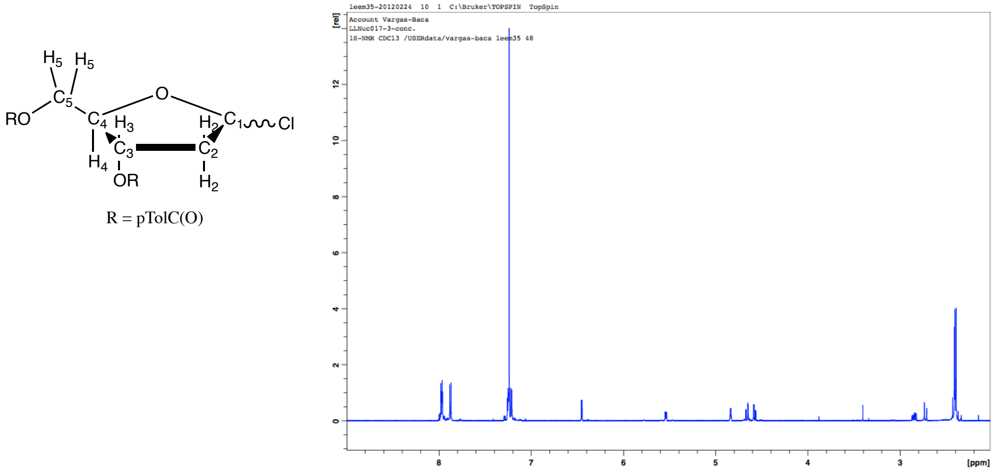

Figure 8.3 ^{1}H NMR spectrum of **26b** acquired in CDCl$_3$.

8.3.3.1 1D COSY and TOCSY NMR

Spectra of **26b** The NMR analysis of carbohydrates can be challenging due to the anomeric hydrogens and the stereochemistry of the molecules. The assignment of the protons in the intermediate used to couple 1,2-phenylenediamine was completed using 1D correlation spectroscopy (COSY) and total correlation spectroscopy (TOCSY). (Figure 8.4) Both experiments give the same ^{1}H coupling information one site at a time without involving a 2D Fourier transform. Selective excitation of H1 or H3 was useful in the assignment of the other protons.

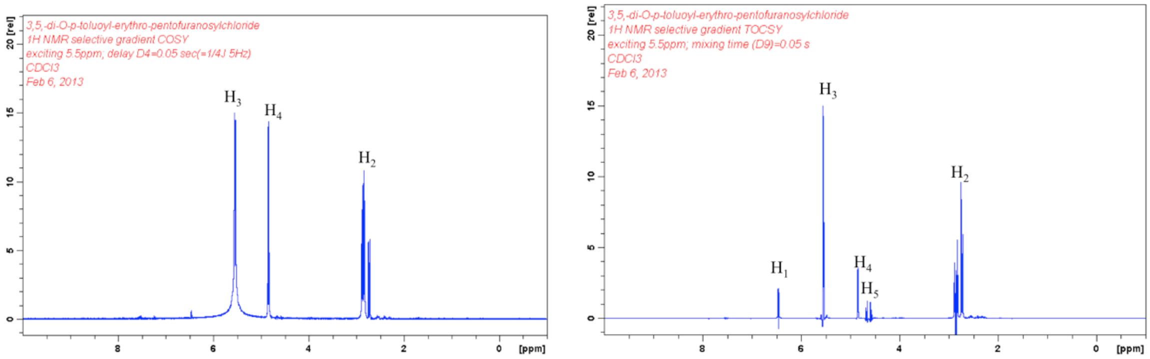

(a) (b)

Figure 8.4 a) 1D COSY and b) TOCSY spectra of **26b** with a selective excitation of H3.

8.3.4 Synthesis of 1-(α,β)-O-(2-amino-phenyl-amino)-3,5-di- (O-p-toluoyl)-2-deoxy-D-ribose (28b)

Two synthetic routes were proposed using a number of literature sources on nucleoside chemistry.[91-93]

8.3.4.1 Route 1: Reaction with fluoro-2-nitrobenzene

Using the first route (Equation 4), compound **28b** would be obtained via selective reduction of the azide then nucleophilic aromatic substitution of the amine. The azide compound obtained from acetylated sugar **28** has overall yield of 38%.[93] In addition, the yield of the next step in which nitro aromatic derivative is added was reported to be 68%. Considering the yield of intermediate compounds, an alternative approach was sought.

8.3.4.2 Route 2: Reaction with o-phenylenediamine.

The second route (Equation 5) was proposed to reduce the number of steps. Among many organic solvents, chloroform was chosen due to the insolubility of the side product, a diamine hydrochloride. The addition of two equivalent of *o*-phenylenediamine (**29)** was added under nitrogen to a solution **26b** in chloroform immediately gave yellow precipitate which was characterized to be **29**·2HCl. The product was filtered, dried under vacuum and isolated using column chromatography (1% methanol in chloroform). Although the HRMS-ES analysis detected the $[M-H]^+$ ion at m/z= 459.1920 (*Cf.* calc. 459.1920) and the TLC (1% methanol in chloroform as eluent) gave only one spot, the ^1H NMR spectrum (Figure 8.5) was complex and characterized by broad resonances. Due to uncertainty about the purity of this product and overall low yields (12%) of the synthetic steps, this line of research was suspended.

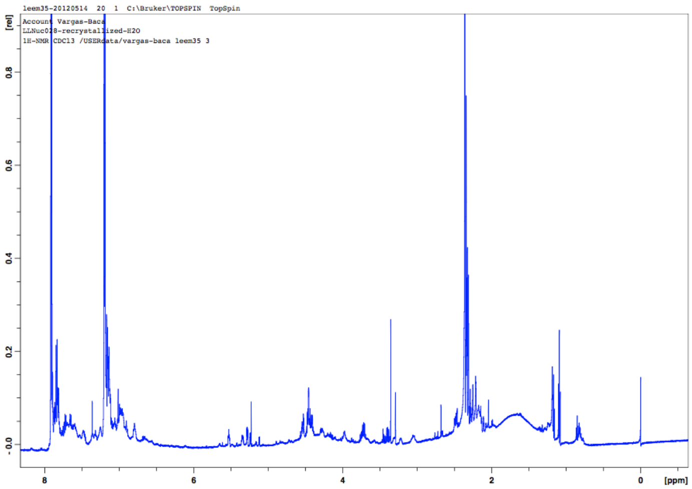

Figure 8.5 ^1H NMR spectrum of **28b** acquired in $CDCl_3$.

Chapter 9. Crystallographic Study of the Supramolecular Aggregates of 1,2-Tellurazole 2-oxides

Investigations described in this chapter have been included the following publication:

P. C. Ho, P. Szydlowski, P. J. W. Elder, J. Sinclair, J. Kübel, C. Gendy, L. M. Lee, H. Jenkins, J. F. Britten, D. R. Morim, I. Vargas-Baca, *"Supramolecular Macrocycles Reversibly Assembled by Te···O Chalcogen Bonding", Nat. Commun.* **2016**, 7, 11299; DOI: 10.1038/ncomms11299.

9.1 Introduction

There is a rich history of studies of the formation of coordination complexes using molecular rings or chains that contain electron-donor atoms. Such studies have focused on the kinetic and thermodynamic control of the formation of the ligands and their ability to bind metal ions.

Transition-metal complexes of selenium macrocycles have been reported and are known to be stable. In contrast, it has been difficult to construct tellurium macrocycles because of the large size of the atom and the high polarizability of the Te-C bond. Hard donor atoms such as N or O have been incorporated to increase the stability of such macrocycles and their complexes. Early examples of tellura-crown ethers include 1,5-ditelluracyclooctane and 1,5,9-tritelluracyclododecane, however these molecules could not form coordination complexes.[163,164] Another tellurium-centred molecule is 1,10-ditellura-4,7,13,16-tetraoxacyclooctadedecane ([18]aneO_4Te_2) (Figure 9.1) which is capable of forming complexes with PtX_2, PdX_2, and $RhCl_2$ (X=Cl, Br). (Figure 9.1). The tellura-polyazamacrocycle in Figure 9.1 coordinates Pd(II) by both Te and N atoms with a distorted square planar geometry.

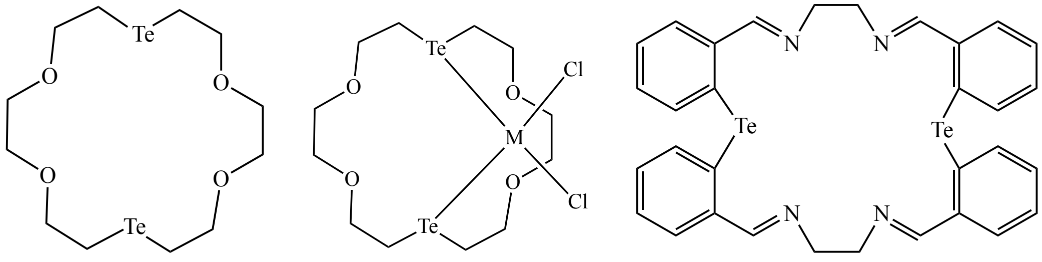

(a) (b) (c)

Figure 9.1 Structures of tellurium-containing macrocycles. 1,10-ditellura-4,7,13,16-tetraoxacyclooctadedecane(a) and its complexes (M=Pd, Pt) (c) a tellurium-centred polyazamacrocycle.

In general, syntheses of macrocycles are laborious and low yielding, although template methods greatly improve the yields of the syntheses. In contrast to the covalent synthesis of macrocycles, *iso*-tellurazole *N*-oxides have a remarkable ability to undergo reversible auto-association through Te-O secondary bonds into annular aggregates (tetramers and hexamers) that are persistent in solution. In the individual *iso*-tellurazole *N*-oxide molecule, the Te atom has two σ holes, one opposite to C and the other, more prominent, opposite to the N atom, this is the point at which the SBI interaction with the oxygen atom is formed. The Te···O interaction also entails the donation of a lone pair on the oxygen atom to the LUMO which predominantly is the $\sigma^*_{Te\text{-}N}$ orbital. The aggregates are best characterized in the case of 3-methyl-5-phenyl-*iso*-tellurazole *N*-oxide (**30**), depending on the solvent, **30** crystallizes in a variety of structures. The aggregates observed in crystals include an infinite spiral chain ($\mathbf{30}_{\infty}$) and cyclic tetra- ($\mathbf{30}_{\mathbf{4}}$) and hexamers ($\mathbf{30}_{\mathbf{6}}$). Each morphology has been identified by single-crystal X-ray diffraction. The annular aggregates of **30** are functional macrocycles, capable of binding transition metal ions, form adducts with fullerenes and host small molecules. The known behaviour of this compound, summarized in Figure 9.2, has been established through a combination of multinuclear NMR spectroscopy and structural single-crystal X-ray diffraction studies. While the syntheses and spectroscopic experiments have been conducted by other members of the Vargas research group, the diffraction experiments, solution and refinement of the structures have been the responsibility of L. M. Lee. This chapter describes the main features of these structures and their refinement, which in most cases was not routine work.

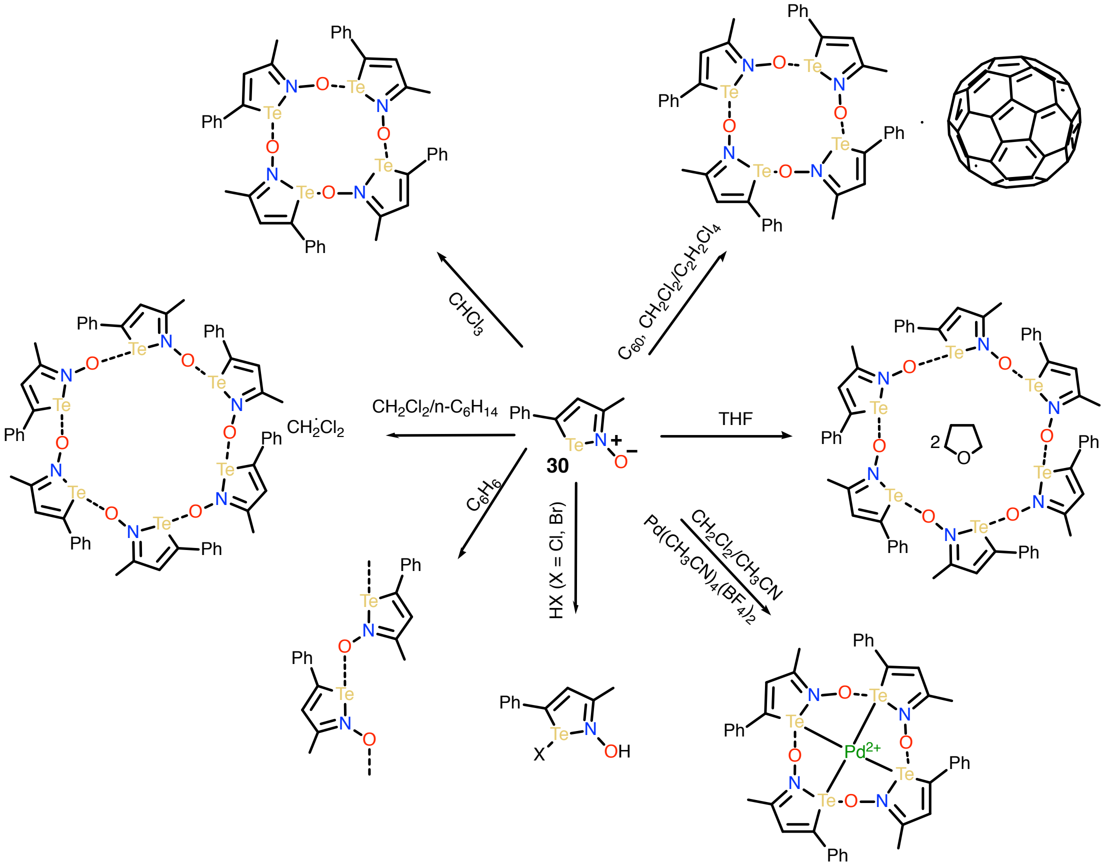

Figure 9.2 Summary of supramolecular species derived from **30**. Adapted with permission from reference 165.

9.2 Results and Discussion

Crystal data, data collection and structure refinement details are summarized in Table 2.1.

9.2.1 Crystal structure of 30_∞

Crystallization from benzene gives infinite spiral chains (**30**$_\infty$) coiling in alternating directions along b with a periodicity of 3. (Figure 9.3) The structure features an oxygen atom of one heterocycle bound to tellurium of the neighbouring unit, always trans to the nitrogen atom and to distance of 2.209(4) Å. The Te-N distance (2.222(5) Å) is slightly longer than that of a typical Te-N single bond (2.10 Å). The three molecules constituting the unit cell are crystallographically independent.

The H atoms on the heterocycle and those on the methyl group were refined with $U_{\mathrm{iso}}(\mathrm{H}) = 1.2U_{\mathrm{eq}}\mathrm{C(H)}$ and $U_{\mathrm{iso}}(\mathrm{H})=1.5\mathrm{C(H,H,H)}$ respectively. The aromatic hydrogens were refined with appropriate riding coordinates.

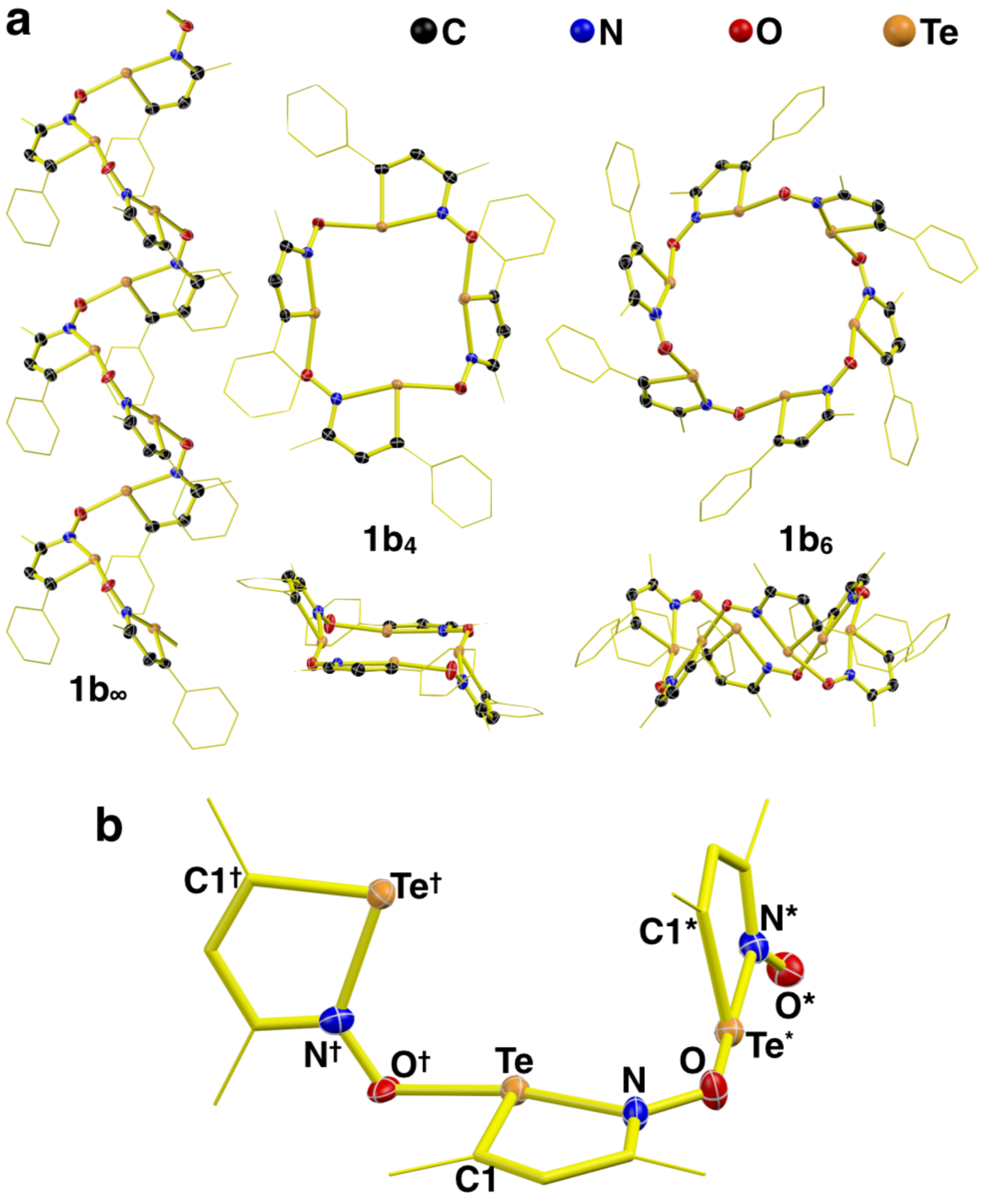

Figure 9.3 Crystallographically characterized aggregates of **30**. (a) **30**$_{\infty}$ (b) **30**$_{\mathbf{4}}$ (c) **30**$_{\mathbf{6}}$. (d) Detail of the structure of **30** displaying the relative orientations of the *iso*-tellurazole planes. Displacement ellipsoids are plotted at 75% probability in all cases. For clarity, hydrogen atoms are omitted, the phenyl and methyl groups are portrayed using a wireframe representation and are partially hidden in (d).

9.2.2 Structure of 30_4

The macrocyclic tetramer **30_4** is formed in non-solvated crystals obtained from $CHCl_3$ or by layering CH_3CN over a CH_2Cl_2 solution. (Figure 9.3) The four-membered macrocycle consists of each heterocycle linked by oxygen bridges between tellurium and nitrogen. (Te-O: 2.242(1) Å and Te-N: 2.198(1) Å) The aggregate is different from the tetramer of 3-methyl-5-(1,1-dimethylethyl)-1,2-tellurazole[166] and the *tert*-butyl derivative. It is in a chair conformation with C_i symmetry and the unit cell consists of two crystallographically independent molecules whereas the *tert*-butyl derivative is in a boat conformation with S_4 geometry and the four constituting molecules are related by symmetry. There are two distinct trans-annular Te–Te distances in **30_4**, 5.5895(2) and 5.3043(2) Å.

Hydrogen atoms were generated geometrically based on the hybridization of the parent atom and refined using the riding model with $U_{iso}(H) = 1.2U_{eq}(C)$ for CH groups, and $U_{iso}(H)=1.5C(H,H,H)$ for CH_3.

9.2.3 Structure of $30_6.(C_4H_8O)_2$

Crystallization from tetrahydrofuran yielded a hexamer aggregate consists of six equivalent molecular units of **30** with a trans-annular Te-Te distance of 7.638(2) Å. The tellurium atom is bound to oxygen with a distance of 2.197(4) Å and the Te-N bond distance is longer than the typical Te-N single bond (2.246(4) Å). Figure 9.4 shows disordered THF molecules occupying the voids external to two crystallographically independent macrocycles. The phenyl groups are also disordered and sit in another cavity.

Vertical stacking of the layers in an ABA sequence alternates the two types of cavity forming tubular channels.

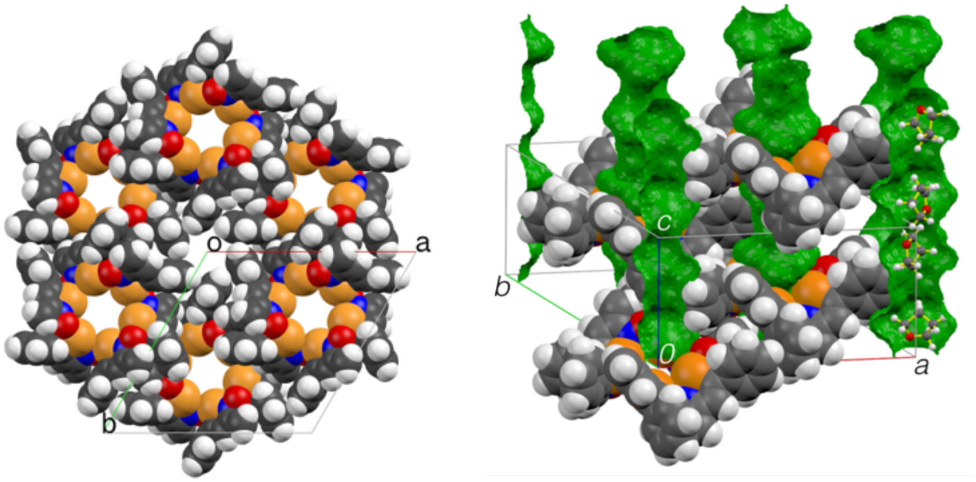

Figure 9.4 From the crystal of composition $\mathbf{30}_6\cdot(C_4H_8O)_2$ (a) packing of a layer in the (0,0,1) plane, (b) channels, location and three orientations of the disordered THF molecules. Reproduced with permission from reference 165.

Positional disorder with rotation of the THF molecule was observed. Initially in the refinement, the disorder was treated with a larger unit cell and less symmetric space groups but the R factor could not be improved. Application of a twinning law made no difference. The THF molecule was finally refined disordered over three positions in the cavities of the macrocycle, above and below the plane defined by the chalcogens. The phenyl rings were also found to be disordered over three positions and their occupancy was held at 0.3333 (Figure 9.5). All H atoms were placed in geometrically calculated positions and were refined isotropically with $U_{\mathrm{iso}}(\mathrm{H}) = 1.2\ U_{\mathrm{eq}}$ for the aromatic C atoms and $U_{\mathrm{iso}}\ (\mathrm{H}) = 1.5\ U_{\mathrm{eq}}$

for the methyl C atoms using a riding model with C-H = 0.95 Å for aromatic and C-H = 0.98 Å for methyl groups.

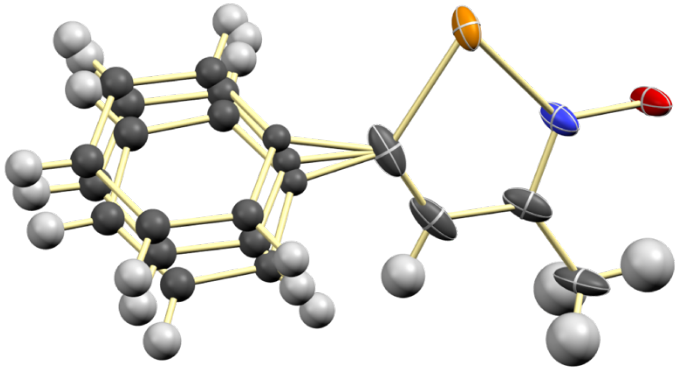

Figure 9.5 Detail of the model used for the refinement of the crystal structure of **30**$_6 \cdot (C_4H_8O)_2$ displaying the disorder three sets of atomic sites. THF molecule is omitted for clarity.

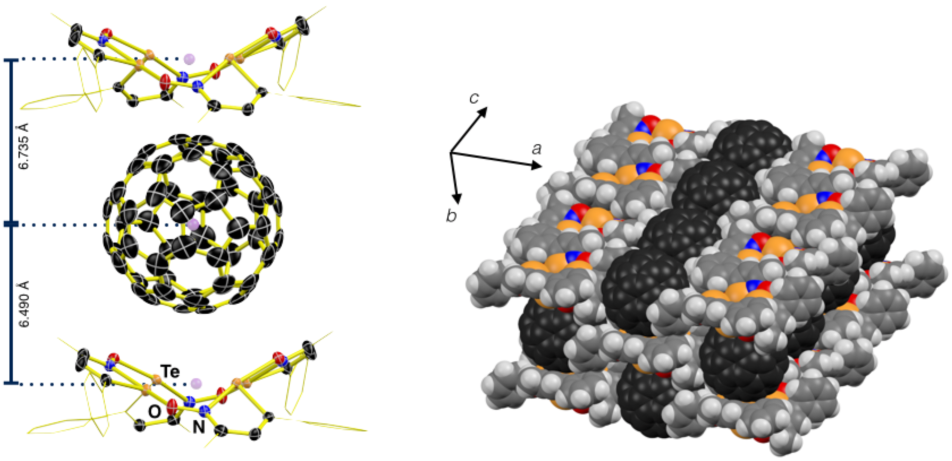

Figure 9.6 ORTEP crystal structure of **30**$_4 \cdot C_{60}$ and space-filling depiction of molecular packing in **30**$_4 \cdot C_{60}$. Reproduced with permission from reference 165.

9.2.4 C_{60} adduct of $\mathbf{30}_4$

A slow diffusion of C_{60} into a solution of hexamer produced crystals of composition $\mathbf{30}_4 \cdot C_{60}$ (Figure 9.6). The positions of H atoms in the structure were refined with appropriate riding coordinates and U_{iso} (H) = $1.2U_{eq}$C(H)/ 1.5 U_{eq} C(H,H,H).

The fullerene molecule in the crystal structure is distorted and features three crystallographically distinct diameter values of 6.952(5), 6.9393(5) and 6.9223(5) Å, which could be explained by the Jahn-Teller distortion that results from electron transfer into the $_{t1u}$ LUMO. Stacks of fullerene molecules and the distorted boat conformers of the *iso*-tellurazole rings alternate along the b-axis. The aggregates of $\mathbf{30}_4$ above and below the fullerene molecule are different and therefore, there exists two distinct distances between the centroids centred on four tellurium atoms of each aggregate. The *iso*-tellurazole rings are tilted towards the meridional plane of the macrocycle to maximize their contact with the fullerene. Along c-axis, the C_{60} molecules are organized in a columnar arrangement with even C···C spacing of 3.496 Å. The distance between C_{60} centroids is 10.533(2) Å, longer than the 10.008 Å observed in the crystal of pure C_{60}[167], and may be determined by the size of the macrocycle.

9.2.5 Structure of $[Pd(\mathbf{30}_4)_2](BF_4)_2.2(CH_2Cl_2)$

The structure of the coordination complex $[Pd(\mathbf{30}_4)_2](BF_4)_2.2(CH_2Cl_2)$ consists of a tetramer in the boat conformation while the metal centre displays a square planar coordination geometry. The Pd-Te distances (2.5805(4) Å) are comparable to those measured in complexes of anionic tellurium ligands[168]; the Te-Pd-Te trans bond angles of

172.38(2)° denote a slight pseudo D_{2d} distortion. (Figure 9.7) The square geometry allows maximum interaction between the Pd ion and the Te atom, and this effect is depicted on the shortening of the Te-O bonds and the lengthening of the Te-N bonds.

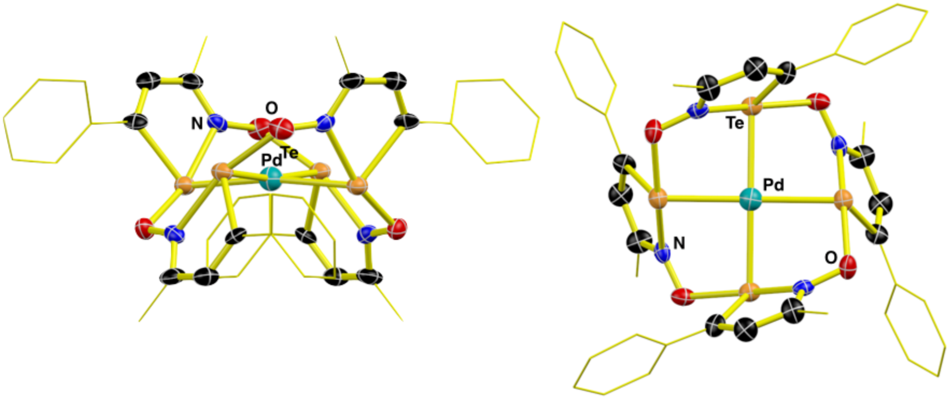

Figure 9.7 ORTEP crystal structure of the $[\mathrm{Pd}(\mathbf{30}_4)_2]^{2+}$ complex along (a) (0,2,0) and (b) along (2,1,0). All displacement ellipsoids are shown at 75% probability.

Two sets of crystallographic data of the same complex showed the coordination of the Pd ion in the tetrameric aggregate, in which the metal ion was disordered over a special position. There was, however, an anomalously low density that was attributed to metal depletion due to partial occupation of the coordination sites. CH_2Cl_2 molecules replaced the tetrafluoroborate anions in proportion to the missing metal ions. (Figure 9.8). To test this effect, diffraction data was collected from crystals grown in separate batches. Both sets of data were refined as a Pd-coordinated complex with a minor component of the neutral parent molecule with a final site-occupation factor of 0.863(7) and 0.797(5). The occupancy parameters on both solvent and tetrafluoroborate molecules were refined to account for this disorder. The refinement of the overall molecule was then aided by the application of rigid body (RIGU) restraints on all non-hydrogen atoms.

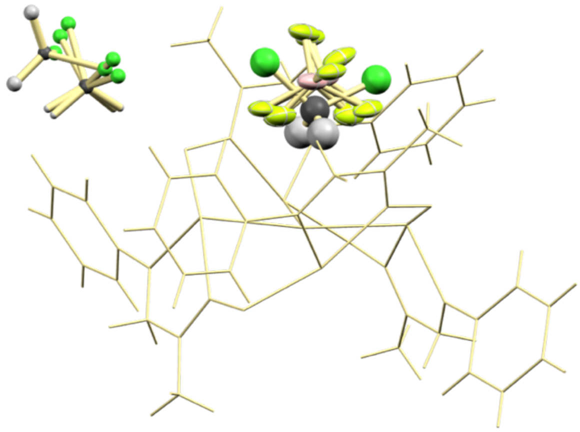

Figure 9.8 Details of the structure Pd($\mathbf{30}_4$)$_2$·(BF_4) highlighting the disordered BF_4 and CH_2Cl_2 molecules.

9.3 Summary

A variety of supramolecular structures of **30** identified by X-ray crystallography indicate that the aggregates **30** undergo reversible dissociation in solution. These structures include cyclic tetramers, hexamers and helical polymers, in which the building blocks are connected by Te···O secondary bonds. The *iso*-tellurazole *N*-oxides also form coordination complexes with a transition metal ion (Pd(II)) and act as fullerene receptors. The structures $\mathbf{30}_6$·(C_5H_8O)$_2$ and Pd($\mathbf{30}_4$)$_2$·(BF_4) featured positional and occupancy disorders. The latter structure was of special interest as the Pd ion was sitting on a special position, causing disorder on the entire structure. Refinement work for other polymorphs of **30** only required calculating positions of H atoms using a riding model.

Chapter 10. Conclusions and Outlook

10.1 Conclusions

The results of the research described in this thesis are examples of the great potential of organo-chalcogen molecules as robust and versatile supramolecular building blocks due to their ability to engage in secondary bonding.

The application of modern Density Functional Theory methods to modelling the auto-association of 1,2,5-chalcogenadiazoles did confirm that the London dispersion force makes a non-negligible stabilizing contribution. All future computational studies of secondary bonding must account for dispersion, even if just as a correction to the Kohn-Sham energy. This approach allowed proper modelling of the secondary ions detected in the mass spectra of 1,2,5-telluradiazoles and conclusively established that the interaction most likely responsible for the stabilization of $[2M + H]^+$ and $[2M]^+$ is formation the $[Te\text{-}N]_2$ supramolecular synthon. The C-Te bond in the N-heterocyclic-carbene adducts of 3,4-dicyano-1,3,5-telluradiazole and benzo-2,1,3-telluradiazole was shown to be a strong dative interaction from the carbene into a $\sigma^*_{Te\text{-}N}$ orbital, akin to SBIs.

N-substituted selenadiazoles were shown to be suitable alternatives to telluradiazoles as supramolecular building blocks. Attachment of an electron withdrawing moiety on one nitrogen greatly enhances the electrophilicity of the chalcogen without degrading the heterocycle or increasing its sensitivity towards hydrolysis. This was shown with boranes, transition-metal ions and alkyl groups (formally carbocations).

However, in the case of transition-metal derivatives, the size of the ion determined the type of structure obtained. The smaller ions (Fe^{II}, Co^{II}, Ni^{II}) preferred forming linear coordination polymers in which benzo-2,1,3-selenadiazole bridges two metal ions. The larger ions (Mn^{II}, Cd^{II}) made structures in which the $[Se\text{-}N]_2$ supramolecular synthon is formed by two heterocycles coordinated the metal atom.

There is also a dichotomy in the structures made by the borane 1:1 adducts of benzo-2,1,3-selenadiazole. While the BF_3 and BCl_3 adducts do form the $[Se\text{-}N]_2$ supramolecular synthon with short Se···N SBIs, BPh_3 and BBr_3 lead to other intermolecular interactions in the crystalline lattice. The BF_3 and BCl_3 compounds provide a proof of concept but would need to be replaced with boranes tolerant of moisture.

N-alkylated cations are more practical because of their stability and flexible methods of preparation. However, the crystallographic study of the monocations showed that the Se···N SBIs face a strong competition from the counterions. The effect is naturally stronger for the dications, which bind to anions such as BF_4^- and $CF_3SO_3^-$. However, it was demonstrated that in some cases it is possible to form the $[Se\text{-}N]_2$ supramolecular synthon.

Structural characterization has been fundamental for these investigations. In addition to problems such as crystal growth, sample quality and disorder, polymorphism (and pseudo-polymorphism) pose a caveat for some of the conclusions of these investigations. In many cases only one crystal structure could be investigated, but the cases of the xylene-bridge dication salt 1,4-$(H_4C_6NSeN\text{-}CH_2)_2\text{-}C_6H_4](BF_4)_2$ and the *iso*-tellurazole oxides constitute a warning against assuming that the observed structures are the only arrangements possible.

10.2 Suggestions of Future Work

The investigations of *d*-metal compounds derived from benzo-2,1,3-selenadiazole presented Chapter 5 are far from being a comprehensive study. As it has been established that the larger cations favour the $[Se\text{-}N]_2$ supramolecular synthon, it is desirable to investigate derivatives of the heavier transition elements. The preference for square planar coordination of d^8 ions in that case would be another factor to investigate.

As the BR_3 (R = F, Cl) the adducts of benzo-2,1,3-selenadiazole promote dimerization through the $[Se\text{-}N]_2$ supramolecular synthon, borane binding would be a convenient method to obtain supramolecular building blocks. However, the synthetic targets should be air stable, in principle. One option would be to make a 1,2-diol derivative such as **31**, alternatively a 2,2'-bipyridine could be used to make **32**. Both compounds would be prepared based on available literature methods[169] and, in spite of their charge, are expected to be air stable. Being cations, formation of Se-N SBIs, with these compounds would be complicated by binding of the anions. In this situation, and in the case of the bis(N-alkyl selenadiazolium cations), the use of much less coordinating anions to promote supramolecular association should be investigated.

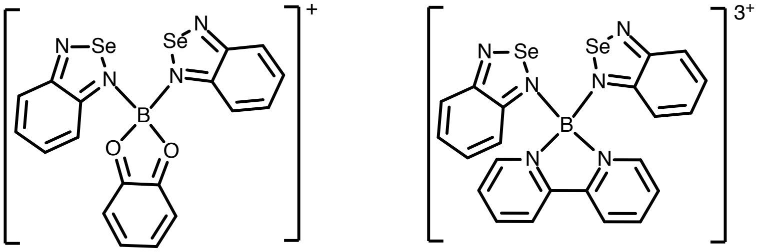

31 **32**

Scheme 10.1 Proposed synthesis of boron-bridged benzo-2,1,3-selenadiazoles

Among the N-alkylated cationic structures, the structure of the pseudotrimer in **3b**[**19a**]$_2$I$_2$ is particularly interesting in that the monocations form the [Se-N]$_2$ supramolecular synthon with a neutral molecule. This suggests that it should be possible to build supramolecular structures by binding the selenadiazolium cations to neutral 1,2,5-chalcogenadiazoles.

REFERENCES

(1) Arunan, E.; Desiraju, G. R.; Klein, R. A.; Sadlej, J.; Scheiner, S.; Alkorta, I.; Clary, D. C.; Crabtree, R. H.; Danninberg, J. J.; Hobza, P.; Kjaergaard, H. G.; Legon, A. C.; Mennucci, B.; Nesbitt, D. J. *Pure Appl. Chem.* **2011**, *83* (8), 1637.

(2) Chen, J.; Sun, L.; Cheng, Y.; Lu, Z.; Shao, K.; Li, T.; Hu, C.; Han, H. *Appl. Mater. Interfaces* **2016**, *8* (36), 24057.

(3) Aldaye, F. A.; Palmer, A. L.; Sleiman, H. F. *Science* **2008**, *321* (5897), 1795.

(4) McLaughlin, C. K.; Hamblin, G. D.; Sleiman, H. F. *Chem. Soc. Rev.* **2011**, *40* (12), 5647.

(5) Vargas Baca, I.; Mitra, D.; Zulyniak, H. J.; Banerjee, J.; Sleiman, H. F. *Angew. Chem.* **2001**, *113* (24), 4765.

(6) and, K. M. S.; McLaughlin, L. W. *J. Am. Chem. Soc.* **2004**, *126* (7), 2050.

(7) Mitra, D.; Di Cesare, N.; Sleiman, H. F. *Angew. Chem. Int. Ed. Engl.* **2004**, *43* (43), 5804.

(8) Curtis, N. F.; Curtis, Y. M.; Powell, H. K. J. *J. Chem. Soc. A* **1966**, 1015.

(9) Curtis, N. F. *J. Chem. Soc.* **1960**, 4409.

(10) Cook, T. R.; Zheng, Y. R.; Stang, P. J. *Chem. Rev.* **2012**, *113* (1), 734.

(11) Mak, T.; Chun-Ying, D.; LIu, Z.-H.; You, X.-Z.; Xue, F. *Chem. Commun.* **1997**, 381.

(12) Stang, P. J.; Persky, N. E.; Manna, J. *J. Am. Chem. Soc.* **1997**, *119* (20), 4777.

(13) Fujita, M.; Fujita, N.; Ogura, K.; Yamaguchi, K. *Nature* **1999**, *400* (6739), 52.

(14) Fujita, M.; Nagao, S.; Ogura, K. *J. Am. Chem. Soc.* **1995**, *117* (5), 1649.

(15) Fujita, W. *Science* **1999**, *286* (5438), 261.

(16) Fujita, M. *Chem. Soc. Rev.* **1998**, *27* (6), 417.

(17) Inokuma, Y.; Arai, T.; Fujita, M. *Nat Chem* **2010**, *2* (9), 780.

(18) Yaghi, O. M.; Li, H.; Eddaoudi, M.; O'Keeffe, M. *Nature* **1999**, *402* (6759), 276.

(19) Eddaoudi, M.; Kim, J.; O'Keeffe, M.; Yaghi, O. M. *CrystEngComm* **2002**, *4* (68), 401.

(20) Rosi, N. L.; Eddaoudi, M.; Kim, J.; O'Keeffe, M.; Yaghi, O. M. *Angew. Chem.* **2002**, *114* (2), 294.

(21) Fujita, M.; Sasaki, O.; Mitsuhashi, T.; Fujita, T.; Yazaki, J.; Yamaguchi, K.; Ogura, K. *Chem. Commun.* **1996**, 1535.

(22) Politzer, P.; Murray, J. S.; Clark, T. In *Halogen Bonding I*; Topics in Current Chemistry; Springer International Publishing: Cham, 2014; Vol. 358, pp 19–42.

(23) Bleiholder, C.; Werz, D. B.; Köppel, H.; Gleiter, R. *J. Am. Chem. Soc.* **2006**, *128* (8), 2666.

(24) Desiraju, G. R.; Ho, P. S.; Kloo, L.; Legon, A. C.; Marquardt, R.; Metrangolo, P.; Politzer, P.; Resnati, G.; Rissanen, K. *Pure Appl. Chem.* **2013**, *85* (8), 1711.

(25) Bauzá, A.; Mooibroek, T. J.; Frontera, A. *Chem. Rec.* **2016**, *16* (1), 473.

(26) Bauzá, A.; Mooibroek, T. J.; Frontera, A. *Chem. Phys. Chem.* **2015**, *16* (12), 2496.

(27) Bauzá, A.; Frontera, A. *Angew. Chem. Int. Ed. Engl.* **2015**, *54* (25), 7340.

(28) Alcock, N. W. *Adv. Inorg, Chem. Radiochem.* **1972***, 15*, 1.

(29) Politzer, P.; Murray, J. S. In *Noncovalent Forces*; Springer International Publishing: Cham, 2015; pp 291–321.

(30) Politzer, P.; Murray, J. S.; Clark, T. *Phys. Chem. Chem. Phys.* **2010**, *12* (28), 7748.

(31) Politzer, P.; Murray, J.; Janjić, G.; Zarić, S. *Crystals* **2014**, *4* (1), 12.

(32) Cavallo, G.; Metrangolo, P.; Milani, R.; Pilati, T.; Priimagi, A.; Resnati, G.; Terraneo, G. *Chem. Rev.* **2016**, *116* (4), 2478.

(33) Bundhun, A.; Ramasami, P.; Murray, J. S.; Politzer, P. *J. Mol. Model.* **2013**, *19* (7), 2739.

(34) Murray, J. S.; Lane, P.; Politzer, P. *J. Mol. Model.* **2009**, *15* (6), 723.

(35) Bauzá, A.; Mooibroek, T. J.; Frontera, A. *Chem. Rec.* **2016**, *16* (1), 473.

(36) Mahmoudi, G.; Bauzá, A.; Amini, M.; Molins, E.; Mague, J. T.; Frontera, A. *Dalton Trans.* **2016**, *45* (26), 10708.

(37) Mahmoudi, G.; Bauzá, A.; Frontera, A. *Dalton Trans.* **2016**, *45* (12), 4965.

(38) Servati Gargari, M.; Stilinović, V.; Bauzá, A.; Frontera, A.; McArdle, P.; Van Derveer, D.; Ng, S. W.; Mahmoudi, G. *Chem. Eur. J.* **2015**, *21* (49), 17951.

(39) Southern, S. A.; Bryce, D. L. *J .Phys. Chem. A* **2015**, *119* (49), 11891.

(40) Thirumoorthi, R.; Chivers, T.; Vargas Baca, I. *Dalton Trans.* **2011**, *40* (32), 8086.

(41) Sánchez-Sanz, G.; Trujillo, C.; Alkorta, I.; Elguero, J. *Phys. Chem. Chem. Phys.* **2016**, *18* (13), 9148.

(42) Barton, A. J.; Genge, A. R. J.; Levason, W.; Reid, G. *J. Chem. Soc., Dalton Trans.* **2000**, 859.

(43) Vickaryous, W. J.; Berryman, O. B.; Johnson, D. W. *In Bottom-Up Nanofabrication: Supramolecules, Self-Assemblies, and Organized Films; Ariga, K., Nalwa, HS, Eds*; 2006.

(44) Pitt, M. A.; Johnson, D. W. *Chem. Soc. Rev.* **2007**, *36* (9), 1441.

(45) Carter, T. G.; Vickaryous, W. J.; Cangelosi, V. M.; Johnson, D. W. *Comments Inorg. Chem.* **2007**, *28* (3-4), 97.

(46) Allen, C. A.; Cangelosi, V. M.; Zakharov, L. N. *Cryst. Growth Des.* **2009**, *9* (7), 3011.

(47) Shuka, R.; Chopra, D. *J. Chem. Sci.* **2016**, *128* (10), 1589.

(48) Bleiholder, C.; Gleiter, R.; Werz, D. B.; Köppel, H. *Inorg. Chem.* **2007**, *46* (6), 2249.

(49) J A Dobado; Henar Martínez-García; José Molina Molina, A.; Markku R Sundberg. *J. Am. Chem. Soc.* **1999**, *121*, 3156.

(50) Guo, X.; An, X.; Li, Q. *J .Phys. Chem. A* **2015**, *119* (14), 3518.

(51) Zhao, Q.; Feng, D.; Sun, Y.; Hao, J.; Cai, Z. *Int. J. Quant. Chem.* **2011**, *111* (14), 3881.

(52) Esrafili, M. D.; Mohammadian-Sabet, F. *Int. J. Quant. Chem.* **2016**, *116* (7), 529.

(53) Elder, P. J. W.; Vargas-Baca, I. *Phys. Chem. Chem. Phys.* **2016**, *18* (44), 30740.

(54) Robertson, S. D.; Chivers, T.; Tuononen, H. M. *Inorg. Chem.* **2009**, *48* (14), 6755.

(55) Mikherdov, A. S.; Kinzhalov, M. A.; Novikov, A. S.; Boyarskiy, V. P.; Boyarskaya, I. A.; Dar'in, D. V.; Starova, G. L.; Kukushkin, V. Y. *J. Am. Chem. Soc.* **2016**, *138*, 14129.

(56) Alotaibi, M. A.; Alharthi, A. I.; Zierkiewicz, W.; Akhtar, M.; Tahir, M. N.; Mazhar, M.; Isab, A. A.; Ahmad, S. *J. Mol. Struct.* **2017**, *1133*, 271.

(57) Manna, D.; Mugesh, G. *J. Am. Chem. Soc.* **2012**, *134* (9), 4269.

(58) Benz, S.; Macchione, M.; Verolet, Q.; Mareda, J.; Sakai, N.; Matile, S. *J. Am. Chem. Soc.* **2016**, *138* (29), 9093.

(59) Garrett, G. E.; Carrera, E. I.; Seferos, D. S.; Taylor, M. S. *Chem. Commun.* **2016**, *52* (64), 9881.

(60) Werz, D. B.; Gleiter, R.; Rominger, F. *J. Am. Chem .Soc.* **2002**.

(61) Werz, D. B.; Gleiter, R.; Rominger, F. *J. Org. Chem.* **2004**, *69* (9), 2945.

(62) Werz, D. B.; Staeb, T. H.; Benisch, C.; Rausch, B. J.; Rominger, F.; Gleiter, R. *Org. Lett.* **2002**, *4* (3), 339.

(63) Werz, D. B.; Gleiter, R.; Rominger, F. *J. Org. Chem.* **2002**, *67* (12), 4290.

(64) Bertini, V.; Dapporto, P.; Lucchesini, F.; Sega, A.; De Munno, A.; *Acta. Cryst. C* **1984**, *40* (4), 653.

(65) Cozzolino, A. F.; Elder, P. J. W.; Vargas Baca, I. *Coord. Chem. Rev.* **2011**, *255* (11-12), 1426.

(66) Cozzolino, A. F.; Vargas Baca, I.; Mansour, S.; Mahmoudkhani, A. H. *J. Am.

Chem. Soc. **2005**, *127* (9), 3184.

(67) Anthony F Cozzolino; James F Britten, A.; Vargas Baca, I. *Cryst. Growth Des.* **2005**, *6* (1), 181.

(68) Chivers, T.; Gao, X.; Parvez, M. *Inorg. Chem.* **1996**, *35* (1), 9.

(69) Pavan, M. S.; Jana, A. K.; Natarajan, S.; Guru Row, T. N. *J. Phys. Chem. B* **2015**, *119* (34), 11382.

(70) Cozzolino, A. F.; Bain, A. D.; Hanhan, S.; Vargas Baca, I. *Chem. Commun.* **2009**, No. 27, 4043.

(71) Cozzolino, A. F.; Whitfield, P. S.; Vargas Baca, I. *J. Am. Chem. Soc.* **2010**, *132* (48), 17265.

(72) Cozzolino, A. F.; Yang, Q.; Vargas Baca, I. *Cryst. Growth Des.* **2010**, *10*, 4959.

(73) Cozzolino, A. F.; Dimopoulos-Italiano, G.; Lee, L. M.; Vargas Baca, I. *Eur. J. Inorg. Chem.* **2013**, *2013* (15), 2751.

(74) Semenov, N. A.; Lonchakov, A. V.; Pushkarevsky, N. A.; Suturina, E. A.; Korolev, V. V.; Lork, E.; Vasiliev, V. G.; Konchenko, S. N.; Beckmann, J.; Gritsan, N. P.; Zibarev, A. V. *Organometallics* **2014**, *33* (16), 4302.

(75) Risto, M.; Reed, R. W.; Robertson, C. M.; Oilunkaniemi, R.; Laitinen, R. S.; Oakley, R. T. *Chem. Commun.* **2008**, No. 28, 3278.

(76) Garrett, G. E.; Gibson, G. L.; Straus, R. N.; Seferos, D. S.; Taylor, M. S. *J. Am. Chem. Soc.* **2015**, *137* (12), 4126.

(77) Langis-Barsetti, S.; Maris, T.; Wuest, J. D. *J. Org. Chem.* **2017**, *82* (10), 5034.

(78) Ivanova, M. V.; Mercier, H. P. A.; Schrobilgen, G. J. *J. Am. Chem. Soc.* **2015**,

137 (41), 13398.

(79) Hughes, M. J.; Mercier, H. P. A.; Schrobilgen, G. J. *Inorg. Chem.* **2009**, *48* (10), 4478.

(80) Brock, D. S.; Mercier, H. P. A.; Schrobilgen, G. J. *J. Am. Chem. Soc.* **2013**.

(81) Elliott, H. S. A.; Lehmann, J. F.; Mercier, H. P. A.; Jenkins, H. D. B.; Schrobilgen, G. J. *Inorg. Chem.* **2010**, *49* (18), 8504.

(82) Smith, G. L.; Schrobilgen, G. J. *Inorg. Chem.* **2009**, *48* (16), 7714.

(83) Koppe, K.; Frohn, H.-J.; Mercier, H. P. A.; Schrobilgen, G. J. *Inorg. Chem.* **2008**, *47* (8), 3205.

(84) Goettel, J. T.; Matsumoto, K.; Mercier, H. P. A.; Schrobilgen, G. J. *Angew. Chem. Int. Ed. Engl.* **2016**, *55* (44), 13780.

(85) Schrobilgen, G. J. *J. Chem. Soc., Chem. Commun.* **1988**, 1506.

(86) MacDougall, P. J.; Schrobilgen, G. J. *Inorg. Chem.* **1989**, *28*, 763.

(87) Sheldrick, G. M. *SADABS: Program for Empirical Absorption Correction of Area Detector Data; University of Göttingen: Germany, 1996.*

(88) Neve, J.; Hanocq, M.; Molle, L. *Talanta* **1979**, *26* (1), 15.

(89) Salavati-Niasari, M. *J. Coord. Chem.* **2009**, *62* (6), 980.

(90) Shi, M.; Qian, H.-X. *Tetrahedron* **2005**, *61* (21), 4949.

(91) Lukin, M.; Minetti, C. A. S. A.; Remeta, D. P.; Attaluri, S.; Johnson, F.; Breslauer, K. J.; de Los Santos, C. *Nucleic Acids Res.* **2011**, *39* (13), 5776.

(92) Ogino, M.; Fujimoto, K. *Angew. Chem. Int. Ed. Engl.* **2006**, *45* (43), 7223.

(93) Hashmi, S. A. N.; Hu, X.; Immoos, C. E.; Lee, S. J.; Grinstaff, M. W. *Org. Lett.*

2002, *4* (26), 4571.

(94) Figge, A.; Altenbach, H. J.; Brauer, D. J.; Tielmann, P. *Tetrahedron: Asymmetry* **2002**, *13* (2), 137.

(95) Cozzolino, A. F.; Elder, P. J. W.; Lee, L. M.; Vargas Baca, I. *Can. J. Chem.* **2013**, *91* (5), 338.

(96) Cozzolino, A. F. Synthesis, Structural Characterization, Spectroscopic Studies and Computational Investigations of 1,2,5-telluradiazoles and Their Supramolecular Assemblies. Ph. D. Thesis, McMaster University, October, 2009.

(97) Velde, te, G.; Bickelhaupt, F. M. *J. Comp. Chem.* **2001**, *22* (9), 932967.

(98) Guerra, C. F.; Snijders, J. G.; Velde, te, G.; Baerends, E. J. *Theor. Chem. Acc.* **1998**, *99* (6), 391.

(99) *ADF,* 2009-2017; SCM, Theoretical Chemistry; Vrije Universiteit, Amsterdam, The Netherlands; from http://www.scm.com.

(100) Van Lenthe, E.; Baerends, E. *J. Chem. Phys.* **1993**, *99* (6), 4597.

(101) Van Lenthe, E.; Baerends, E. J.; Snijders, J. G. *J. Chem. Phys.* **1994**, *101* (11), 9783.

(102) van Lenthe, E.; Ehlers, A.; Baerends, E.-J. *J. Chem. Phys.* **1999**, *110* (18), 8943.

(103) Van Lenthe, E.; Van Leeuwen, R.; Baerends, E. J.; Snijders, J. G. *Int. J. Quant. Chem.* **1996**, *57* (3), 281.

(104) Van Lenthe, E.; Snijders, J. G.; Baerends, E. J. *J. Chem. Phys.* **1996**, *105* (15), 6505.

(105) Perdew, J. P.; Burke, K.; Ernzerhof, M. *Phys. Rev. Lett* **1996**, *77* (18), 3865.

(106) Cramer, C. J. *Essentials of Computational Chemistry: Theories and Models*; New York, 2004, 1-772.

(107) Perdew, J. P.; Wang, Y. *Phys. Rev. B* **1992**, *45* (23), 13244.

(108) Medvedev, M. G.; Bushmarinov, I. S.; Sun, J.; Perdew, J. P.; Lyssenko, K. A. *Science* **2017**, *356* (6337), 496.

(109) Bader, R. *Atoms in Molecules: a quantum theory, International series of monographs on chemistry, 22*; Oxford University Press, 1990.

(110) Matta, C. F.; Boyd, R. J. *The Quantum Theory of Atoms in Molecules*; 2007.

(111) Bickelhaupt, F. M.; Baerends, E.-J. *Kohn-Sham Density Functional Theory: Predicting and Understanding Chemistry*; Lipkowitz, K. B., Boyd, D. B., Eds.; John Wiley & Sons, Inc.: Hoboken, NJ, USA, 2007; Vol. 15, 1–86.

(112) Ziegler, T.; Rauk, A. *Inorg. Chem.* **1979**, *18* (6), 1558.

(113) Ziegler, T.; Rauk, A. *Inorg. Chem.* **1979**, *18* (7), 1755.

(114) Grimme, S.; Antony, J.; Ehrlich, S.; Krieg, H. *J. Chem. Phys.* **2010**, *132* (15), 154104.

(115) Cozzolino, A. F.; Vargas Baca, I. *Cryst. Growth Des.* **2011**, *11* (3), 668.

(116) Legon, A. C. *Angew. Chem. Int. Ed. Engl.* **1999**, *38* (18), 2686.

(117) Lee, L. M.; Elder, P. J. W.; Cozzolino, A. F.; Yang, Q.; Vargas Baca, I. *Main Group Chem.* **2010**, *9* (1,2), 117.

(118) Zenobi, R.; Knochenmuss, R. *Mass Spectrom. Rev.* **1998**, *17*, 337.

(119) Cozzolino, A. F.; Gruhn, N. E.; Lichtenberger, D. L.; Vargas Baca, I. *Inorg.*

Chem. **2008**, *47* (14), 6220.

(120) Steed, J. W.; Atwood, J. L. *Supramolecular Chemistry* Wiley: New York, 2000, 722.

(121) Dutton, J. L.; Ragogna, P. J. *Inorg. Chem.* **2009**, *48* (4), 1722.

(122) Gieren, A.; Hübner, T.; Lamm, V.; Neidlein, R.; Droste, D. *Z. Anorg. Allg. Chem.* **1985**, *523* (4), 33.

(123) Beckmann, J.; Finke, P.; Heitz, S.; Hesse, M. *Eur. J. Inorg. Chem.* **2008**, *2008* (11), 1921.

(124) Ziegler, T.; Rauk, A. *Theoret. Chim. Acta* **1977**, *46* (1), 1.

(125) Foster, J. M.; Boys, S. F. *Rev. Mod. Phys.* **1960**, *32* (2), 300.

(126) Mitoraj, M. P.; Michalak, A.; Ziegler, T. *J. Chem. Theory Comput.* **2009**, *5* (4), 962.

(127) Rezabal, E.; Frison, G. *J. Compt. Chem.* **2015**, *36* (8), 564.

(128) Mayer, I. *Chem. Phys. Lett.* **1983**, *97* (3), 270.

(129) Michalak, A.; DeKock, R. L.; Ziegler, T. *J .Phys. Chem. A* **2008**, *112* (31), 7256.

(130) Nalewajski, R. F.; Mrozek, J. *Int. J. Quant. Chem.* **1994**, *51* (4), 187.

(131) Nalewajski, R. F.; Mrozek, J.; Michalak, A. *Int. J. Quant. Chem.* **1997**, *61* (3), 589.

(132) Nalewajski, R. F.; Michalak, A. *J .Phys. Chem. A* **1998**, *102* (3), 636.

(133) Nalewajski, R. F.; Mrozek, J.; Mazur, G. *Can. J. Chem.* **2011**, *74* (6), 1121.

(134) Wiberg, K. B. *Tetrahedron* **1968**, *24* (3), 1083.

(135) Mulliken, R. S. *J. Chem. Phys.* **2004**, *23* (10), 1833.

(136) Mulliken, R. S. *J. Chem. Phys.* **2004**, *23* (10), 1841.

(137) Mulliken, R. S. *J. Chem. Phys.* **2004**, *23* (12), 2338.

(138) Mulliken, R. S. *J. Chem. Phys.* **2004**, *23* (12), 2343.

(139) Reed, A. E.; Curtiss, L. A.; Weinhold, F. *Chem. Rev.* **1988**, *88*, 899.

(140) Reed, A. E.; Weinstock, R. B.; Weinhold, F. *J. Chem. Phys.* **1998**, *83* (2), 735.

(141) Bader, R. F. W. *Acc. Chem. Res.* **1985**, *18* (1), 9.

(142) Lee, L. M.; Elder, P. J. W.; Dube, P. A.; Greedan, J. E.; Jenkins, H. A.; Britten, J. F.; Vargas Baca, I. *CrystEngComm* **2013**, *15* (37), 7434.

(143) Lee, L. M.; Corless, V. B.; Tran, M.; Jenkins, H.; Britten, J. F.; Vargas Baca, I. *Dalton Trans.* **2016**, *45* (8), 3285.

(144) Baudron, S. A. *CrystEngComm* **2010**, *12* (8), 2288.

(145) Constable, E. C. *Coord. Chem. Rev.* **2008**, *252* (8-9), 842.

(146) Clemente-Juan, J. M.; Coronado, E.; Mínguez Espallargas, G.; Adams, H.; Brammer, L. *CrystEngComm* **2010**, *12* (8), 2339.

(147) Milios, C. J.; Ioannou, P. V.; Raptopoulou, C. P.; Papaefstathiou, G. S. *Polyhedron* **2009**, *28* (15), 3199.

(148) Milios, C. J.; Ioannou, P. V.; Raptopoulou, C. P.; Papaefstathiou, G. S. *Polyhedron* **2009**, *28* (15), 3199.

(149) Gomes, A. C.; Biswas, G.; Banerjee, A.; Duax, W. L.; IUCr. *Acta. Cryst. C* **1989**, *45* (1), 73.

(150) Fisher, M. E. *Am. J. Phys.* **1964**, *32* (5), 343.

(151) Rodríguez Fortea, A.; Alemany, P.; Alvarez, S.; Ruiz, E. *Chem. Eur. J.* **2001**, *7* (3), 627.

(152) Jeon, I.-R.; Jeannin, O.; Clérac, R.; Rouzières, M.; Fourmigué, M. *Chem. Commun.* **2017**, *53* (36), 4989.

(153) Risto, M.; Assoud, A.; Winter, S. M.; Oilunkaniemi, R.; Laitinen, R. S.; Oakley, R. T. *Inorg. Chem.* **2008**, *47* (21), 10100.

(154) Nunn, A. J.; Ralph, J. T. *J. Chem. Soc.* **1965**, 6769.

(155) Nunn, A. J.; Ralph, J. T. *J. Chem. Soc., C* **1966**, 1568.

(156) Berionni, G.; Pegot, B.; Marrot, J.; Goumont, R. *CrystEngComm* **2009**, *11*, 986.

(157) Dutton, J. L.; Tindale, J. J.; Jennings, M. C.; Ragogna, P. J. *Chem. Commun.* **2006**, 2474.

(158) Eremeeva, G. I.; Strelets, B. K.; Efros, L. S. *Khim. Geterotsikl. Soedin.* **1975**, 276.

(159) Eremeeva, G. I.; Akulin, Y. I.; Timofeeva, T. N.; Strelets, B. K.; Efros, L. S. *Chem. Heterocycl. Compd.* **1982**, *18* (8), 870.

(160) Prochaska, E. S.; Loewenschuss, A. *Inorg. Chem.* **1980**.

(161) Schreckenbach, G.; Morales, Y. R.; Ziegler, T. *J. Chem. Phys.* **1998**, *104* (21), 8605.

(162) Mukherjee, G.; Singh, P.; Ganguri, C.; Sharma, S.; Singh, H. B.; Goel, N.; Singh, U. P.; Butcher, R. J. *Inorg. Chem.* **2012**, *51* (15), 8128.

(163) Fujihara, H.; Ninoi, T.; Akaishi, R.; Erata, T.; Furukawa, N. *Tetrahedron Lett.* **1991**, *32* (35), 4537.

(164) Yutaka Takaguchi; Ernst Horn, A.; Furukawa, N. *Organometallics* **1996**, *15* (24), 5112.

(165) Ho, P. C.; Szydlowski, P.; Sinclair, J.; Elder, P. J. W.; Kübel, J.; Gendy, C.; Lee, L. M.; Jenkins, H.; Britten, J. F.; Morim, D. R.; Vargas Baca, I. *Nat. Commun.* **2016**, *7*, 11299.

(166) Kübel, J.; Elder, P. J. W.; Jenkins, H. A.; Vargas Baca, I. *Dalton Transactions* **2010**, *39* (46), 11126.

(167) Kratschmer, W.; Lamb, L. D.; Fostiropoulos, K.; Huffman, D. R. *Nature* **1990**, *347*, 354.

(168) Robertson, S. D.; Ritch, J. S.; Chivers, T. *Dalton Trans.* **2009**, *345* (40), 8582.

(169) Vargas Baca, I.; Findlater, M.; Powell, A.; Vasudevan, K. V.; Cowley, A. H. *Dalton Trans.* **2008**, *346* (45), 6421.

APPENDIX

Distance Ranges for Secondary Bonding [Σr(cov) to Σr(vdW)] for Selected Pairs of Elements

	C	Si	Ge	Sn	Pb	N	P	As	Sb	Bi	O	S	Se	Te	F	Cl	Br	I	Xe
C	1.54	1.88	1.99	2.18	2.24	1.52	1.83	2.62	2.15	2.23	1.50	1.79	1.93	2.12	1.48	1.76	1.91	2.10	2.22
	3.40	3.80	1.70	3.87	3.72	3.25	3.50	3.55	1.70	1.70	3.22	3.50	3.60	3.76	3.17	3.45	3.55	3.68	3.86
Si		2.22	2.33	2.52	2.58	1.86	2.17	2.96	2.49	2.57	1.84	2.13	2.27	2.46	1.82	2.10	2.25	2.44	2.56
		4.20	2.10	4.27	4.12	3.65	3.90	3.95	2.10	2.10	3.62	3.90	4.00	4.16	3.57	3.85	3.95	4.08	4.26
Sn				2.82	2.88	2.16	2.47	3.26	2.79	2.87	2.14	2.43	2.57	2.76	2.12	2.40	2.55	2.74	2.86
				4.34	4.19	3.72	3.97	4.02	2.17	2.17	3.69	3.97	4.07	4.23	3.64	3.92	4.02	4.15	4.33
Pb					2.94	2.22	2.53	3.32	2.85	2.93	2.20	2.49	2.63	2.82	2.18	2.46	2.61	2.80	2.92
					4.04	3.57	3.82	3.87	2.02	2.02	3.54	3.82	3.92	4.08	3.49	3.77	3.87	4.00	4.18
N						1.50	1.81	2.60	2.13	2.21	1.48	1.77	1.91	2.10	1.46	1.74	1.89	2.08	2.20
						3.10	3.35	3.40	1.55	1.55	3.07	3.35	3.45	3.61	3.02	3.30	3.40	3.53	3.71
P							2.12	2.91	2.44	2.52	1.79	2.08	2.22	2.41	1.77	2.05	2.20	2.39	2.51
							3.60	3.65	1.80	1.80	3.32	3.60	3.70	3.86	3.27	3.55	3.65	3.78	3.96
As								3.70	3.23	3.31	2.58	2.87	3.01	3.20	2.56	2.84	2.99	3.18	3.30
								3.70	1.85	1.85	3.37	3.65	3.75	3.91	3.32	3.60	3.70	3.83	4.01
O											1.46	1.75	1.89	2.08	1.44	1.72	1.87	2.06	2.18
											3.04	3.32	3.42	3.58	2.99	3.27	3.37	3.50	3.68
S												2.04	2.18	2.37	1.73	2.01	2.16	2.35	2.47
												3.60	3.70	3.86	3.27	3.55	3.65	3.78	3.96
Se													2.32	2.51	1.87	2.15	2.30	2.49	2.61
													3.80	3.96	3.37	3.65	3.75	3.88	4.06
Te														2.70	2.06	2.34	2.49	2.68	2.80
														4.12	3.53	3.81	3.91	4.04	4.22
F															1.42	1.70	1.85	2.04	2.16
															2.94	3.22	3.32	3.45	3.63
Cl																1.98	2.13	2.32	2.44
																3.50	3.60	3.73	3.91
Br																	2.28	2.47	2.59
																	3.70	3.83	4.01
I																		2.66	2.78
																		3.96	4.14
Xe																			2.90
																			4.32

Data from:

1) R.T. Sanderson in *Chemical Periodicity*, Reinhold, New York, USA, 1962.
2) L.E. Sutton (ed.) in *Table of interatomic distances and configuration in molecules and ions*, Supplement 1956-1959, Special publication No. 18, Chemical Society, London, UK, 1965.
3) W.W. Porterfield in *Inorganic chemistry, a unified approach*, Addison Wesley Publishing Co., Reading Massachusetts, USA, 1984.
4) A.M. James and M.P. Lord in *Macmillan's Chemical and Physical Data*, Macmillan, London, UK, 1992.
5) A. Bondi, *J. Phys. Chem.*, **1964,** *68,* 441.
6) L. Pauling, *The Nature of the Chemical Bond*, Cornell University Press, USA, 1945.
7) J.E. Huheey, E.A. Keiter, and R.L. Keiter in *Inorganic Chemistry : Principles of Structure and Reactivity*, 4th edition, HarperCollins, New York, USA, 1993.W.W. Porterfield in *Inorganic chemistry, a unified approach*, Addison Wesley Publishing Co., Reading Massachusetts, USA, 1984.
8) A.M. James and M.P. Lord in *Macmillan's Chemical and Physical Data*, Macmillan, London, UK, 1992.

As compiled in www.webelements.com/periodicity/van_der_waals_radius/ on June 22, 2017.